

A Study on Space Structure Attitude Stabilization and Actuator Degradation

Thesis submitted for the degree of
Doctor of Philosophy
at the University of Leicester

by

Rihan Ahmed Irfan Ahmad
B.E. (Electrical & Electronics), M.Sc. (Aerospace Engineering)
Control and Instrumentation Research Group
Department of Engineering
University of Leicester

March 2012

Abstract

A Study on Space Structure Attitude Stabilization and Actuator Degradation

Rihan Ahmed Irfan Ahmad

This thesis first addresses an important topic concerning space structure control systems, namely, attitude stabilization and control, which is followed by a study on subsystem interactions of general Multi Input Multi Output (MIMO) systems for better performance and actuator fault tolerance.

A novel and simple output feedback stabilization approach is proposed for a space structure system characterized with kinematics and dynamics. The approach globally, asymptotically stabilizes the plant and the closed-loop stability is proved using Lyapunov analysis. The simplicity and robustness of the designed controller are demonstrated by investigating the closed-loop response after reducing the degree of freedom in control structure. The stability of the closed-loop system is further analyzed and the performance is compared with two other robust control approaches.

The study carries on to another space plant, a Large Space Telescope (LST). Its dynamic model which is fitted with reaction wheels initially developed by NASA is analyzed and the fully coupled dynamics are derived by taking into account the nonlinear coupling phenomena and other terms neglected in their original (NASA) form. The dynamics are combined with Quaternion based kinematics to form an intricate yet realistic LST attitude model. The attitude of the nonlinear LST model is stabilized using a state feedback controller and the LST model is shown to track a time varying attitude reference. Structure configuration is an imperative task in the design of MIMO control systems. In order to make use of interactions between multiple channels so that the system can deal with vulnerability due to actuator degradation, a novel interaction measure is proposed. It is defined as Relative Dependency Index (*RDI*) and is based on H_∞ norms. Such a measurement is effective in understanding the influence of the j^{th} input on the i^{th} output of a system. *RDI* based guidelines are outlined for configuring a system towards coupling/decoupling. *RDI* is further extended to the Input Impact Index (*i.i.i.*) which helps in determining how much an actuator degradation would affect the output of a system. The validity of *RDI* and *i.i.i.* is illustrated by simulation results and tested on the linearized spacecraft attitude model presented in the former part of the thesis.

Acknowledgments

All praise and thanks are due to Almighty ALLAH swt, The Most Gracious and The Most Merciful who has created everything and taught the creation which they knew not and may ALLAH's peace and blessings be upon the Prophet Muhammad and all of us.

I am thankful to ALLAH swt for giving me the strength, courage and opportunity to successfully start and finish my PhD at the University of Leicester. This journey started in January 2008 and I awarded a PhD in March 2012. I am greatly indebted to my parents, Irfan Ahmad and Najma Sultana, my wife Dr. Ayesha Fatima, my dearest and loving daughter Nuha, special aunt Aijazunnisa, younger brother Ridwan Ahmad and my in-laws for their most valuable prayers, patience, encouragement and sacrifice which helped me throughout this journey.

I would like to express my profound gratitude to my supervisor Prof. Da-Wei Gu for his consistent help, guidance and attention that he devoted throughout my PhD study. His supervision has enlightened me the way I do research and through him I have acquired a great deal of research knowledge and experience that will help me in future as well. I am also thankful to Prof. Ian Postlethwaite for his belief and trust in me by awarding me the UKIERI (United Kingdom & India Education & Research Initiative) award. Thanks are due to my fellow colleagues Bharani Chandra for the valuable discussions I had with him and to Mirza Tariq Hamayun for his best wishes during my PhD. My thanks are also due to Halim Alwi, Rosli Omar, Naeem Khan, Mangal Kothari, Emmanuel Prempain and Rafael Morales.

Finally, I would like to dedicate this thesis to my late grandfathers (paternal and maternal). May ALLAH swt have mercy on them, Mr. Muhammad Ahmad (Inventor of smokeless chulah) and Syed Hasan Al-zaman (Advocate). I cherish their memories which are and will be a source of inspiration.

Contents

Acknowledgments	i
Nomenclature and Abbreviations	xii
List of Publications	xiv
1 Introduction	1
1.1 Overview	1
1.2 Literature Review	4
1.3 Contribution and Thesis Organization	6
1.3.1 Thesis Contribution	6
1.3.2 Thesis Organization	8
2 Spacecraft Dynamics and Kinematics	11
2.1 Introduction	11
2.2 Direction Cosine Matrix	12
2.3 Euler Angles	13
2.4 Euler's Theorem	15
2.5 Euler's Symmetric Parameters	16
2.6 Classical Rodrigues Parameters	17
2.7 Modified Rodrigues Parameters	18
2.8 Euler's Equation of Rotational Dynamics	19
2.9 Nonlinear Spacecraft Attitude Model	20

2.9.1	MRP based Attitude Model	21
2.9.2	Quaternion based Attitude Model	21
2.10	Linearized Spacecraft Attitude Model	21
2.10.1	MRP based Linearized Attitude Model	22
3	An Attitude Stabilization Approach	25
3.1	Introduction	25
3.2	Lyapunov Theory	26
3.3	Nonlinear Spacecraft Model Formulation	27
3.4	Motivation and Previous Work in Attitude Stabilization	28
3.4.1	Slotine and Benedetto Approach [51]	29
3.4.2	Slotine and Li Approach [52]	29
3.4.3	Bong Wie Approach [62]	30
3.4.4	Tsiotras Approach [56]	30
3.5	Problem Formulation	31
3.6	Output Feedback Controller Design	31
3.6.1	Stability Analysis	33
3.6.2	Simulation Results	35
3.6.3	A Modified Approach to Lyapunov Based Output Feedback Control Law	42
3.6.4	Modified Output Feedback Control Law	43
3.6.5	Stability Analysis	44
3.6.6	Attitude Tracking System Design	45
3.6.7	Simulation Results	47
3.7	Output Feedback Controller Tuning using PSO	56
3.7.1	Preliminary	57
3.7.2	PSO algorithm	59
3.7.3	Parameter Determination and Simulation Results	61
3.8	H_∞ Controllers Design of Spacecraft Attitude	63

3.8.1	H_∞ Loop-Shaping Controller Design	64
3.8.2	H_∞ Mixed Sensitivity Controller Design	66
3.8.3	Simulation Results	68
3.9	Output Feedback Control in Quaternion Formulation	73
3.9.1	Output Feedback Control Law	73
3.9.2	Stability Analysis	75
3.9.3	Simulation Results	77
3.10	Conclusions	80
3.10.1	Extension to Chapter 4	81
3.10.2	Extension to Chapter 5	82
4	Attitude Stabilization and Control of a Large Space Telescope Model	83
4.1	Introduction	83
4.2	LST Model Description	84
4.3	LST Model Equations of Motion	87
4.4	Derivation of Coupled Equations for LST Model	90
4.5	LST Reaction Wheels	92
4.6	Attitude Stabilization and Tracking of LST Model	94
4.6.1	Attitude Model Design	96
4.6.2	State Feedback Controller	97
4.7	Simulation Results	98
4.7.1	Initial Conditions	98
4.7.2	Attitude Tracking	100
4.8	Conclusions and Future Work	102
5	Study of MIMO Subsystem Interactions for Better Performance and Fault Tolerance	106
5.1	Introduction	106
5.2	Existing Interaction Measures	108

5.2.1	Relative Gain Array	109
5.2.2	Implications of RGA	110
5.2.3	Relative Interaction Array	112
5.2.4	Niederlinski Index	113
5.2.5	Effective Relative Gain Array	116
5.2.6	Effective Relative Energy Array	119
5.3	RMSE based Performance Measure	122
5.4	H_∞ Norm based Interaction Index	125
5.4.1	Decoupling in Open-loop Stable System	125
5.4.2	Decoupling in Closed-loop System	133
5.4.3	Predicting Channel Vulnerability in Case of Actuator Degradation for Open-loop Stable Systems	139
5.4.4	Predicting Channel Vulnerability in Case of Actuator Degradation for Closed-loop Systems	146
5.5	Conclusions	152
6	Conclusions	156
6.1	Accomplishments	156
6.2	Suggestions for Future Work	160
A	Linearization of Spacecraft Attitude Model based on Euler's Equation of Rotational Dynamics and MRP	162
A.1	Introduction	162
A.1.1	Linearization	162
B	Dynamic Formulation of Euler's Equation of Rotational Dynamics and MRP	170
B.1	Introduction	170
B.1.1	Dynamic Formulation	170

C	Dynamic Formulation of Euler’s Equation of Rotational Dynamics and Quaternions	173
C.1	Introduction	173
C.1.1	Dynamic Formulation	173
D	Reaction Wheel Specifications	176
D.1	Introduction	176
D.1.1	Functional Characteristics	176
D.1.2	Physical Characteristics	177
D.1.3	Current Consumption	177
D.1.4	Interfaces	177

List of Figures

2.1	Direction cosines between reference frames \mathbb{B} and \mathbb{N}	12
2.2	Euler angle orientation	13
2.3	Nonlinear spacecraft attitude model with MRP	21
2.4	Nonlinear spacecraft attitude model with quaternions	22
3.1	Attitude stabilization using output feedback	32
3.2	Closed-loop attitude stabilization in state space	33
3.3	Case-I step response and error	37
3.4	Case-I control torque input	38
3.5	Case-II step response and error	38
3.6	Case-II control torque input	39
3.7	Case-III step response and error	39
3.8	Case-III control torque input	40
3.9	Case-IV step response and error	40
3.10	Case-IV control torque input	41
3.11	Case-III ramp response and error	41
3.12	Case-III ramp excited control torque input	42
3.13	Attitude stabilization using modified output feedback	43
3.14	Attitude tracking control system	46
3.15	Case-I attitude stabilization	49
3.16	Case-I control torque input	49
3.17	Case-II attitude stabilization	50

3.18 Case-II control torque input	50
3.19 Case-III attitude stabilization	51
3.20 Case-III control torque input	51
3.21 Case-IV attitude stabilization	52
3.22 Case-IV control torque input	52
3.23 Case-III attitude tracking	53
3.24 Case-III attitude tracking error	53
3.25 Case-III attitude tracking control torque input	54
3.26 Case-IV attitude tracking	54
3.27 Case-IV attitude tracking error	55
3.28 Case-IV attitude tracking control torque input	55
3.29 Learning curve of PSO algorithm	63
3.30 Step response of the stabilized N.L. plant	64
3.31 Step response error	64
3.32 Angular velocity plot	65
3.33 Control torque input	66
3.34 H_∞ Loop shaping controller design	66
3.35 S/T Mixed sensitivity controller design	66
3.36 Channel-1 step response and control torque input of linear plant using LSDP	68
3.37 Channel-1 step response and control torque input of nonlinear plant using LSDP	69
3.38 Channel-1 step response and control torque input of linear plant using mixed sensitivity approach	70
3.39 Channel-1 step response and control torque input of nonlinear plant using mixed sensitivity approach	70
3.40 Linearized plant step response and control torque input with saturation of ± 50 Nm using output feedback control law	72

3.41	Quaternion based attitude stabilization using output feedback	73
3.42	Quaternion based time varying attitude tracking	79
3.43	Quaternion based attitude tracking control torque	79
4.1	LST spacecraft configuration [44]	85
4.2	Basic elements of LST [44]	85
4.3	Reaction wheel configuration of LST model	86
4.4	Reaction wheel [1]	93
4.5	LST model attitude tracking control system	94
4.6	Attitude model design in simulink	96
4.7	LST model attitude stabilization	97
4.8	Attitude tracking of coupled and decoupled LST model	102
4.9	Attitude tracking control torque input for coupled and decoupled LST model	103
4.10	Attitude error quaternions of coupled and decoupled LST model	103
4.11	Roll axis stabilization and control of coupled and decoupled LST model .	104
4.12	Roll axis stabilization control torque input for coupled and decoupled LST model	104
4.13	Roll axis stabilization error for coupled and decoupled LST model	105
5.1	RMSE based plant-model performance measure in open-loop	122
5.2	Multivariable output feedback control system	133
5.3	RMSE based plant-model performance measure in closed-loop	137
5.4	Open-loop stable MIMO system with actuator uncertainty	139
5.5	RMSE based performance measure in case of actuator degradation for open-loop stable systems	142
5.6	System response with channel-1 actuator degradation	144
5.7	System response with channel-2 actuator degradation	144
5.8	System response with channel-3 actuator degradation	145
5.9	RMSE plot for actuator degradation in channels-1, 2 & 3	145

5.10	Multivariable output feedback control system with actuator uncertainty .	146
5.11	Spacecraft attitude stabilization using output feedback	149
5.12	RMSE based performance measure in case of actuator degradation for closed-loop systems	150
5.13	Attitude stabilization with channel-1 actuator degradation	153
5.14	Attitude stabilization with channel-2 actuator degradation	153
5.15	Attitude stabilization with channel-3 actuator degradation	154
5.16	RMSE plot for actuator degradation in channels-1, 2 & 3	154

List of Tables

3.1	Controller gains, inertia matrix selection & channel excitation - Output feedback approach	36
3.2	Controller gains and inertia matrix selection - Modified output feedback approach	48
3.3	Parameters for PSO algorithm	62
5.1	Loop configurations and their respective RGA	111
5.2	Loop configurations and their respective RIA, NI & $\Phi_{min}(G_1(s))$	115
5.3	Existing interaction measures for $G_2(s)$	121
5.4	RMSE for different system configurations and Δ_{OL} for $G_2(s)$	123
5.5	Existing interaction measures for $G_3(s)$	129
5.6	RMSE for system configurations of $G_3(s)$	130
5.7	Existing interaction measures for $G_4(s)$	132
5.8	RMSE for system configurations uy_{123} and Δ_{OL} for $G_4(s)$	132
5.9	RMSE for system configurations of $\tilde{P}_{c1}(s)$	138
5.10	RMSE for system configurations of $\tilde{P}_{c2}(s)$	138

Nomenclature and Abbreviations

ADCS	Attitude Determination and Control System
SISO	Single Input Single Output
MIMO	Multi Input Multi Output
DCM	Direction Cosine Matrix
PI	Proportional Integral
PD	Proportional Differential
MRP	Modified Rodrigues Parameter
PSO	Particle Swarm Optimization
GA	Genetic Algorithm
LSDP	Loop Shaping Design Procedure
LST	Large Space Telescope
RGA	Relative Gain Array
RIA	Relative Interaction Array
NI	Niederlinski Index
DRGA	Dynamic Relative Gain Array
PRGA	Partial Relative Gain Array
ERGA	Effective Relative Gain Array
EREA	Effective Relative Energy Array
RDI	Relative Dependency Index
RDIA	Relative Dependency Index Array
i.i.i.	Input Impact Index

RMSE	Root Mean Square Error
\mathbb{B}, \mathbb{N}	Reference frames with mutually perpendicular sets of vectors
ϕ, θ, ψ	Roll, pitch and yaw angles
$\omega_1, \omega_2, \omega_3$	Angular velocity about roll, pitch and yaw axes
$\hat{k}, \hat{\Phi}$	Axis and angle of rotation
$I_{n \times n}$	Identity matrix with ' n ' rows and columns
$S(a)$	Skew symmetric matrix for vector a
$\beta_{qo}, \beta_{q1}, \beta_{q2}, \beta_{q3}$	Euler symmetric parameters (Quaternions)
$\sigma_1, \sigma_2, \sigma_3$	Gibbs vector
q_1, q_2, q_3	Modified Rodrigues parameter
$\tilde{q}, \tilde{\beta}_q$	Attitude error in terms of MRP and Quaternions
q_d, β_{qd}	Reference attitude in terms of MRP and Quaternions
J, h_b	Spacecraft inertia matrix
τ_1, τ_2, τ_3	Control torque input about roll, pitch and yaw axes
$V(t)$	Positive definite function
k_a, k_b, k_p, k_c, k_d	Constant symmetric positive definite gain matrices
$s_p, s_d, \alpha, v, \beta$	Constant symmetric positive definite gain matrices
\mathbb{S}, \mathbb{T}	Sensitivity and Complementary sensitivity
W_2, W_3	Weighting functions
K_{LS}	Loop-shaping controller
K_{ST}	Mixed sensitivity controller
G_{mrp}	MRP based linear state space model
ω_o	Closed-loop bandwidth in rad/sec
I	LST model inertia
I_1, I_2, I_3	Reaction wheel inertia
M_x, M_y, M_z	External torques acting on LST
k, c, s_a, s_b, γ	Constant symmetric positive definite gain matrices

List of Publications

1. **Rihan Ahmed**, Da-wei Gu & Ian Postlethwaite, "A Simple Stabilization Approach for a Nonlinear Spacecraft Attitude Model Using a Lyapunov Function", Proceedings of ICEAE 2009, International Conference and Exhibition on Aerospace Engineering, 18th – 22nd May 2009, Bangalore, India.
2. **Rihan Ahmed**, Da-wei Gu & Ian Postlethwaite, "Attitude Tracking of a Rotating Rigid Body System", 11th IASTED International Conference on Control and Applications, CA 2009, 13th – 15th July 2009, Cambridge, United Kingdom.
3. **Rihan Ahmed**, Hamza Chaal & Da-wei Gu, "Spacecraft Controller Tuning using Particle Swarm Optimization", ICCAS-SICE 2009, International Joint Conference, 18th – 21st August 2009, Fukuoka, Japan.
4. **Rihan Ahmed**, Da-wei Gu & Ian Postlethwaite, "A Case Study on Spacecraft Attitude Control", 48th IEEE Conference on Decision and Control and 28th Chinese Control Conference, 16th – 18th December 2009, Shanghai, China.
5. Naeem khan, **Rihan Ahmed** & Da-wei Gu, "A Fault Tolerant Scheme for Attitude Estimation", 7th International Bhurban Conference on Applied Sciences and Technology, IBCAST 2010, 11th – 14th January 2010, Islamabad, Pakistan.
6. **Rihan Ahmed**, Da-wei Gu & Ian Postlethwaite, "System Structure Configuration and Actuator Degradation", 23rd Chinese Control and Decision Conference, CCDC-2011, 23rd – 25th May 2011, Mianyang, China.

-
7. Naeem Khan, Sajjad Fekri, **Rihan Ahmed** & Da-wei Gu, "Robust State Estimation in Spacecraft Attitude Control", 50th IEEE Conference on Decision and Control & European Control Conference, CDC-ECC-2011, 12th – 15th December 2011, Orlando, Florida, USA.

Chapter 1

Introduction

1.1 Overview

The motion of a rigid body in space such as a spacecraft can be distinctly divided into two types namely, translational and rotational. The position and velocity of a spacecraft describe its translational motion. The rotational motion is specified in terms of the spacecraft's attitude and attitude motion. The attitude of a spacecraft is defined as its orientation in space with respect to a reference system. The process of orienting a spacecraft in a specified, predetermined direction is called as **attitude control**. It consists of two areas namely, **attitude stabilization**, which is the process of maintaining an existing orientation, and **attitude maneuver control**, which is the process of controlling the reorientation of the spacecraft from one attitude to another [61]. This thesis addresses the problem of attitude stabilization and control of nonlinear rigid space structures. **Attitude Determination and Control System (ADCS)** is an important subsystem in all types of spacecrafts. Some of the important operations of an ADCS are as follows:

- Pointing of solar panels normal to the sun for the purpose of solar power generation.
- Pointing at selected ground targets accurately by an earth observing remote sensing spacecraft.

- Pointing of a space observing spacecraft away from earth with an additional requirement to avoid pointing the sun.
- Pointing of directional antenna and transceiver for transmission and reception.
- Avoiding solar and atmospheric damage to sensitive components.

The key aspects of attitude control are pointing in the right direction, maintaining the angular velocity and control inputs at the desired value. For example, attitude tracking would require that the spacecraft be oriented such that its sensor always points at a moving target. Such a maneuver is accomplished through a control law that generates control torques to re-orient the spacecraft to the desired attitude and angular velocity. A spacecraft's attitude is affected by disturbance torques that tend to perturb the spacecraft's attitude. The major environmental torques that affect the attitude are as follows [61]:

- Aerodynamic torques caused by the rapid spacecraft motion through the tenuous upper atmosphere.
- Gravity gradient torque due to the small difference in gravitational attraction from one end of the spacecraft to the other.
- Magnetic torque due to the interaction between the spacecraft's magnetic field and the earth's magnetic field.
- Solar radiation torque due to the electromagnetic radiation and particles radiating outward from the sun.

In order to overcome such perturbations the spacecraft's attitude is stabilized and controlled using different techniques such as spin-stabilization where the spacecraft is rotated about its axis. The angular momentum of a spin-stabilized spacecraft will remain approximately fixed and its attitude is maintained as desired. A spacecraft is three-axis stabilized when its three mutually perpendicular axes are controlled. In addition to

the three-axis stabilization the control torques are also required to compensate for the disturbance torques mentioned earlier which causes the spacecraft's orientation to drift. Hence the attitude control of a spacecraft involves the application of torques which can be generated externally by thrusters, internally by means of momentum wheels, or by a combination of both by using a wide variety of hardware and techniques. The choice of hardware depends on the requirements for maneuverability, pointing accuracy, stability and other mission requirements such as cost and lifetime. Sidi [47], has presented a notable appendix on hardware specifications.

Common means of validating control laws are numerical simulations and implementations on mathematical models reflecting the attributes of the real system to be controlled. The control concepts are effectively illustrated and verified by such simulations.

This thesis can be broadly divided into two parts, the former deals with attitude stabilization and control of two rigid space structures comprised as follows:

1. Spacecraft attitude model defined using Euler's equation of rotational dynamics and kinematic differential equations given by Quaternions and Modified Rodrigues parameters (MRP). This model is stabilized using an output feedback control law and the stability is proved in the sense of Lyapunov.
2. A Large Space Telescope (LST) attitude model is formulated by deriving the coupled nonlinear dynamics considering the coupling phenomena neglected in [44] and combining it with Quaternion based kinematics. This model is stabilized with a state feedback control law.

The latter part presents a systematic study of subsystem interactions of general Multi-Input-Multi-Output (MIMO) systems to achieve better performance and actuator fault tolerance. A simple and effective interaction index is proposed which helps in understanding the effect of one input on an output of a multivariable system with the objective of system structure configuration towards decoupling and prediction of channel vulnerability to actuator faults and failures.

In the next section a literature review is presented to familiarize oneself with the prior work in spacecraft attitude control followed by the contribution and organization of this thesis.

1.2 Literature Review

George Meyer [34], in 1971, was one of the first to present the problem of attitude control. He in [34], developed a general procedure for the design and analysis of three-axis, large angle attitude control system. Properties of three dimensional rotations were used to formulate a rigid spacecraft model. Error functions were used to assign numerical values to attitude error. These functions were used to construct asymptotically stable control laws. This method provided a useful alternative to Lyapunov analysis for determination of system stability, responsiveness, and sensitivity to disturbances, parameter variations, and target attitude motion.

Slotine et al [51], proposed a new approach to accurate attitude tracking of rigid spacecrafts handling large loads of unknown mass properties in 1990. The method was based on the construction of a physically motivated Lyapunov like function inspired from the adaptive robot manipulator control algorithm. The authors made a comparison between PD control law and an adaptive control law.

Salcudean [40], presented a new nonlinear angular velocity observer for rigid body motion in 1991. The observer structure was derived by exploiting the structure of the dynamics of rigid body motion and the simplicity of the Euler Quaternion representation of rotation.

Wen et al [60], presented an attitude controller in 1991. The controller structure was of the form of proportional and derivative feedback and a feed forward compensation. The proportional term is either the vector Quaternion feedback or the vector Quaternion and scalar Quaternion product. The research is an extension of the work done in [34].

Shuster [46], in 1993, made a survey of the different type of attitude representations. The paper discussed in detail the advantages and disadvantages in the three-parameter

as well as four parameter representations and the relationship between the various representations of the attitude and their kinematic equations.

Lizarralde et al [32], in 1996, proposed a new attitude stabilization technique when the angular velocity is not available. In contrast to the past observer based approach, a passivity approach was used to derive a large class of filters for the error Quaternion which replaced the angular velocity in the standard PD control law.

Ahmed et al [4], in 1998, addressed the problem of spacecraft tracking a desired trajectory using adaptive feedback control. The algorithm assumes no knowledge of inertia of the spacecraft and is thus unconditionally robust with respect to this parametric uncertainty. Periodic commands are used to identify the inertia matrix.

Miroslav et al [30], in 1999, presented an approach for constructing optimal feedback control laws for the regulation of a rotating rigid spacecraft. The inverse optimal control approach requires the knowledge of a control Lyapunov function and a stabilizing control law is constructed using integrator backstepping. The resulting design includes a penalty on the angular velocity, orientation and the control torque.

Wong et al [66], in 2001, addressed the problem of attitude tracking of uncertain spacecraft without angular velocity measurements. The adaptive control incorporated a velocity generating filter from attitude measurements. A high pass filter was used to generate a pseudo velocity tracking error signal while a gradient type, adaptive law accounted for the inertia uncertainty.

Sharma et al [45], in 2004, devised a nonlinear-optimal controller for the attitude tracking problem of spacecraft maneuvers through Hamilton-Jacobi formulation, applying penalty on angular velocity and attitudinal kinematics resulting in closed-form expressions for unknown Lyapunov parameters.

Gollu et al [19], in 2007 presented a Lyapunov based controller synthesis performed using sum of squares technique for large angle attitude maneuvers. The rigid body attitude was parameterized in terms of MRP's.

Doruk [16], in 2009, linearized the nonlinear satellite model which uses MRP as the

attitude representation mechanism based on Jacobian matrix linearization, around the origin and the reference values of MRP. A linear quadratic regulation approach was designed for attitude stabilization and it was shown that the closed-loop system converges but there exists a tracking error which can be reduced by increasing the controller coefficients.

Chen et al-a [15], in 2010, presented sliding mode control based on RBF neural network using reaction wheels for attitude tracking. The controller is divided into two parts, the former is the traditional sliding mode control, and the latter part is neural network based and is used for estimating the plant's uncertainties.

Hu et al [23], in 2011 improved the basic PSO algorithm and applied it to a flexible satellite attitude controller for parameter optimization.

Chen et al-b [14], in 2011 applied the PSO algorithm to optimize the controller parameters presented in [15].

1.3 Contribution and Thesis Organization

1.3.1 Thesis Contribution

The thesis has attained the following objectives:

- A novel and simple output feedback stabilization approach is proposed for the nonlinear spacecraft attitude model defined in terms of Euler's equation of rotational dynamics and the kinematic formulation using MRP and Euler's symmetric parameters (Quaternions).
- The output feedback approach is proved to be globally asymptotically stable with the help of Lyapunov stability analysis and requires only the plant output as a measurement. It is in contrast to the previously proposed approaches in literature which require additional state measurements such as angular velocity.
- The proposed control law is shown to be robust because of its non-dependency on

the spacecraft inertia and degree of freedom in the controller parameters selection. This is illustrated by reducing the degree of freedom in the controller and proving its global asymptotic stability in the sense of Lyapunov.

- A nonlinear attitude model of a LST fitted with reaction wheels as actuators is analyzed and its nonlinear coupled dynamic equations are derived by taking into account the nonlinear coupling terms, inertia tensors and the angular velocity terms neglected in the original work [44].
- The derived nonlinear coupled dynamic system is combined with a Quaternion based kinematic model to form a nonlinear attitude model of the LST system with reaction wheels as actuators. A state feedback control law is shown to stabilize the nonlinear LST attitude model and track a time varying attitude reference.
- A new measure of interaction known as Relative Dependency Index (*RDI*) and some guidelines are presented for stable open-loop MIMO systems. *RDI* is defined in terms of H_∞ norm of the individual subsystems and helps in understanding the effect of one input on an output. *RDI* based guidelines are shown to configure a MIMO system structure towards coupling and decoupling and the veracity of this approach is verified using a performance measure defined in terms of Root Mean Square Error (RMSE). The effectiveness of the approach is illustrated by simulation results and the approach is compared with the existing measures.
- *RDI* is extended to the case of closed-loop MIMO systems. A similar performance measure is used to verify the *RDI* based approach and its associated guidelines in studying the subsystem interactions. Suitable examples are demonstrated.
- *RDI* is further extended to understand the tendency of fault and failure and the influence of actuator input on system output by presenting an index known as Input Impact Index (*i.i.i.*) based on *RDI*. The *i.i.i.* and its associated guidelines are shown to predict the actuator fault/failure that would least and most affect the

overall performance of open-loop stable and closed-loop systems. The effectiveness of this approach is illustrated by examples.

- The research carried out has resulted in a few conference publications [9], [7], [5], [8], [28], [6] & [29]. Some journal papers are currently under preparation.

1.3.2 Thesis Organization

The thesis is organized into six chapters including this chapter and four appendices. A summary of each is given below:

- **Chapter 1:** This is the current chapter in which the concept of attitude is familiarized and the importance of attitude control as a major subsystem in a spacecraft is described. A literature review is presented describing the prior work in the field of attitude stabilization and control.
- **Chapter 2:** This chapter covers the fundamentals of spacecraft attitude dynamics. Different types of attitude representations to be used in the proposed work are discussed. Their pros and cons are pointed out. Euler's equation of rotational dynamics are introduced. The nonlinear spacecraft attitude model comprising of the dynamics and the kinematics is formulated using two different types of attitude representations, namely, MRP and Quaternions. Nonzero equilibrium points are found for the nonlinear attitude model and are then linearized at these operating points based on Jacobian linearization.
- **Chapter 3:** In this chapter a novel and simple output feedback stabilization approach is proposed for the nonlinear spacecraft attitude model presented in chapter two. The approach is shown to globally asymptotically stabilize the nonlinear plant and the overall closed-loop stability is proved in the sense of Lyapunov. Particle Swarm Optimization (PSO) algorithm is used as a tool to infer the best controller parameters depending on an objective function which minimizes the absolute value of the attitude error. Two robust controllers are synthesized namely,

H_∞ loop shaping and H_∞ mixed sensitivity for the linearized spacecraft attitude model presented in chapter two. The robust controllers are tested on the nonlinear attitude model and the simulation results are compared with the proposed Lyapunov based output feedback approach.

The proposed output feedback control law is modified by reducing the degree of freedom in the control structure. The overall closed-loop stability is proved with a modified Lyapunov function which globally asymptotically stabilizes the nonlinear plant. Simulation results are illustrated for attitude stabilization and time varying attitude tracking of the nonlinear plant.

- **Chapter 4:** In this chapter a LST model developed by NASA [44] in 1973, fitted with reaction wheels as actuators is described. The LST model is further developed into a fully coupled nonlinear dynamic equation of the original model itself and the reaction wheels (actuators), which are derived by taking into account the nonlinear coupling phenomena and the inertia terms neglected by [44]. The dynamic equations are then combined with a Quaternion based kinematic formulation to form a nonlinear LST attitude model. This model is globally asymptotically stabilized using a state feedback control structure and is shown to track time varying attitude.
- **Chapter 5:** In this chapter a systematic study of subsystem interactions for MIMO systems is performed. The existing interaction measures required to decouple the structure configuration and their shortcomings are outlined. A new approach for structure configuration of MIMO systems in open and closed-loop systems is presented by proposing interaction indexes defined in terms of H_∞ norm. The new interaction index helps in understanding the effect of one input on an output of a multivariable system in open-loop stable and closed-loop systems. Additionally, it is also shown that the index identifies the least and most vulnerable channel to an actuator degradation. Sufficient examples are illustrated to show the effectiveness of the index and its guidelines which help in structure

configuration of distillation column examples. The index is also shown to predict the least and most vulnerable channel prone to actuator degradation for the linearized spacecraft attitude model presented in chapter two and stabilized with an output feedback controller proposed in chapter three.

- **Chapter 6:** In this chapter a summary of the achieved results is presented followed by some thoughts on future research.
- **Appendix-A:** In this appendix the Jacobian linearization of nonlinear spacecraft attitude model defined in terms of MRP's and Euler's equation of rotational dynamics is presented.
- **Appendix-B:** The Euler's equation of rotational dynamics and the MRP's based kinematic differential equation are combined to form a second order nonlinear equation of the Hamiltonian form.
- **Appendix-C:** The Euler's equation of rotational dynamics and the Quaternion's based kinematic differential equation are combined to form a second order nonlinear equation of the Hamiltonian form.

Chapter 2

Spacecraft Dynamics and Kinematics

2.1 Introduction

The spacecraft is considered to be a rigid body, i.e. the distance between any two points on the body is fixed all the time. The rigid body attitude can be described by two sets of equations, namely, Kinematic equation and Dynamic equation [61] and [25]. They are defined as follows.

1. **Kinematic Equations of Motion:** The study of motion irrespective of forces that bring about motion. They are set of first order differential equations specifying time evolution of attitude parameters. It relates the time derivatives of the orientation angles to the angular velocity vector.
2. **Kinetic or Dynamic Equations of Motion:** The study of motion with respect to forces that cause motion. The equation expresses time dependence of angular velocity. This equation describes the time evolution of the angular velocity vector due to torque. It is also known as the Euler's equation of rotational dynamics.

The equations of motion of a rigid spacecraft deals with two frames of reference. The first is the body axis system which is fixed to the body of the spacecraft and is constantly

moving and the other is inertial axis system which is fixed to the center of the Earth. A transformation is needed to transform the orientation between the body axis and the inertial axis. Rigid body orientation has been studied by great scholars such as Euler, Jacobi, Hamilton, Cayley, Klein, Rodrigues and Gibbs [42]. A detailed description of the various attitude representations, their advantages, disadvantages and their respective kinematic differential equations can be found in [46].

2.2 Direction Cosine Matrix

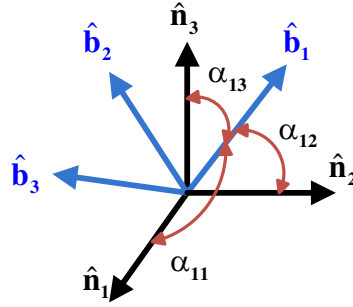


Figure 2.1: Direction cosines between reference frames \mathbb{B} and \mathbb{N}

Direction Cosine Matrix (DCM) is one of the basic coordinate transformation that maps the vectors from the body axis system to the inertial axis system. Let the two reference frames \mathbb{N} and \mathbb{B} each be defined with sets of mutually perpendicular sets of vectors given as follows:

$$\mathbb{N} \triangleq \begin{pmatrix} n_1 \\ n_2 \\ n_3 \end{pmatrix} \quad \mathbb{B} \triangleq \begin{pmatrix} b_1 \\ b_2 \\ b_3 \end{pmatrix} \quad (2.1)$$

The unit vectors of the frames \mathbb{N} and \mathbb{B} are shown in Fig. 2.1. Let α_{11} , α_{12} and α_{13} be the angles formed between the first body vector b_1 and the three inertial axes namely, n_1 , n_2 and n_3 . The cosines of these angles are called the direction cosines of b_1 relative to the \mathbb{N} frame. The unit vector b_1 can be projected onto the frame \mathbb{N} as follows:

$$b_1 = \cos \alpha_{11}n_1 + \cos \alpha_{12}n_2 + \cos \alpha_{13}n_3 \quad (2.2)$$

Analogously, the direction cosines of b_2 and b_3 relative to n_2 and n_3 can be written as follows:

$$\begin{aligned} b_2 &= \cos \alpha_{21}n_1 + \cos \alpha_{22}n_2 + \cos \alpha_{23}n_3 \\ b_3 &= \cos \alpha_{31}n_1 + \cos \alpha_{32}n_2 + \cos \alpha_{33}n_3 \end{aligned} \quad (2.3)$$

In matrix form the reference frame \mathbb{B} can be expressed in terms of reference frame \mathbb{N} as follows:

$$\mathbb{B} \triangleq \begin{pmatrix} \cos \alpha_{11} & \cos \alpha_{12} & \cos \alpha_{13} \\ \cos \alpha_{21} & \cos \alpha_{22} & \cos \alpha_{23} \\ \cos \alpha_{31} & \cos \alpha_{32} & \cos \alpha_{33} \end{pmatrix} \mathbb{N} \equiv [C_{rot}] \mathbb{N} \quad (2.4)$$

where $[C_{rot}]$ is called the DCM.

2.3 Euler Angles

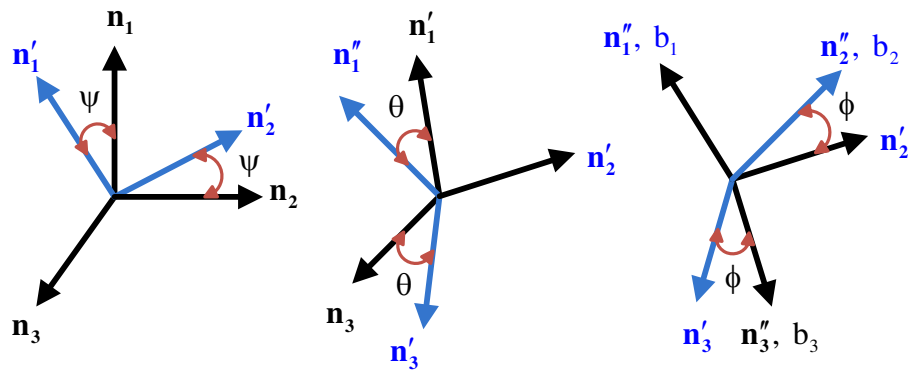


Figure 2.2: Euler angle orientation

The attitude parameters are most commonly represented using Euler angles. They describe the attitude of the reference frame \mathbb{B} relative to the frame \mathbb{N} by a sequence of three principal rotations. One possible sequence is shown in Fig. 2.2 as follows:

1. A rotation of angle ψ about the original n_3 axis.
2. A rotation of angle θ about the intermediate n_2 axis.
3. A rotation of angle ϕ about the transformed n_1 axis.

This transformation is called a 3-2-1 attitude sequence or the yaw-pitch-roll convention and is very common in aerospace applications. In this case the rotation matrix C_{rot} from \mathbb{B} to \mathbb{N} is given by:

$$C_{rot}(\psi, \theta, \phi) = \begin{pmatrix} c\theta c\psi & c\theta s\psi & -s\theta \\ s\phi s\theta c\psi - c\phi s\psi & s\phi s\theta s\psi + c\phi c\psi & s\phi c\theta \\ c\phi s\theta c\psi + s\phi s\psi & c\phi s\theta s\psi - s\phi c\psi & c\phi c\theta \end{pmatrix} \quad (2.5)$$

where the short hand notation $c = \cos$ and $s = \sin$. There are 12 possible sets of Euler angle rotations. Six of them are called symmetric sets because the first and last axis of rotation are the same. The other set of six rotations are called the asymmetric Euler angles. They are also referred to as Cardan, Tait or Bryant angles [46].

Symmetric sets		Asymmetric sets	
1-2-1	1-3-1	1-2-3	1-3-2
2-3-2	2-1-2	2-3-1	2-1-3
3-1-3	3-2-3	3-1-2	3-2-1

If the Euler angle set is symmetric, then singular orientation occurs at $\theta = 0$ or 180° and for an asymmetric set there is a singular orientation at $\theta = \pm 90^\circ$ [42]. The Euler angles are a compact, three parameter attitude representation whose coordinates are easy to visualize. The main drawback in Euler angles is that a reference frame is never further than a 90° rotation away from a singular orientation [46]. Hence their use in describing large rotations is limited. Euler angles based kinematic differential equations are fairly nonlinear comprising of computationally intensive trigonometric functions and their linearized form are only valid for a relatively small domain of rotations [42].

The kinematic differential equation of the (3-2-1) Euler angles is given by:

$$\begin{pmatrix} \dot{\psi} \\ \dot{\theta} \\ \dot{\phi} \end{pmatrix} = \frac{1}{\cos \theta} \begin{pmatrix} 0 & \sin \phi & \cos \phi \\ 0 & \cos \phi \cos \theta & -\sin \phi \cos \theta \\ \cos \theta & \sin \phi \sin \theta & \cos \phi \sin \theta \end{pmatrix} \begin{pmatrix} \omega_1 \\ \omega_2 \\ \omega_3 \end{pmatrix} \quad (2.6)$$

where ω_1 , ω_2 and ω_3 are the angular velocities of the rigid body about the roll, pitch and yaw axes in the body fixed frame.

2.4 Euler's Theorem

One of the important contributions of Euler is the Euler's theorem which tells us that only one rotation is necessary in order to reorient from one frame to another. This is formally stated as follows [61]:

Euler's Theorem: *The most general displacement of a rigid body with one point fixed is a rotation about some axis.*

Thus a single rotation about a fixed axis is sufficient to keep track of rotational motion instead of three rotations about three angles. The axis of rotation is called Euler axis or eigenaxis, denoted as $\hat{\Phi}$ and the angle of rotation is called as Euler angle or eigenangle, denoted as \hat{k} where $\hat{k} = [k_1 \ k_2 \ k_3]^T$. Each vector of frame \mathbb{B} can be expressed with respect to reference frame \mathbb{N} in terms of \hat{k} and $\hat{\Phi}$ as follows [46]

$$\mathbb{B} \triangleq [\cos \hat{\Phi} [I_{3 \times 3}] + (1 - \cos \hat{\Phi}) \hat{k} \hat{k}^T - \sin \hat{\Phi} S(\hat{k})] \mathbb{N} \equiv [\mathbb{C}] \mathbb{N} \quad (2.7)$$

where $I_{3 \times 3}$ is an identity matrix with 3 rows and 3 columns, $\hat{k} \hat{k}^T$ is the outer vector dot product of the vector \hat{k} and $S(\hat{k})$ is the skew-symmetric matrix representing the cross product operation of \hat{k} as follows:

$$S(\hat{k}) = \begin{pmatrix} 0 & -k_3 & k_2 \\ k_3 & 0 & -k_1 \\ -k_2 & k_1 & 0 \end{pmatrix} \quad (2.8)$$

The eigenaxis and eigenangle can be computed from the DCM, \mathbb{C} in (2.7) using the

following relationship [42]:

$$\hat{\Phi} = \cos^{-1} \left[\frac{1}{2} (\text{trace}(\mathbb{C}) - 1) \right] \quad (2.9)$$

$$\hat{k} = \begin{pmatrix} k_1 \\ k_2 \\ k_3 \end{pmatrix} = \frac{1}{2 \sin \hat{\Phi}} \begin{pmatrix} \mathbb{C}_{2,3} - \mathbb{C}_{3,2} \\ \mathbb{C}_{3,1} - \mathbb{C}_{1,3} \\ \mathbb{C}_{1,2} - \mathbb{C}_{2,1} \end{pmatrix} \quad (2.10)$$

where $\mathbb{C}_{i,j}$ represents the i^{th} row and j^{th} column element of \mathbb{C} matrix.

2.5 Euler's Symmetric Parameters

The Euler symmetric parameters also known as Quaternions are the preferred form of attitude representation as they globally represent the spacecraft attitude without any singularities. They provide a very convenient parametrization of attitude which is more compact than the DCM as only four parameters, rather than nine, are needed and is also superior to Euler angle parametrization which involves computationally intensive trigonometric functions, requiring time consuming computer operations [61]. They are defined in terms of the eigenaxis and eigenangle as follows:

$$\begin{aligned} \beta_{q_0} &\triangleq \cos \left(\frac{\hat{\Phi}}{2} \right) \\ \beta_{q_1} &\triangleq k_1 \sin \left(\frac{\hat{\Phi}}{2} \right) \\ \beta_{q_2} &\triangleq k_2 \sin \left(\frac{\hat{\Phi}}{2} \right) \\ \beta_{q_3} &\triangleq k_3 \sin \left(\frac{\hat{\Phi}}{2} \right) \end{aligned} \quad (2.11)$$

The Quaternions are not independent and satisfy the following constraint equation

$$\beta_{q_0}^2 + \beta_{q_1}^2 + \beta_{q_2}^2 + \beta_{q_3}^2 = 1 \quad (2.12)$$

The kinematic differential equation in terms of the Euler symmetric parameters is given as follows [42] :

$$\begin{pmatrix} \dot{\beta}_{q_0} \\ \dot{\beta}_{q_1} \\ \dot{\beta}_{q_2} \\ \dot{\beta}_{q_3} \end{pmatrix} = \begin{pmatrix} 0 & -\omega_1 & -\omega_2 & -\omega_3 \\ \omega_1 & 0 & \omega_3 & -\omega_2 \\ \omega_2 & -\omega_3 & 0 & \omega_1 \\ \omega_3 & \omega_2 & -\omega_1 & 0 \end{pmatrix} \begin{pmatrix} \beta_{q_0} \\ \beta_{q_1} \\ \beta_{q_2} \\ \beta_{q_3} \end{pmatrix} \quad (2.13)$$

Alternatively (2.13) can also be written as follows:

$$\begin{pmatrix} \dot{\beta}_{q_0} \\ \dot{\beta}_{q_1} \\ \dot{\beta}_{q_2} \\ \dot{\beta}_{q_3} \end{pmatrix} = \begin{pmatrix} \beta_{q_0} & -\beta_{q_1} & -\beta_{q_2} & -\beta_{q_3} \\ \beta_{q_1} & \beta_{q_0} & -\beta_{q_3} & \beta_{q_2} \\ \beta_{q_2} & \beta_{q_3} & \beta_{q_0} & -\beta_{q_1} \\ \beta_{q_3} & -\beta_{q_2} & \beta_{q_1} & \beta_{q_0} \end{pmatrix} \begin{pmatrix} 0 \\ \omega_1 \\ \omega_2 \\ \omega_3 \end{pmatrix} \quad (2.14)$$

2.6 Classical Rodrigues Parameters

The classical Rodrigues parameter vector also known as the Gibbs vector is another set of attitude parametrization which reduces the redundant Euler symmetric parameters to a minimal three parameter set through the following transformation

$$\sigma_i \triangleq \frac{\beta_{qi}}{\beta_{q_0}} \text{ for } i = 1, 2, 3 \quad (2.15)$$

The Gibbs vector is defined in terms of the eigenaxis and eigenangle as follows:

$$\begin{pmatrix} \sigma_1 \\ \sigma_2 \\ \sigma_3 \end{pmatrix} \triangleq \begin{pmatrix} k_1 \\ k_2 \\ k_3 \end{pmatrix} \tan \left(\frac{\hat{\Phi}}{2} \right) \quad (2.16)$$

The kinematic differential equation in terms of the Gibbs vector is given by [42]

$$\begin{pmatrix} \dot{\sigma}_1 \\ \dot{\sigma}_2 \\ \dot{\sigma}_3 \end{pmatrix} = \frac{1}{2} \begin{pmatrix} 1 + \sigma_1^2 & \sigma_1\sigma_2 - \sigma_3 & \sigma_1\sigma_3 + \sigma_2 \\ \sigma_2\sigma_1 + \sigma_3 & 1 + \sigma_2^2 & \sigma_2\sigma_3 - \sigma_1 \\ \sigma_3\sigma_1 - \sigma_2 & \sigma_3\sigma_2 + \sigma_1 & 1 + \sigma_3^2 \end{pmatrix} \begin{pmatrix} \omega_1 \\ \omega_2 \\ \omega_3 \end{pmatrix} \quad (2.17)$$

The kinematic differential equation in terms of Gibbs vector has no trigonometric functions as in the case of Euler angle approach. It is also a three parameter attitude representation. Hence, the additional constraint of four parameters in quaternion's is not present. However, the Gibbs vector has a drawback that it is defined for any rotation except for $\hat{\Phi} = \pm 180^\circ$. Although it has more freedom of rotation in comparison to Euler angles but a singularity is encountered whenever $\hat{\Phi} \rightarrow \pm 180^\circ$. This impediment is overcome in the modified form of Gibbs vector and is presented in the next section.

2.7 Modified Rodrigues Parameters

The MRP are a recent form of attitude representation. They are defined in terms of the eigenaxis and eigenangle as follows:

$$\begin{pmatrix} q_1 \\ q_2 \\ q_3 \end{pmatrix} \triangleq \begin{pmatrix} k_1 \\ k_2 \\ k_3 \end{pmatrix} \tan \left(\frac{\hat{\Phi}}{4} \right) \quad (2.18)$$

The MRP's reduce the redundant Euler symmetric parameters to a minimal three parameter set through the following transformation

$$q_i \triangleq \frac{\beta_{qi}}{1 + \beta_{qo}} \quad \text{for } i = 1, 2, 3 \quad (2.19)$$

The MRP's have a singularity at $\hat{\Phi} = \pm 360^\circ$. Hence any rotation can be described except a complete revolution back to the original orientation. It has twice the rotational range of the Gibbs vector. The kinematic differential equation in terms of MRP's is given by [42]

$$\begin{pmatrix} \dot{q}_1 \\ \dot{q}_2 \\ \dot{q}_3 \end{pmatrix} = \frac{1}{4} \begin{pmatrix} 1 + q_1^2 - q_2^2 - q_3^2 & 2(q_1q_2 - q_3) & 2(q_1q_3 + q_2) \\ 2(q_2q_1 + q_3) & 1 - q_1^2 + q_2^2 - q_3^2 & 2(q_2q_3 - q_1) \\ 2(q_3q_1 - q_2) & 2(q_3q_2 + q_1) & 1 - q_1^2 - q_2^2 + q_3^2 \end{pmatrix} \begin{pmatrix} \omega_1 \\ \omega_2 \\ \omega_3 \end{pmatrix} \quad (2.20)$$

In addition to these, there exists other attitude parameterizations and will not be discussed here. Interested readers can refer to [42] and [46].

2.8 Euler's Equation of Rotational Dynamics

The Euler's equation of rotational dynamics also known as the dynamic or kinetic equations are defined as follows:

$$J\dot{\omega} \triangleq -\omega \times J\omega + \tau = -S(\omega)J\omega + \tau \quad (2.21)$$

where J is the spacecraft's constant inertia matrix defined as follows:

$$J \triangleq \begin{pmatrix} J_{11} & J_{12} & J_{13} \\ J_{21} & J_{22} & J_{23} \\ J_{31} & J_{32} & J_{33} \end{pmatrix} \quad (2.22)$$

$\omega = [\omega_1 \ \omega_2 \ \omega_3]^T$ is the angular velocity of the rigid spacecraft in body fixed frame. $S(\omega)$ is the skew symmetric matrix representing the cross product operation of the angular velocity vector given by

$$S(\omega) = \begin{pmatrix} 0 & -\omega_3 & \omega_2 \\ \omega_3 & 0 & -\omega_1 \\ -\omega_2 & \omega_1 & 0 \end{pmatrix} \quad (2.23)$$

$\tau = [\tau_1 \ \tau_2 \ \tau_3]^T$ is the control torque input. The rigid body dynamics can be further simplified by choosing a particular orientation of the body fixed frame relative to the rigid body such that the products of inertia in (2.22) vanish. Such a frame is called the principal body fixed frame [55]. The moment of inertia in this case will be given as follows:

$$J \triangleq \begin{pmatrix} J_{11} & 0 & 0 \\ 0 & J_{22} & 0 \\ 0 & 0 & J_{33} \end{pmatrix} \quad (2.24)$$

In (2.24) all non-diagonal elements will be zero. The Euler's equation defined in (2.21) for the principal moment of inertia is given by the following equations:

$$\begin{aligned} J_{11}\dot{\omega}_1 + (J_{33} - J_{22})\omega_2\omega_3 &= \tau_1 \\ J_{22}\dot{\omega}_2 + (J_{11} - J_{33})\omega_1\omega_3 &= \tau_2 \\ J_{33}\dot{\omega}_3 + (J_{22} - J_{11})\omega_1\omega_2 &= \tau_3 \end{aligned} \quad (2.25)$$

If the spacecraft is assumed to be axis-symmetric, for instance, $J_{11} = J_{22}$, then (2.25) can be simplified as follows:

$$\begin{aligned} J_{11}\dot{\omega}_1 + (J_{33} - J_{22})\omega_2\omega_3 &= \tau_1 \\ J_{22}\dot{\omega}_2 + (J_{11} - J_{33})\omega_1\omega_3 &= \tau_2 \\ J_{33}\dot{\omega}_3 &= \tau_3 \end{aligned} \quad (2.26)$$

2.9 Nonlinear Spacecraft Attitude Model

In this thesis, the nonlinear spacecraft attitude model is formulated using both MRP's and Quaternions. Both these attitude representations have some advantages and disadvantages over each other and the Euler angles approach. A few of these can be summarized below

1. MRP's have a singularity occurrence only at $\pm 360^\circ$, whereas, in Euler angles no rotation is more than 90° .

2. Singularity can be completely avoided in Quaternions but it suffers from non-minimal parameterizations.
3. Both MRP and Quaternions do not involve computationally intensive trigonometric functions as in the case of Euler angles.

2.9.1 MRP based Attitude Model

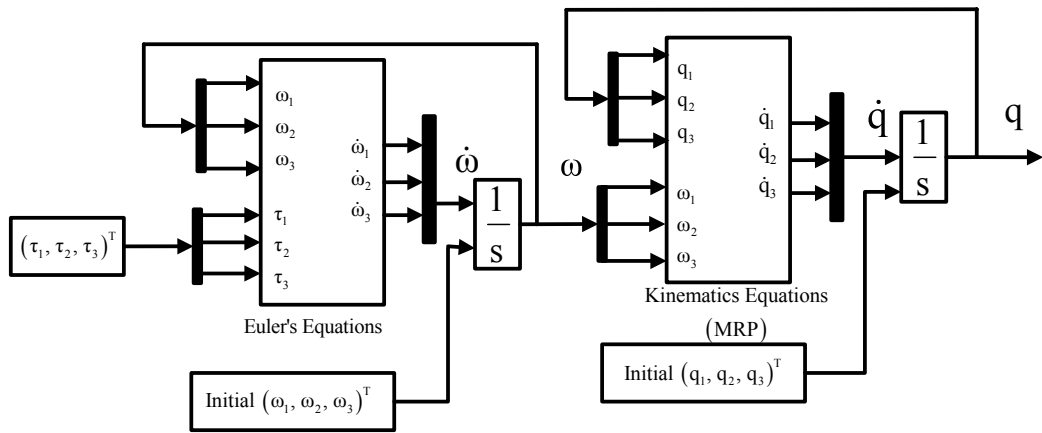


Figure 2.3: Nonlinear spacecraft attitude model with MRP

The kinematic differential equations in terms of MRP described in (2.20) and the Euler's equation of rotational dynamics described in (2.21) are cascaded to form the nonlinear spacecraft attitude model as shown in Fig. 2.3.

2.9.2 Quaternion based Attitude Model

The kinematic differential equations in terms of Quaternions described in (2.14) and the Euler's equation of rotational dynamics described in (2.21) are cascaded to form the nonlinear spacecraft attitude model as shown in Fig. 2.4.

2.10 Linearized Spacecraft Attitude Model

In this section the linearized spacecraft attitude model formulated in terms of MRP's and Euler's equation of rotational dynamics is presented.

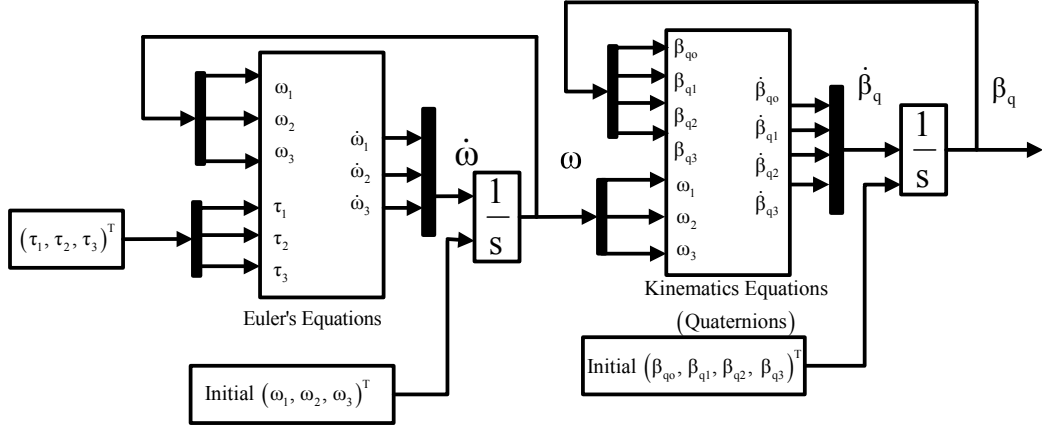


Figure 2.4: Nonlinear spacecraft attitude model with quaternions

2.10.1 MRP based Linearized Attitude Model

The spacecraft attitude model described in section 2.9.1 is nonlinear and is linearized based on Jacobian matrix linearization approach. The linearized plant approximates the nonlinear model about a set of operating points which are the angular velocities and the attitude respectively. The Jacobian matrix linearization is performed based on non-zero equilibrium points of the nonlinear model. Non-zero equilibrium points are the set of attitude and angular velocities such that the angular acceleration and the rate of change of attitude is zero. These set of points are considered as the operating points here. The characterization of equilibrium points for this class of systems is discussed in detail in chapter 7 of [10]. The analysis of Jacobian matrix linearization of satellite attitude dynamics with MRP's as attitude representation is given in [16].

Mathematically, this can be written as follows

$$\begin{bmatrix} \dot{\omega} \\ \dot{q} \end{bmatrix} = 0 \quad (2.27)$$

such that $\omega, q, \tau \neq 0$ in (2.20 & 2.21). The detailed Jacobian matrix linearization of the nonlinear model is presented in Section A.1.1 of Appendix A. The linearized spacecraft attitude model is given by

$$\begin{bmatrix} \dot{q} \\ \dot{\omega} \end{bmatrix} = A_{mrp} \begin{bmatrix} q \\ \omega \end{bmatrix} + B_{mrp} \tau \quad (2.28)$$

$$q = C_{mrp} \begin{bmatrix} q \\ \omega \end{bmatrix}$$

where A_{mrp} , B_{mrp} and C_{mrp} are found to be

$$A_{mrp} = \begin{pmatrix} -0.0656 & -0.0595 & -0.1955 & 0.2148 & 0.1227 & -0.2206 \\ 0.0595 & -0.0656 & -0.0680 & -0.2248 & 0.2248 & -0.0938 \\ 0.1955 & 0.0680 & -0.0656 & 0.1149 & 0.2104 & 0.1882 \\ 0 & 0 & 0 & -0.0245 & -0.0350 & -0.0106 \\ 0 & 0 & 0 & 0.0194 & -0.0104 & 0.0689 \\ 0 & 0 & 0 & 0.1055 & -0.0142 & 0.0349 \end{pmatrix} \quad (2.29)$$

$$B_{mrp} = \begin{pmatrix} 0 & 0 & 0 \\ 0 & 0 & 0 \\ 0 & 0 & 0 \\ 0.0503 & -0.0033 & -0.0027 \\ -0.0033 & 0.0595 & -0.0054 \\ -0.0027 & -0.0054 & 0.0673 \end{pmatrix} \quad (2.30)$$

$$C_{mrp} = \begin{pmatrix} 1 & 0 & 0 & 0 & 0 & 0 \\ 0 & 1 & 0 & 0 & 0 & 0 \\ 0 & 0 & 1 & 0 & 0 & 0 \end{pmatrix} \quad (2.31)$$

The rigid spacecraft inertia matrix is taken from [66] given as follows:

$$J = \begin{pmatrix} 20 & 1.2 & 0.9 \\ 1.2 & 17 & 1.4 \\ 0.9 & 1.4 & 15 \end{pmatrix} (kgm^2) \quad (2.32)$$

Chapter 3

An Attitude Stabilization Approach

3.1 Introduction

In this chapter, a novel and simple approach to stabilize the nonlinear spacecraft attitude model (plant) is proposed. The plant is a second order, nonlinear, MIMO system composed of the kinematic differential equations in terms of MRP and the Euler's equation of rotational dynamics presented in Section 2.9 of Chapter 2. The plant is stabilized using an output feedback controller comprising of two loops (inner and outer) wherein the angular velocity is not measured directly. The spacecraft's attitude (plant output) expressed in terms of MRP's is the only measurable state. The inner loop has a first order controller and the outer loop has a proportional gain matrix. The control scheme inherits the simplicity and robustness of a PD (Proportional-Derivative) controller, but does not require the measurement of attitude rates or use of differentiators, which makes the approach more practically useful and acceptable by practising engineers. A Lyapunov argument is used to show that the nonlinear plant can be globally stabilized using the proposed output feedback control structure. The control law does not directly depend on plant inertia matrix or its structure parameters (principal inertia matrix or inertia matrix with all non-zero elements). The overall closed-loop gives robust stability and zero tracking error performance. Particle swarm optimization is used as a tool to find the best controller parameters with regard to an objective function which minimizes the ab-

solute value of the attitude error. For the purpose of comparison, two robust controllers are synthesized, namely, H_∞ loop shaping and H_∞ mixed sensitivity for the linearized spacecraft attitude model presented in chapter two. The robust controllers are tested on the nonlinear attitude model and the simulation results are compared with the proposed output feedback approach, wherein the output feedback control law is modified by reducing the degree of freedom in the control structure. Simulation results demonstrate the effectiveness of the proposed approaches. The effectiveness of the output feedback control structure is further demonstrated in a Quaternion formulation where the plant is defined by Euler's equation of rotational dynamics and Quaternion based kinematics. The approach is shown to globally stabilize the plant based on Quaternions instead of MRP's in the sense of Lyapunov using a new candidate Lyapunov function. Simulations are again showing good results on attitude stabilization and time varying attitude acquisition.

3.2 Lyapunov Theory

The most important question for a control system is whether it is stable, because an unstable control system is undesirable. A system can be qualitatively described as being stable if it is in operation about a desired operating point and it would stay around that point ever after [52]. Every control system, whether linear or nonlinear, involves a stability problem which should be carefully studied. The most useful and general approach for studying the stability of nonlinear control systems is the theory introduced at the end of the nineteenth century by the Russian Mathematician Aleksandr Mikhailovich Lyapunov [53] and [52]. Lyapunov theory constitutes of two methods namely, a direct method and an indirect method. The direct method deals with the energy concepts associated with a mechanical system and states that a system is stable if its total mechanical energy decreases with time. This method can be used in stability analysis of nonlinear systems by the construction of a Lyapunov function and its first order derivative should be negative definite for a system to be stable. Nonlinear controllers can be designed

with the help of the direct method. For such an analysis, a Lyapunov function has to be formulated and a control structure has to be designed such that the Lyapunov function decreases with time. The major drawback in the direct method is the identification of a suitable Lyapunov function. It is common practice to use the energy of the system in constructing the Lyapunov function [51]. The Lyapunov's stability theorem can be stated as follows [50]

Theorem I: Lyapunov's stability theorem: *Given a positive definite function $V(x(t)) > 0 \forall x(t) \neq 0$ and an autonomous system $\dot{x}(t) = f(x(t))$, then the system $\frac{dx}{dt} = f(x(t))$ is stable if*

$$\dot{V}(x(t)) = \frac{\partial V}{\partial x} f(x(t)) < 0 \quad \forall x \neq 0 \forall t \quad (3.1)$$

3.3 Nonlinear Spacecraft Model Formulation

The Euler's equation of rotational dynamics and the kinematic differential equations using any one of the attitude representation such as Euler angles, Euler symmetric parameters, Gibbs vector or MRP discussed in chapter 2 can be combined to form a second order nonlinear dynamic equation known as the Hamiltonian form [52]. A detailed derivation of such a formulation in terms of Euler's dynamic equation and the MRP's can be found in Section B.1.1 of Appendix B. The second order nonlinear model in terms of MRP is given by the following equation [66]:

$$J^* \ddot{q} + C^* \dot{q} = P^T \tau \quad (3.2)$$

where

$$J^* \triangleq P^T J P \quad (3.3)$$

$$C^* \triangleq -J^* \dot{T} P - P^T S(J P \dot{q}) P$$

The inertia matrix J^* is positive definite and symmetric, and can be bounded as follows [66].

$$j_1 \|x\|^2 \leq x^T J^*(q)x \leq j_2(\|q\|)\|x\|^2, \forall x \in \mathbb{R}^3 \quad (3.4)$$

where j_1 is a positive constant, and $j_2(\|q\|)$ is a positive non decreasing function. The matrices J^* and C^* satisfy the following skew-symmetric relationship [51], [66] and [52]

$$x^T \left(\frac{1}{2} \dot{J}^* - C^* \right) x = 0 \quad (3.5)$$

The derivation of (3.5) can be found in [17].

3.4 Motivation and Previous Work in Attitude Stabilization

In literature, the rigid spacecraft attitude model has been stabilized using state feedback wherein additional measurements such as rate of change of attitude is required [51], [52], [62] and [56]. Additional requirement also includes measurement of the angular velocity vector, [34], [4], [60] and [62]. In reality such requirements are not always available. Hence it is a common practice to approximate the angular velocity vector through an adhoc numerical differentiation of the attitude angles or with the design of angular velocity observers, [40] and [32].

[51], [52], [62] and [56] have proposed state feedback control laws for stabilization of the nonlinear attitude model comprising of the nonlinear kinematic and dynamic equations. These approaches will be briefly discussed as they form the basis of the proposed work to be presented in the forthcoming sections.

3.4.1 Slotine and Benedetto Approach [51]

The spacecraft attitude model is defined using the Euler's equation of rotational dynamics and Gibbs vector stated in (2.21) and (2.17). The kinematic and dynamic equations are formulated to form second order nonlinear equation given as

$$J^*(\sigma)\ddot{\sigma} + C^*(\sigma, \dot{\sigma})\dot{\sigma} = [B(\sigma)]^{-T}\tau_a \quad (3.6)$$

A PD control law is proposed by [51] to stabilize the second order nonlinear equation in (3.6) given by

$$\tau_a = -[B(\sigma)]^T(k_p\tilde{\sigma} + k_d\dot{\tilde{\sigma}}) \quad (3.7)$$

where k_p and k_d are constant symmetric positive definite matrices. The stability is proved by taking a Lyapunov candidate function of the form

$$V_1(t) = \frac{1}{2} [\dot{\tilde{\sigma}}^T J^* \dot{\tilde{\sigma}} + \tilde{\sigma}^T k_p \tilde{\sigma}] \quad (3.8)$$

The time derivative of $V_1(t)$ is given as

$$\dot{V}_1(t) = -\dot{\tilde{\sigma}}^T k_d \dot{\tilde{\sigma}} \leq 0 \quad (3.9)$$

The drawback in this approach is the assumption that the system's state vectors, namely σ and $\dot{\sigma}$, are available or computable from measurements.

3.4.2 Slotine and Li Approach [52]

A similar approach is presented in chapter 9 of [52]. The control input is given by

$$\tau_b = -k_p\tilde{\sigma} - k_d\dot{\tilde{\sigma}} \quad (3.10)$$

where k_p and k_d as before are constant symmetric positive definite matrices. The stability is proved by taking a Lyapunov candidate function of the form

$$V_2(t) = \frac{1}{2} [\dot{\sigma}^T J^* \dot{\sigma} + \tilde{\sigma}^T k_p \tilde{\sigma}] \quad (3.11)$$

The time derivative of $V_2(t)$ is given as

$$\dot{V}_2(t) = -\dot{\sigma}^T k_d \dot{\sigma} \leq 0 \quad (3.12)$$

This approach also has the drawback of two measurement requirements namely σ and $\dot{\sigma}$.

3.4.3 Bong Wie Approach [62]

The spacecraft attitude model is defined by the Euler's equation of rotational dynamics and quaternions described in (2.21) and (2.14).

A state feedback control law is presented in chapter 7 of [62]. The control input is given by

$$\tau_c = -k_a \beta_q - k_b \omega \quad (3.13)$$

where k_a and k_b are constant symmetric positive definite matrices. [63] and [64] have shown global asymptotic stability for selected control gain selections in (3.13). The drawback of this stabilization approach is that the control law requires the measurement of attitude and the angular velocity.

3.4.4 Tsiotras Approach [56]

The spacecraft attitude model given by the Euler's equation of rotational dynamics and MRP vector are given by

$$\begin{aligned} J\dot{\omega} &= -\omega \times J\omega + \tau_d \\ \dot{q} &= T(q) \omega \end{aligned} \quad (3.14)$$

[56] presented a globally stabilizing feedback control law of the form

$$\tau_d = -k_c \omega - k_d q \quad (3.15)$$

where, k_c and k_d are constant symmetric positive definite matrices.

The stability is proved by taking a Lyapunov candidate function of the form

$$V_3(\omega, q) = \frac{1}{2} \omega^T J \omega + 2 k_d \log(1 + q^T q) \quad (3.16)$$

The time derivative of $V_3(\omega, q)$ is given as

$$\dot{V}_3(\omega, q) = -\omega^T k_c \omega \quad (3.17)$$

This approach also requires the measurement of both the attitude and angular velocity. A similar control law is presented in [57].

3.5 Problem Formulation

The objective of this chapter is to design an output feedback control structure such that the nonlinear spacecraft attitude model described in terms of MRP and Euler's equation is stabilized and gives zero steady state error for a step input. It is assumed that the spacecraft attitude is the only measurable quantity. Let \tilde{q} represent the attitude error i.e. $\tilde{q} = q_d(t) - q(t)$, where $q_d(t)$ is the desired reference attitude and $q(t)$ is the actual attitude. The stabilization objective is accomplished if

$$\lim_{t \rightarrow \infty} \tilde{q}(t) = 0 \quad (3.18)$$

3.6 Output Feedback Controller Design

The closed loop system for the proposed output feedback control structure is shown in Fig. 3.1. The control approach is relatively simple. It involves two loops, namely an inner and an outer loop. The outer loop has a negative feedback path and a feed-forward

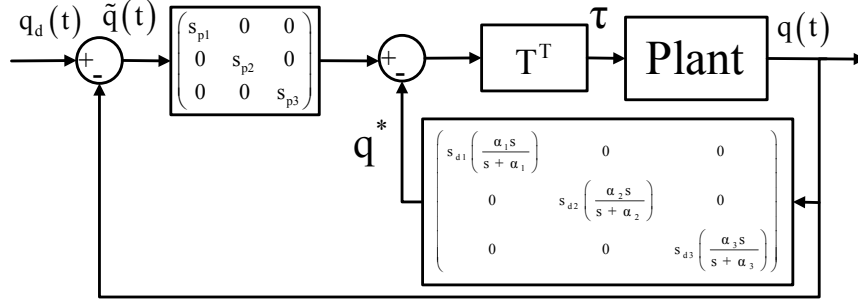


Figure 3.1: Attitude stabilization using output feedback

gain. The inner loop has a first order controller. This approach globally asymptotically stabilizes the nonlinear model in closed-loop and the overall stability is proved in the sense of Lyapunov. The control parameters can be any positive values as far as stability is concerned. However, they can be selected accordingly based on a design requirement. This will be illustrated by way of simulation results. The proposed control law is given as follows:

$$\tau \triangleq T^T (s_p \tilde{q} - q^*) \quad (3.19)$$

where

$$s_p = \text{diag}(s_{p1}, s_{p2}, s_{p3}) \quad (3.20)$$

$$q^* = \text{diag}(q_1^*, q_2^*, q_3^*) \quad (3.21)$$

q^* is defined as follows, for $i=1, 2, 3$.

$$q_i^* = s_{di} \frac{\alpha_i s}{s + \alpha_i} q_i \quad (3.22)$$

The design parameters in the control scheme are s_p in (3.20) and s_d and α are defined as follows:

$$s_d = \text{diag}(s_{d1}, s_{d2}, s_{d3}) \quad (3.23)$$

$$\alpha = \text{diag}(\alpha_1, \alpha_2, \alpha_3) \quad (3.24)$$

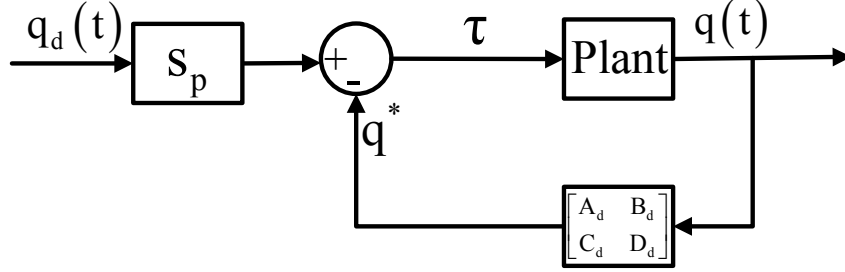


Figure 3.2: Closed-loop attitude stabilization in state space

The closed-loop system in state space for the output feedback controller is shown in Fig. 3.2. The plant represents the nonlinear system described in section (2.9.1), where, $\text{Plant} = f(q, \omega) + \tau$. The control signal is given as follows:

$$\tau = s_p q_d - q^* \quad (3.25)$$

where

$$\begin{aligned} \dot{u}_1 &= A_d u_1 + B_d q \\ q^* &= C_d u_1 + D_d q \end{aligned} \quad (3.26)$$

A_d, B_d and C_d matrices are defined from (3.20, 3.23 & 3.24) as follows:

$$A_d = -\alpha, B_d = s_d \alpha, C_d = \text{diag}(1, 1, 1), D_d = s_p \quad (3.27)$$

3.6.1 Stability Analysis

The control law described by (3.19) ensures the global asymptotic stability as delineated by the following theorem.

Theorem II: *For the nonlinear system given in (2.20 & 2.21), the control scheme in (3.19) makes the closed-loop system stable and the tracking error $\tilde{q}(t)$ in (3.18) converges to zero.*

Proof: Consider the following positive function

$$V_4(q^*, \dot{q}, \tilde{q}) = \frac{1}{2} [\dot{q}^T J^* \dot{q} + \tilde{q}^T s_p \tilde{q} + q^{*T} (s_d \alpha)^{-1} q^*] \quad (3.28)$$

The positive definite function is composed of mechanical energy given by $\frac{1}{2}[\dot{q}^T J^* \dot{q}]$ and the three gains discussed in (3.20, 3.23 and 3.24). The time derivative of the positive definite function in (3.28) can be written as follows:

$$\begin{aligned} \dot{V}_4 &= \frac{1}{2} [\dot{q}^T J^* \ddot{q} + \dot{q}^T \dot{J}^* \dot{q} + \tilde{q}^T J^* \dot{\tilde{q}}] + \frac{1}{2} [\tilde{q}^T s_p \dot{\tilde{q}} \\ &\quad + \dot{\tilde{q}}^T s_p \tilde{q}] + \frac{1}{2} [q^{*T} (s_d \alpha)^{-1} \dot{q}^* + \dot{q}^{*T} (s_d \alpha)^{-1} q^*] \end{aligned} \quad (3.29)$$

$$\dot{V}_4 = \dot{q}^T J^* \ddot{q} + \frac{1}{2} \dot{q}^T \dot{J}^* \dot{q} + \tilde{q}^T s_p \dot{\tilde{q}} + q^{*T} (s_d \alpha)^{-1} \dot{q}^* \quad (3.30)$$

$$\dot{V}_4 = \dot{q}^T (-C^* \dot{q} + P^T \tau) + \frac{1}{2} \dot{q}^T \dot{J}^* \dot{q} + \tilde{q}^T s_p \dot{\tilde{q}} + q^{*T} (s_d \alpha)^{-1} \dot{q}^* \quad (3.31)$$

$$\dot{V}_4 = \dot{q}^T \left(\frac{1}{2} \dot{J}^* - C^* \right) \dot{q} + \dot{q}^T P^T \tau + \tilde{q}^T s_p \dot{\tilde{q}} + q^{*T} (s_d \alpha)^{-1} \dot{q}^* \quad (3.32)$$

By the property of skew symmetry from (3.5), (3.32) can be written as follows

$$\dot{V}_4 = \dot{q}^T P^T \tau + \tilde{q}^T s_p \dot{\tilde{q}} + q^{*T} (s_d \alpha)^{-1} \dot{q}^* \quad (3.33)$$

Then substituting the control law from (3.19) in (3.33)

$$\dot{V}_4 = \dot{q}^T P^T T^T (s_p \tilde{q} - q^*) + \tilde{q}^T s_p \dot{\tilde{q}} + q^{*T} (s_d \alpha)^{-1} \dot{q}^* \quad (3.34)$$

$$\dot{V}_4 = \dot{q}^T s_p \tilde{q} - \dot{q}^T q^* + \tilde{q}^T s_p \dot{\tilde{q}} + q^{*T} (s_d \alpha)^{-1} \dot{q}^* \quad (3.35)$$

From $P^T T^T = I$, $\dot{\tilde{q}} = -\dot{q}$, we can get

$$\dot{V}_4 = -\dot{q}^T q^* + q^{*T} (s_d \alpha)^{-1} \dot{q}^* \quad (3.36)$$

Substituting \dot{q}_i^* from (3.22) in (3.36) we get

$$\dot{V}_4 = -\dot{q}^T q^* + q^{*T} (s_d \alpha)^{-1} (s_d \alpha \dot{q} - \alpha q^*) \quad (3.37)$$

$$\dot{V}_4 = -q^{*T} (s_d \alpha)^{-1} \alpha q^* \leq 0 \quad (3.38)$$

It is critical to verify that the system does not get "stuck" at a stage where $\dot{V}_4 = 0$ by invoking the invariant set theorem [52]. If $\dot{V}_4 = 0$ then it can be shown that $V_4 = 0$ as follows:

When $\dot{V}_4 = -q^{*T} (s_d \alpha)^{-1} \alpha q^* = 0$, then this implies that q^* is identically zero ($q^* \equiv 0$). From (3.22), $q_i^* = s_{di} \dot{q}_i - \frac{1}{\alpha_i} \dot{q}_i^*$ and if $q^* \equiv 0$ then $\dot{q}^* = 0$ so $\dot{q} = 0$. This is a regulator problem, hence without loss of generality, the reference input q_d can be assumed to be zero, hence q is zero.

Therefore, q is a constant. If \tilde{q} is a nonzero constant, then this implies that τ is also a nonzero constant. Such a τ does not generate a constant output of the system. Hence $\tilde{q} = 0$. Therefore, $V_4 = 0$, when $\dot{V}_4 = 0$.

Hence it can be stated that the nonlinear spacecraft attitude model can be globally stabilized by the control law in (3.19). The advantage of using the proposed scheme is that the plant stabilization is achieved by selecting a total of nine positive gains in the feedback and feedforward path of the closed loop system wherein the feedback consists of only the plant output.

3.6.2 Simulation Results

To demonstrate the application of the proposed scheme, the simulation results are illustrated in this section. The mathematical model of the spacecraft attitude given by (2.20 & 2.21) is simulated with (3.19) as the control input and the inertia matrices are given by (2.32) and as follows

$$h_b = \begin{pmatrix} 200 & 1.2 & 0.9 \\ 1.2 & 150 & 1.4 \\ 0.9 & 1.4 & 100 \end{pmatrix} (kgm^2) \quad (3.39)$$

The initial conditions are taken from [42] given as follows:

$$\begin{aligned} q(0) &= [-0.3 \quad -0.4 \quad 0.2]^T \\ \omega(0) &= [0.2 \quad 0.2 \quad 0.2]^T \text{ rad/sec} \end{aligned} \quad (3.40)$$

The selection of the nine gains namely s_p , s_d and α to stabilize the nonlinear plant can be any positive values as far as convergence is concerned, as shown in the Theorem II in Section 3.6.1. Since there are no specific design requirements with respect to each individual channel in this example, we choose for simplicity the same values for the controllers on the three channels. We vary the parameter values over the range from 0 to 100. By trial and error, the following values are chosen to illustrate the results. All of the four cases shown in Table 3.1 show satisfactory step responses in terms of rise time, overshoot and settling time, though different in different channels and the four case plots explain the effect of gain variation on the plant output. In addition to step input the closed-loop system is excited with a ramp signal for a single channel. The purpose of such an illustration is to visualize the inter-axis coupling and how a specific output can be achieved in spite of the interactions from the other channels. The control signal is limited to $\pm 10Nm$ in all the cases.

Table 3.1: Controller gains, inertia matrix selection & channel excitation - Output feedback approach

Case	s_p	s_d	α	Inertia matrix	Channel Excitation
Case-I	1	2	1.5	J	channels - 1, 2 & 3
Case-II	10	20	15	J	channels - 1, 2 & 3
Case-III	20	100	50	J	channel - 1
Case-IV	20	100	50	h_b	channel - 1

Figures (3.3 & 3.5) shows the step responses and errors for cases I and II and their

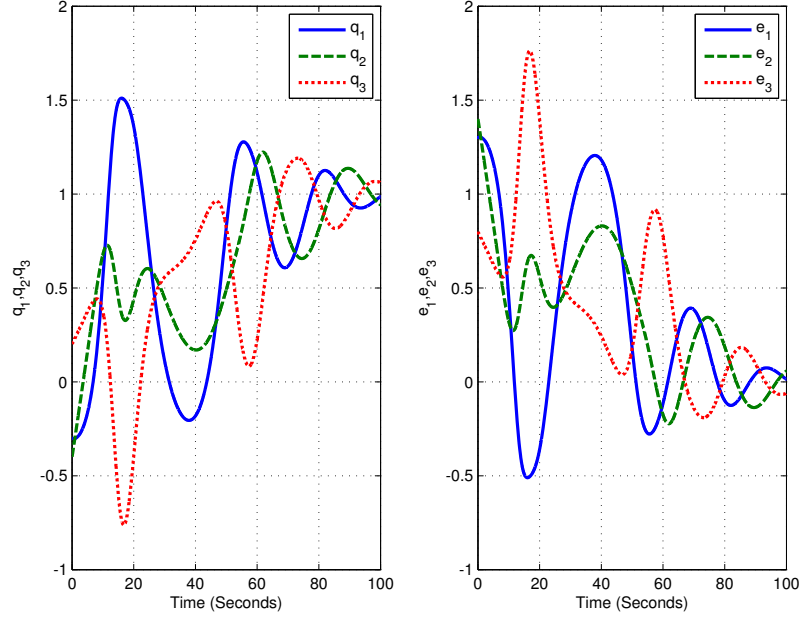


Figure 3.3: Case-I step response and error

respective controller efforts are shown in Figs (3.4 & 3.6). In both these cases all the three input channels are excited with the reference signal.

Fig. (3.7) shows the step responses and errors for case III and the respective controller effort is shown in Fig. (3.8). Fig. (3.9) shows the step response and error of the closed loop system with case III controller gains and increased inertia matrix i.e. (h_b). The required controller effort can be seen in Fig. 3.10. In both these cases (III & IV) the first input channel alone is excited with the reference signal. Cases III and IV illustrates the robustness of the proposed control law. It can be inferred that the step response of the system is not affected for a certain amount of variation in the inertia and the control law does not directly depend on the inertia matrix. In addition to the step response, the closed-loop system is excited with a ramp signal of slope 0.01. Fig. (3.11) shows the ramp response for case III and the required controller is shown in Fig. (3.12).

The nonlinear spacecraft attitude model and the inertia matrix discussed in (2.20, 2.21 & 2.32) is taken from [66], wherein the authors have synthesized an adaptive tracking control structure. The maximum control torque input in this case was bounded between 4 and -2 Nm and zero steady state error was achieved in about 80 seconds. In our case the steady state response is achieved in less time and it depends on the

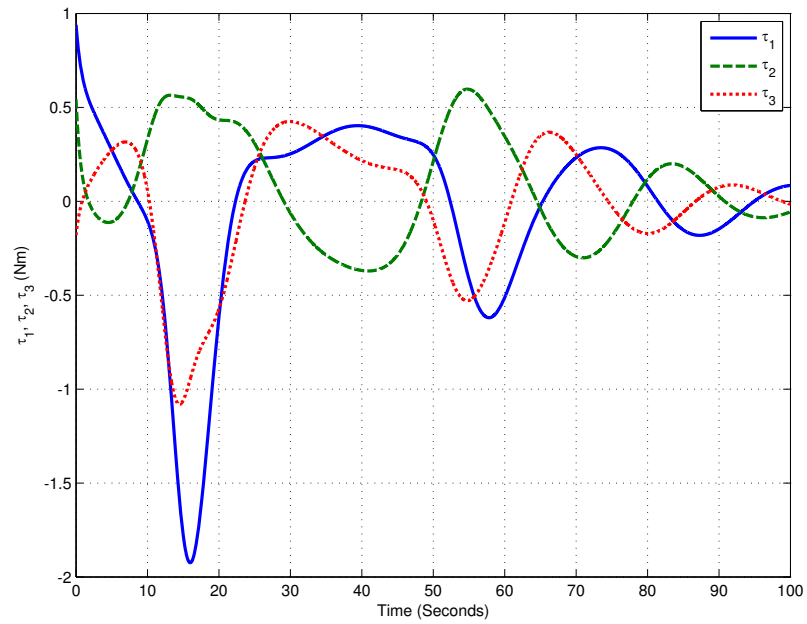


Figure 3.4: Case-I control torque input

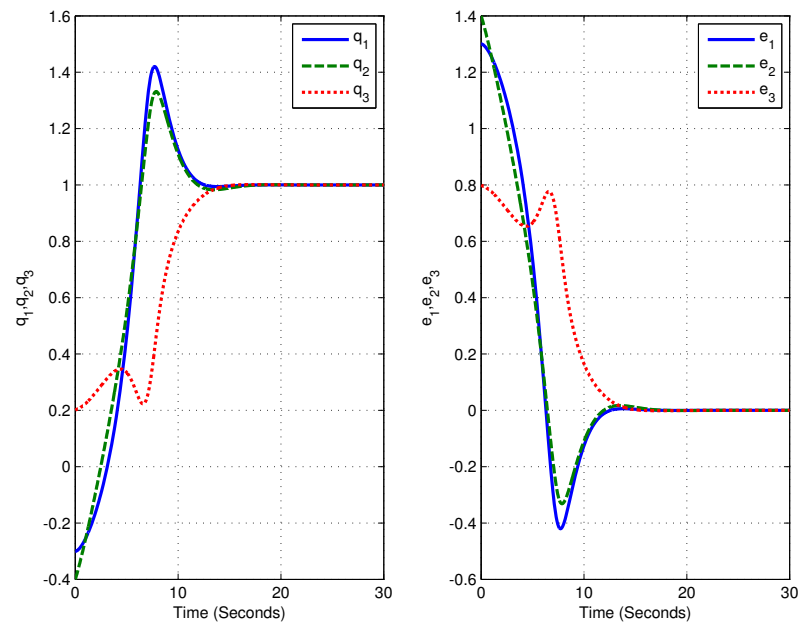


Figure 3.5: Case-II step response and error

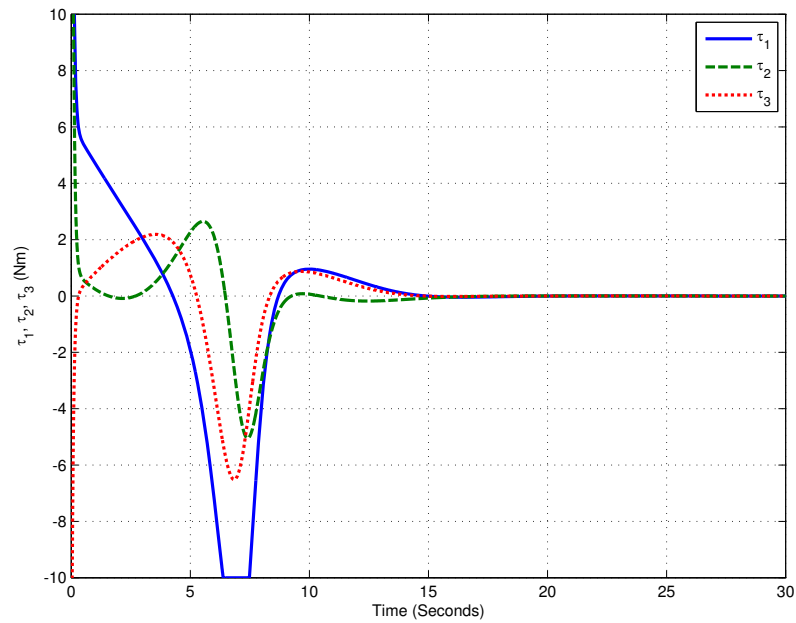


Figure 3.6: Case-II control torque input

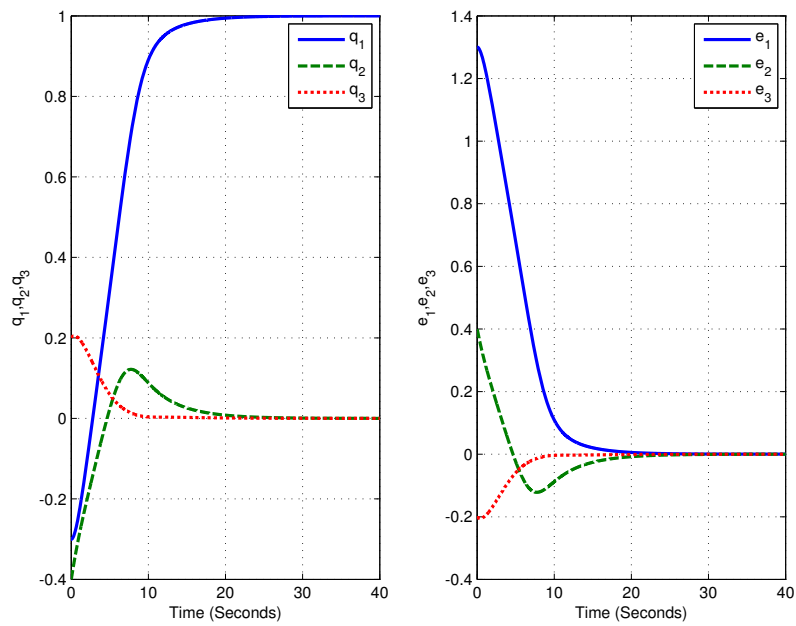


Figure 3.7: Case-III step response and error

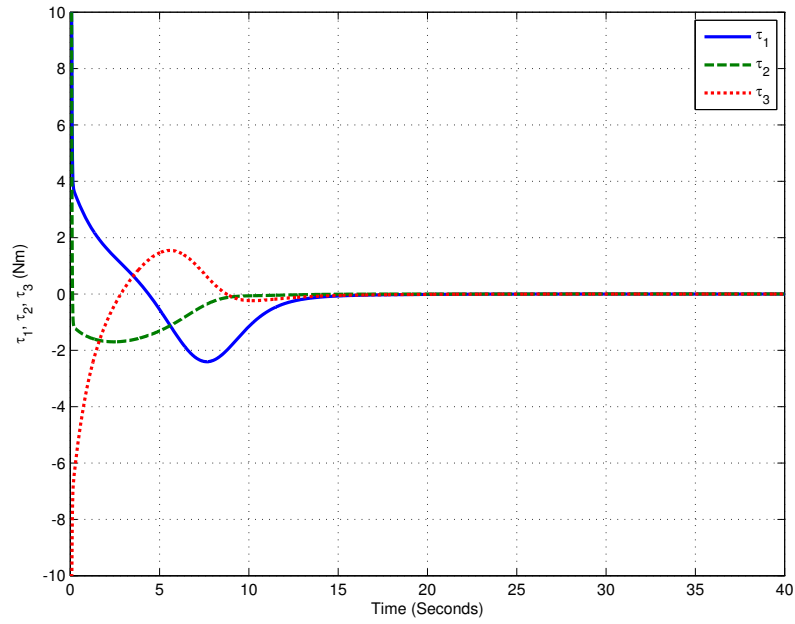


Figure 3.8: Case-III control torque input

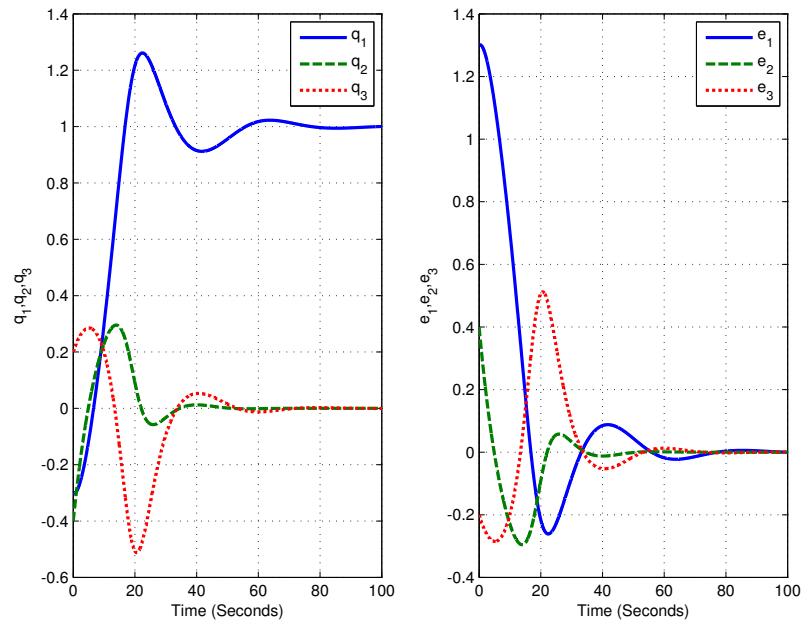


Figure 3.9: Case-IV step response and error

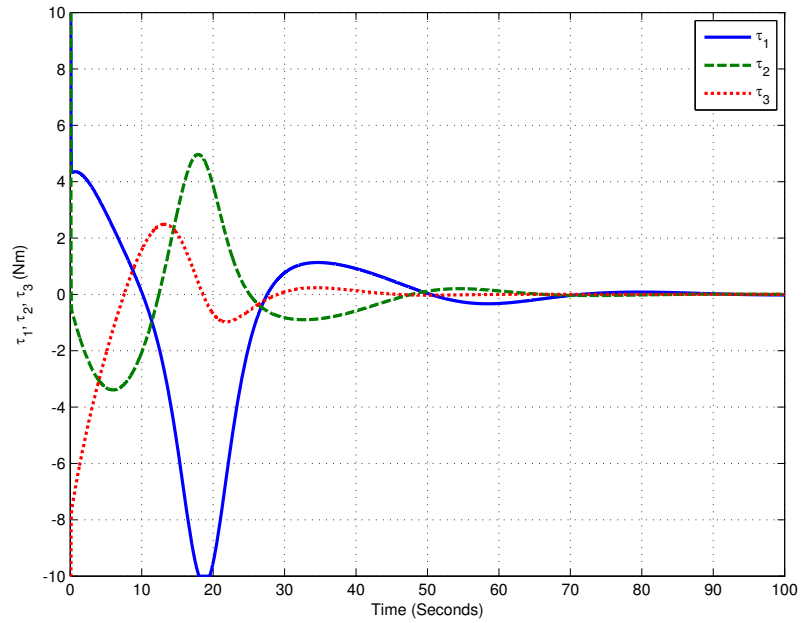


Figure 3.10: Case-IV control torque input

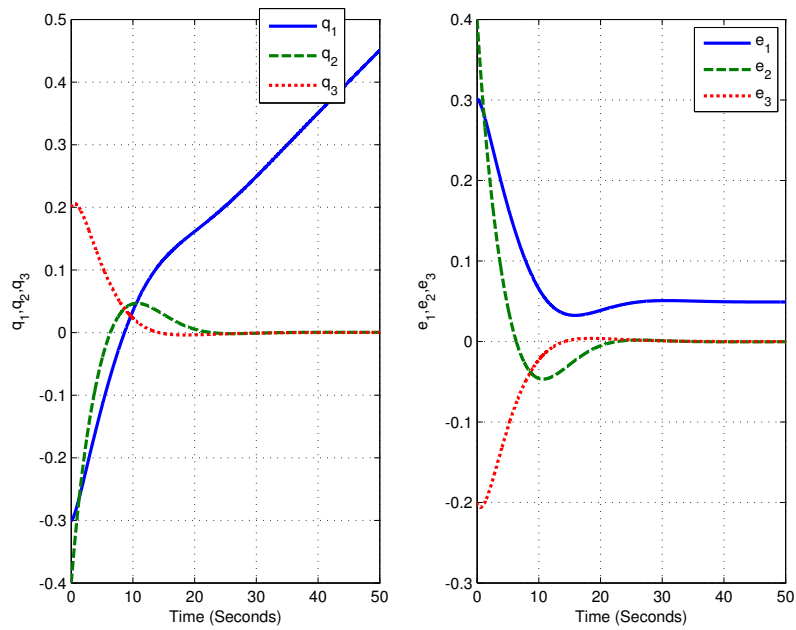


Figure 3.11: Case-III ramp response and error

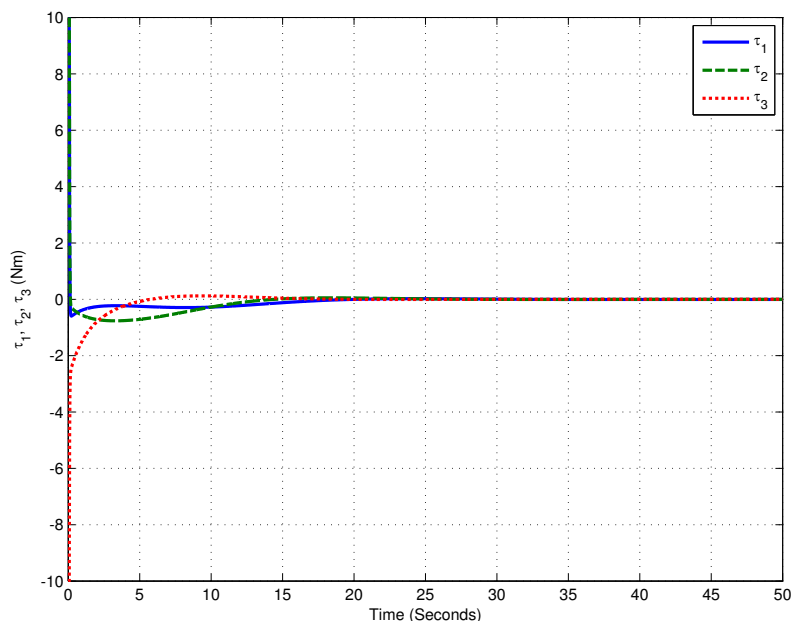


Figure 3.12: Case-III ramp excited control torque input

tuning of controller parameters. In the next subsection, the effectiveness, simplicity and robustness is further demonstrated by reducing the degree of freedom in the control structure and illustrate the stabilization capability by way of simulation results.

3.6.3 A Modified Approach to Lyapunov Based Output Feedback Control Law

In this section the output feedback control law proposed in Section 3.6 is modified by reducing the control freedom in the selection of the controller gains. The modified control law is shown to stabilize the nonlinear attitude model. Global asymptotic stability is proved for the modified approach by a new candidate Lyapunov function. Similar cases of simulations are performed as presented before in Table 3.1. It is illustrated by way of simulations that the modified approach demonstrates very close results to the former approach. In addition to stabilization, time varying attitude acquisition of the nonlinear plant is also demonstrated using the modified output feedback approach.

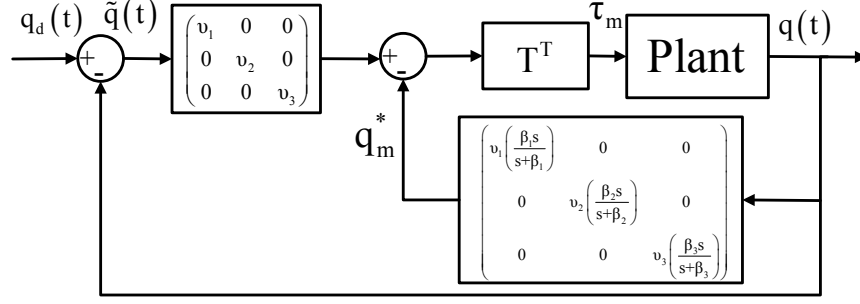


Figure 3.13: Attitude stabilization using modified output feedback

3.6.4 Modified Output Feedback Control Law

The closed loop system for the modified control structure is shown in Fig. 3.13 and the modified control law is chosen to be as follows:

$$\tau_m \triangleq T^T (v\tilde{q} - q_m^*) \equiv T^T v \left\{ q_d - \text{diag} \left[\left(1 + \frac{\beta_1 s}{s + \beta_1} \right), \left(1 + \frac{\beta_2 s}{s + \beta_2} \right), \left(1 + \frac{\beta_3 s}{s + \beta_3} \right) \right] q \right\} \quad (3.41)$$

where

$$v = \text{diag}(v_1, v_2, v_3) \quad (3.42)$$

$$q_m^* = \text{diag}(q_{m1}^*, q_{m2}^*, q_{m3}^*) \quad (3.43)$$

q_{mi}^* is defined as follows, for $i=1,2,3$.

$$q_{mi}^* = v_i \frac{\beta_i s}{s + \beta_i} q_i \quad (3.44)$$

$$q_{mi}^* s + \beta_i q_{mi}^* = v_i \beta_i s q_i \quad (3.45)$$

Taking inverse laplace transform of (3.45)

$$q_{mi}^* = v_i \dot{q}_i - \frac{1}{\beta_i} \dot{q}_{mi}^* \quad (3.46)$$

The control law in (3.41) differs from the previously proposed approach in (3.19) in terms of controller parameters. There are a total of nine tunable parameters in (3.19), whereas, there are only six tunable parameters in (3.41) which are v in (3.42) and β defined as follows:

$$\beta = \text{diag}(\beta_1, \beta_2, \beta_3) \quad (3.47)$$

3.6.5 Stability Analysis

The control law described by (3.41) ensures the global asymptotic stability as delineated by the following theorem.

Theorem III: *For the nonlinear system given in (2.20 & 2.21), the control scheme in (3.41) makes the closed-loop system stable and the tracking error $\tilde{q}(t)$ in (3.18) converges to zero.*

Proof: Define the following non-negative function

$$V_5(\dot{q}, \tilde{q}, q_m^*) = \frac{1}{2} [\dot{q}^T J^* \dot{q} + \tilde{q}^T v \tilde{q} + q_m^{*T} (v\beta)^{-1} q_m^*] \quad (3.48)$$

Differentiating (3.48) with respect to time, we get

$$\begin{aligned} \dot{V}_5 &= \frac{1}{2} [\dot{q}^T J^* \ddot{q} + \dot{q}^T \dot{J}^* \dot{q} + \ddot{q}^T J^* \dot{q}] + \frac{1}{2} [\dot{\tilde{q}}^T v \dot{\tilde{q}} \\ &\quad + \dot{\tilde{q}}^T v \tilde{q}] + \frac{1}{2} [q_m^{*T} (v\beta)^{-1} \dot{q}_m^* + \dot{q}_m^{*T} (v\beta)^{-1} q_m^*] \end{aligned} \quad (3.49)$$

$$\dot{V}_5 = \dot{q}^T J^* \ddot{q} + \frac{1}{2} \dot{q}^T \dot{J}^* \dot{q} + \dot{\tilde{q}}^T v \tilde{q} + q_m^{*T} (v\beta)^{-1} \dot{q}_m^* \quad (3.50)$$

$$\dot{V}_5 = \dot{q}^T (-C^* \dot{q} + P^T \tau_m) + \frac{1}{2} \dot{q}^T \dot{J}^* \dot{q} + \dot{\tilde{q}}^T v \tilde{q} + q_m^{*T} (v\beta)^{-1} \dot{q}_m^* \quad (3.51)$$

$$\dot{V}_5 = \dot{q}^T \left[\frac{1}{2} J^* - C^* \right] \dot{q} + \dot{q}^T P^T \tau_m + \check{q}^T v \tilde{q} + q_m^{*T} (v\beta)^{-1} \dot{q}_m^* \quad (3.52)$$

By the property of skew symmetry from (3.5) and substituting the control law from (3.41), (3.52) can be written as follows

$$\dot{V}_5 = \dot{q}^T P^T T^T (v\tilde{q} - q_m^*) + \check{q}^T v \tilde{q} + q_m^{*T} (v\beta)^{-1} \dot{q}_m^* \quad (3.53)$$

$$\dot{V}_5 = \dot{q}^T v \tilde{q} - \dot{q}^T q_m^* + \check{q}^T v \tilde{q} + q_m^{*T} (v\beta)^{-1} \dot{q}_m^* \quad (3.54)$$

$$P^T T^T = I, \quad \dot{\check{q}} = -\dot{q}$$

$$\dot{V}_5 = -\dot{q}^T q_m^* + q_m^{*T} (v\beta)^{-1} \dot{q}_m^* \quad (3.55)$$

Substituting \dot{q}_m^* from (3.46) in (3.55) we get

$$\dot{V}_5 = -\dot{q}^T q_m^* + q_m^{*T} (v\beta)^{-1} (v\beta \dot{q} - \beta q_m^*) \quad (3.56)$$

$$\dot{V}_5 = -q_m^{*T} (v\beta)^{-1} \beta q_m^* \leq 0 \quad (3.57)$$

The time derivative of the non-negative function is negative semi-definite for all nonzero values of q_m^* and v by invoking the invariant set theorem [52]. This shows that the nonlinear attitude model can be globally stabilized using the proposed control structure by selection of just six gains which can be any positive values instead of nine gains as discussed earlier. The stabilization results in the simulation results section illustrate this fact more clearly.

3.6.6 Attitude Tracking System Design

The attitude tracking control system is shown in Fig. 3.14. The desired attitude is expressed in terms of roll (ϕ), pitch (θ) and yaw (ψ) angles in degrees. The Euler angles are transformed to the DCM using (3-2-1) Euler angle sequence wherein the z, y & x

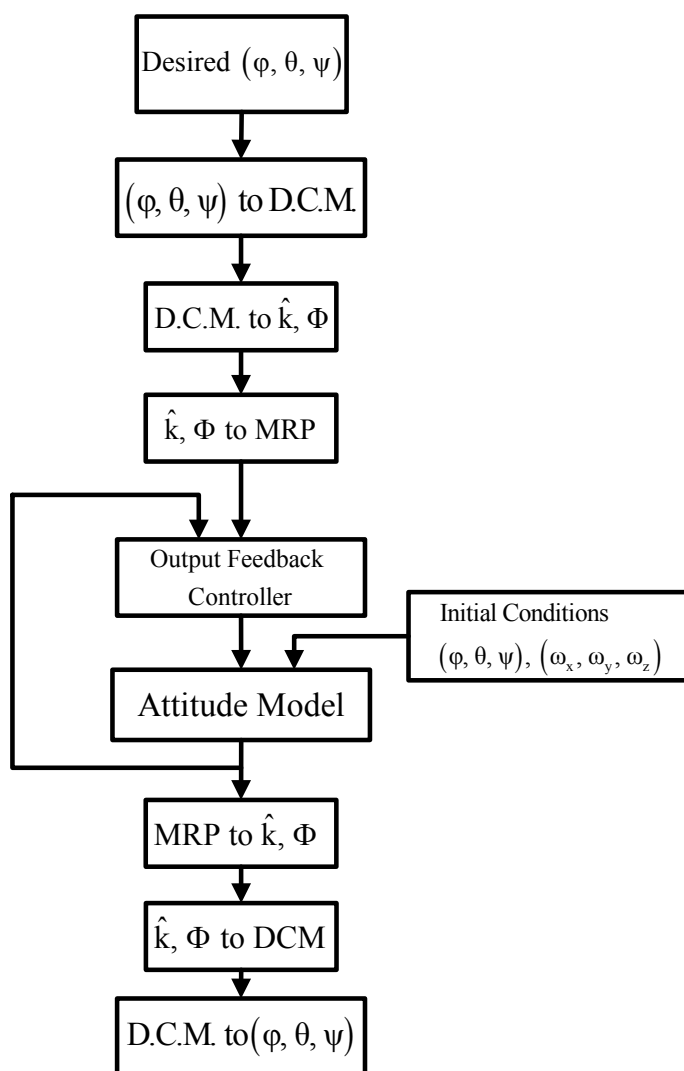


Figure 3.14: Attitude tracking control system

axis are rotated about an angle of ψ, θ & ϕ degrees. The resulting DCM is given by the relationship stated in (2.5). The Euler eigenangle, Φ and Euler eigenaxis, \hat{k} are calculated from the DCM using the relationships discussed in (2.9 & 2.10). The MRP's, q_x, q_y & q_z are calculated from the Euler eigenangle, Φ and Euler eigenaxis, \hat{k} using the relationship stated in (2.18).

The attitude model consisting of the Euler's equations of rotational dynamics and the MRP based kinematic differential equations described in (2.20 & 2.21) is modeled in simulink as shown in Fig. 2.3. The attitude model consists of two integrators blocks. The first block calculates the angular velocity vector, ω with initial conditions specified in degrees/second. The second integrator calculates the attitude of the rigid body with

initial attitude specified in terms of roll, pitch and yaw angles expressed in degrees. The control torque is applied in the Euler's equations block and the kinematics equations block calculates the plant's output. The output feedback controller schematic was shown in Fig. 3.13 with the control law stated in (3.41). The regulated attitude from the attitude model is transformed from MRP's to roll, pitch and yaw angles using the inverse transformations from MRP to Euler eigenaxis and eigenangle and DCM respectively.

3.6.7 Simulation Results

The following initial conditions taken from [7] are chosen for the simulations of the attitude model given in (2.20 & 2.21) and the proposed control law given in (3.41).

$$\omega(0) = [11.45 \quad 11.45 \quad 11.45]^T \text{ rad/sec} \quad (3.58)$$

$$\begin{aligned} \phi &= 10^\circ \\ \theta &= 8^\circ \\ \psi &= 5^\circ \end{aligned} \quad (3.59)$$

The inertia matrices are given by (2.32) and (3.39). The selection of the six positive gains namely, ν in (3.42) and β in (5.29) to stabilize the nonlinear plant can be any positive values as far as convergence is concerned, as shown in Theorem III in Section 3.6.3. Since there are no specific design requirements with respect to each individual channel in this example, we choose for simplicity the same values for the controllers on the three channels. The controller parameters are varied over the range from 0 to 100. By trial and error, the controller values shown in Table 3.2 are chosen to illustrate the results. All the four cases shown in Table 3.2 show satisfactory step response in terms of rise time, overshoot and settling time, though different in different channels and the four case plots explain the effect of gain variation on the plant output. The model under

study is nonlinear and the output feedback controller gains in closed-loop are selected on trial and error. A more formal approach could have been considered if the model was linear. Particle swarm optimization algorithm is used as a tool to infer the optimal controller gains based on a cost function which minimizes the absolute value of tracking error and is discussed in the next section.

Table 3.2: Controller gains and inertia matrix selection - Modified output feedback approach

Cases	v	β	Inertia Matrix
Case-I	1	2	J
Case-II	10	20	J
Case-III	50	100	J
Case-IV	50	100	h_b

Fig. 3.15 shows the step response for case-I and the required controller effort is shown in Fig. 3.16. Likewise the step responses for case-II and case-III are shown in Figs. (3.17 & 3.19) and the required controller effort is shown in Figs. (3.18 & 3.20). Fig. 3.21 shows the step response for case-IV which has same controller gains as in case-III with a large variation in the inertia matrix from J to h_b . The respective control signal in case-IV is shown in Fig. 3.22. Case-IV step response shows the robustness of the modified control law. The step response of the attitude model is satisfactory even when the inertia matrix is varied to large diagonal values keeping the controller parameters unchanged.

The desired attitude is selected to be time varying and is expressed in terms of Euler angles as follows:

$$[\phi_1, \theta_1, \psi_1 = 20^\circ, 15^\circ, 10^\circ]^T \text{ for time } t = (0 - 200) \text{ sec}$$

$$[\phi_2, \theta_2, \psi_2 = 30^\circ, 25^\circ, 20^\circ]^T \text{ for time } t = (200 - 400) \text{ sec}$$

$$[\phi_3, \theta_3, \psi_3 = 45^\circ, 35^\circ, 30^\circ]^T \text{ for time } t = (400 - 600) \text{ sec}$$

Figs. (3.23 & 3.24) show the case-III attitude tracking and the observed error. The respective control signal is shown in Fig. 3.25. Figs. (3.26 & 3.27) show the attitude tracking and the observed error for case-IV and the respective controller effort is shown in Fig. 3.28

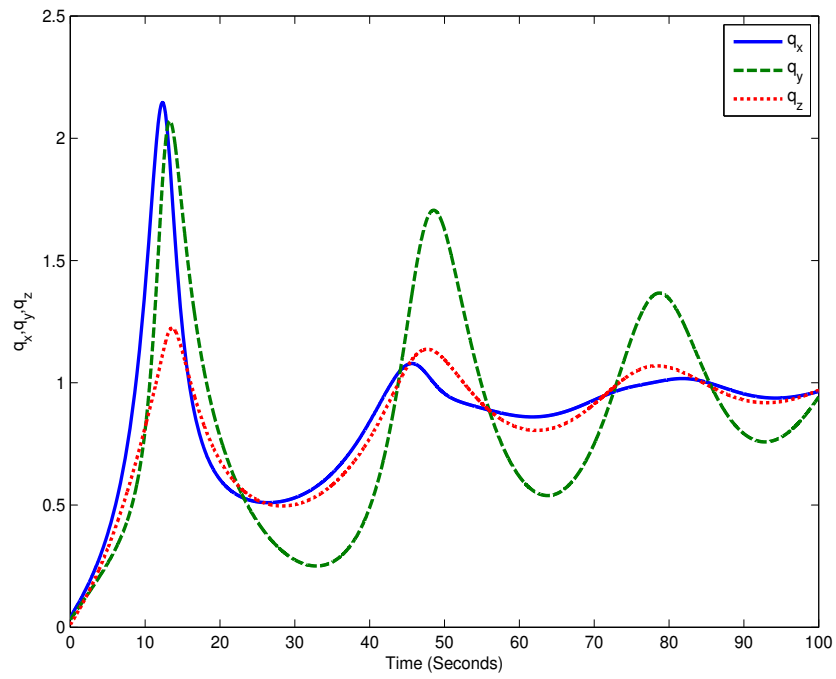


Figure 3.15: Case-I attitude stabilization

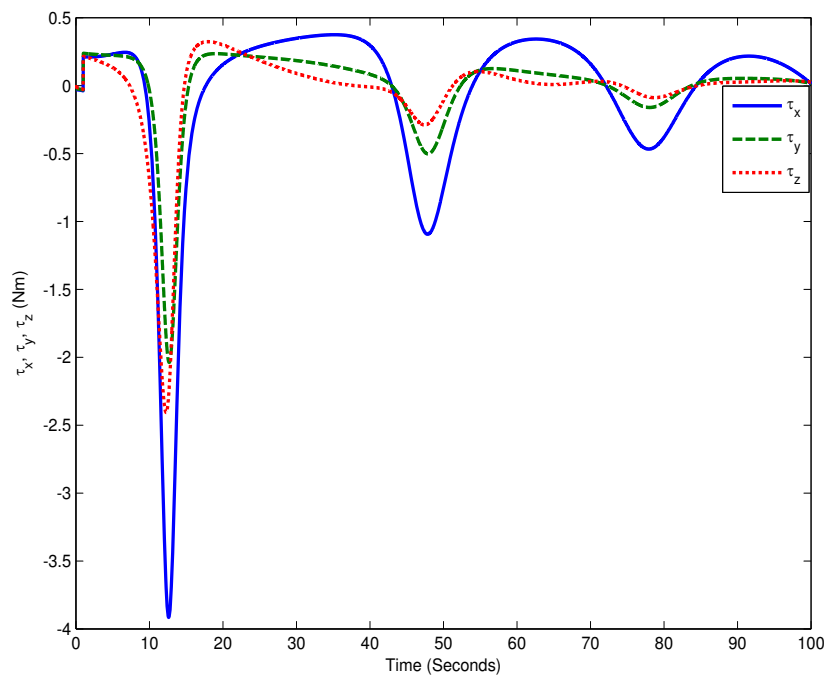


Figure 3.16: Case-I control torque input

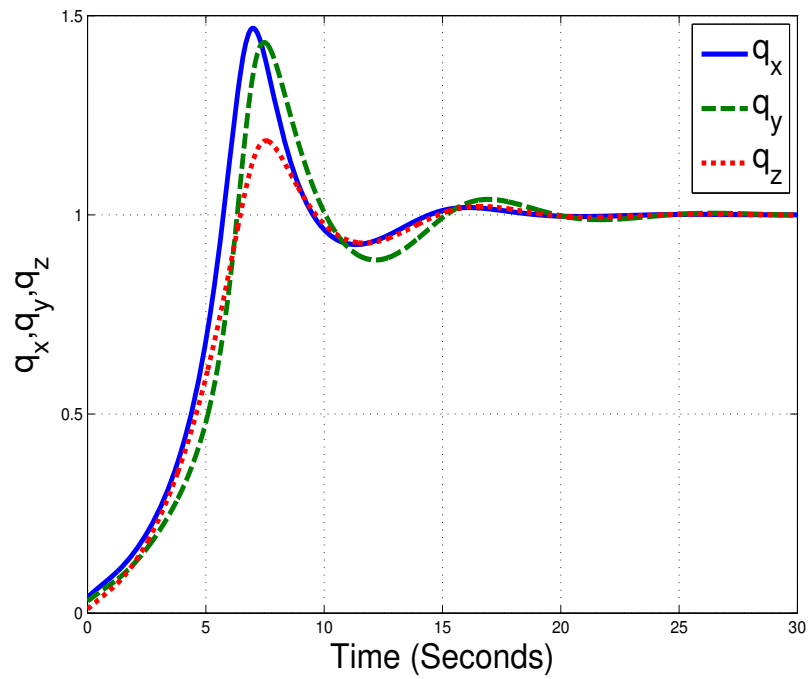


Figure 3.17: Case-II attitude stabilization

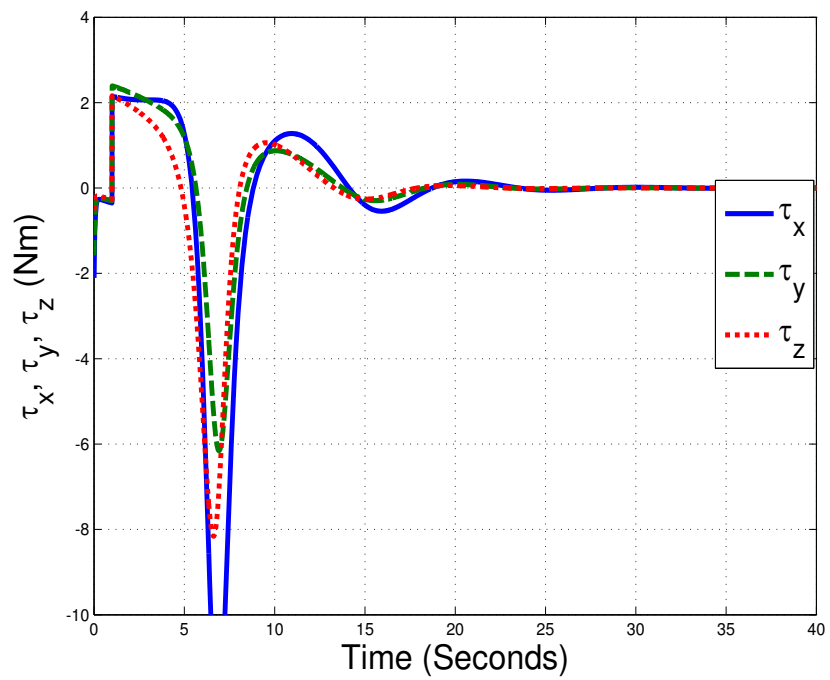


Figure 3.18: Case-II control torque input

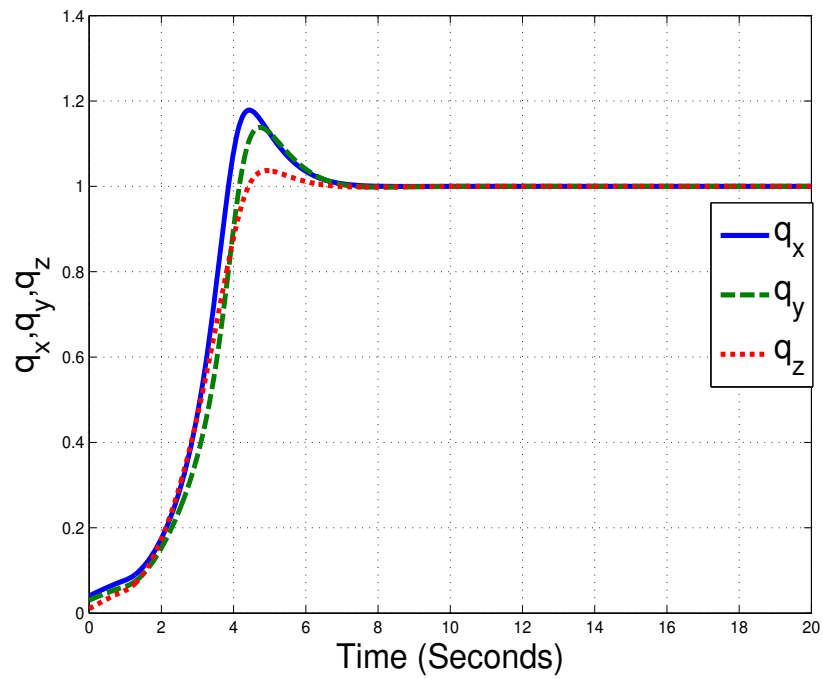


Figure 3.19: Case-III attitude stabilization

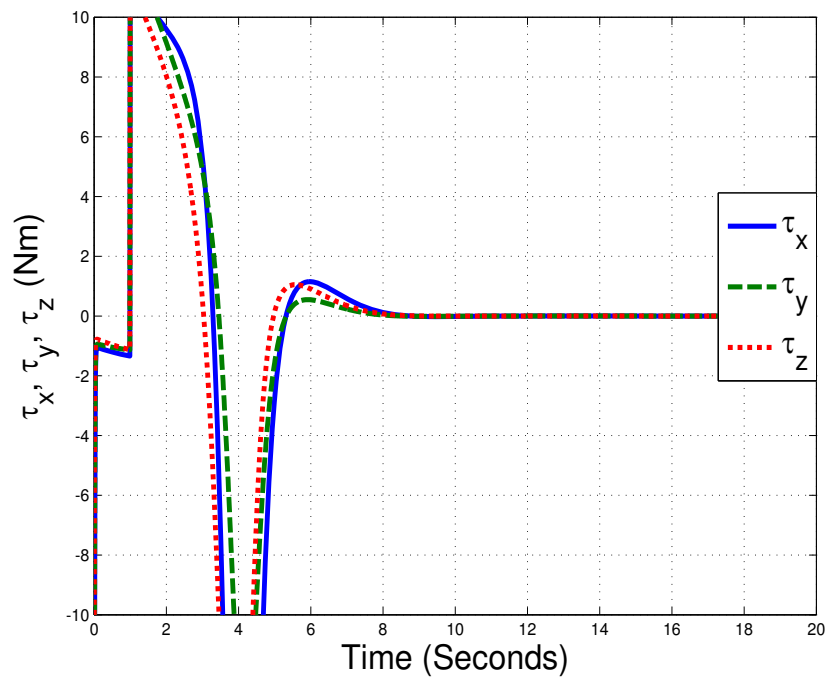


Figure 3.20: Case-III control torque input

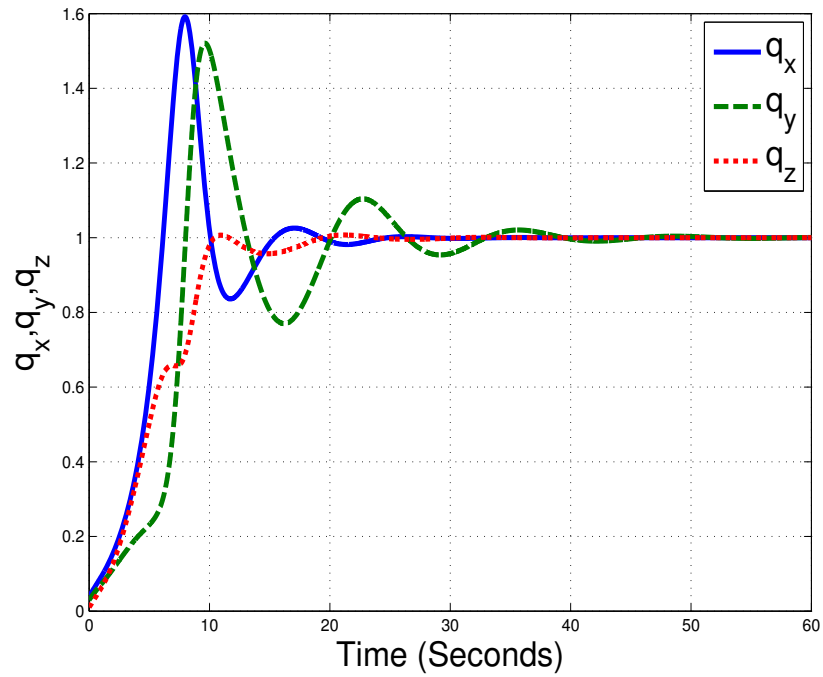


Figure 3.21: Case-IV attitude stabilization

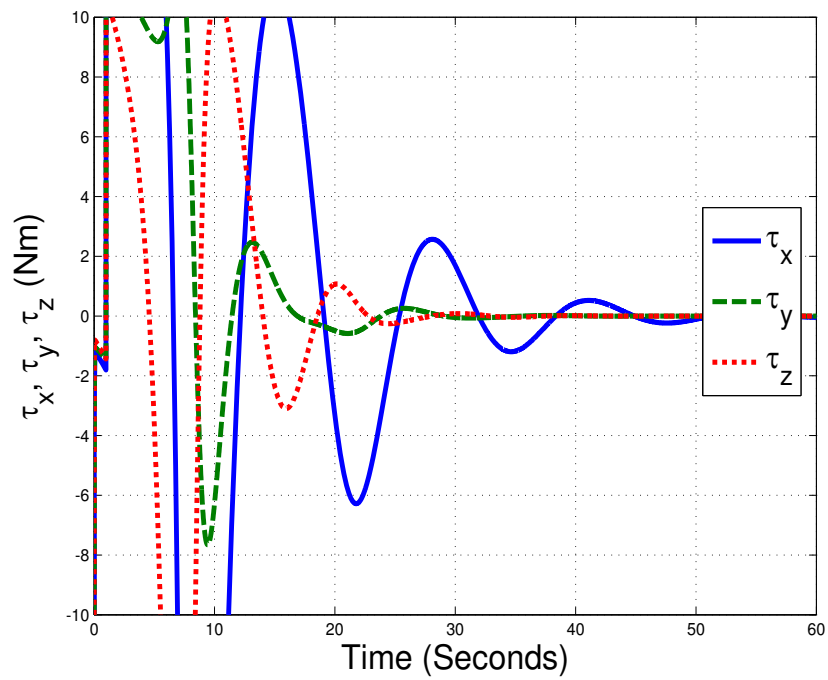


Figure 3.22: Case-IV control torque input

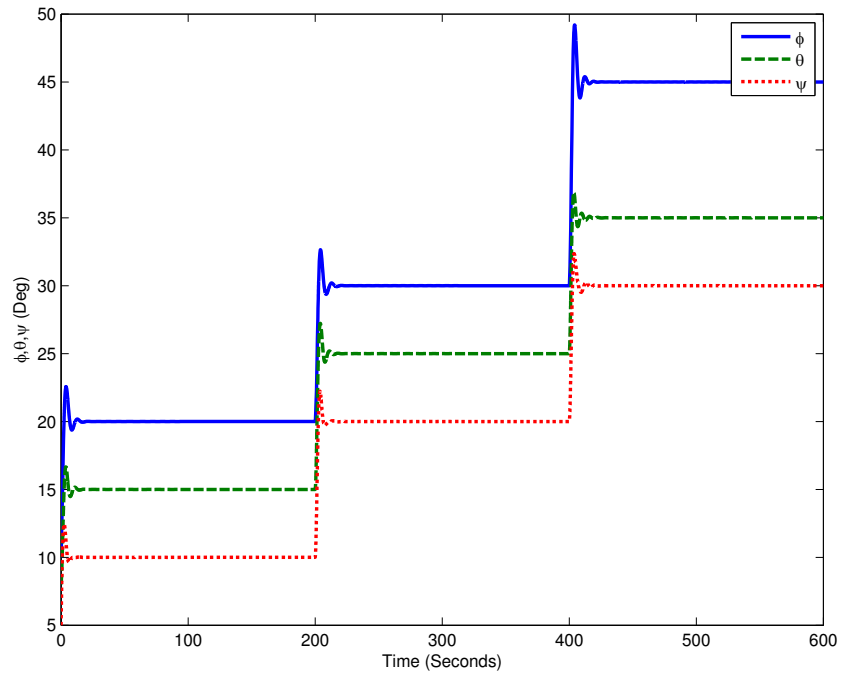


Figure 3.23: Case-III attitude tracking

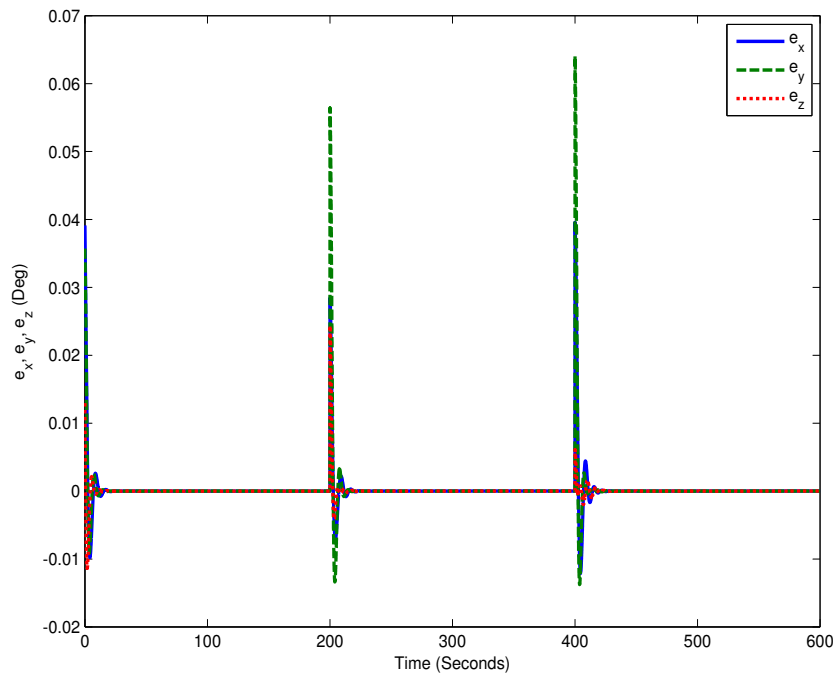


Figure 3.24: Case-III attitude tracking error

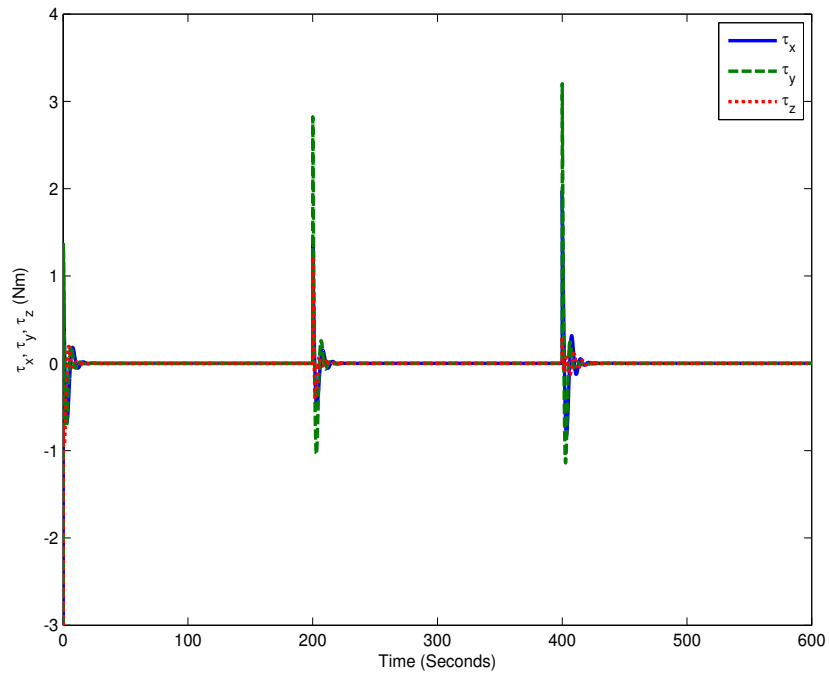


Figure 3.25: Case-III attitude tracking control torque input

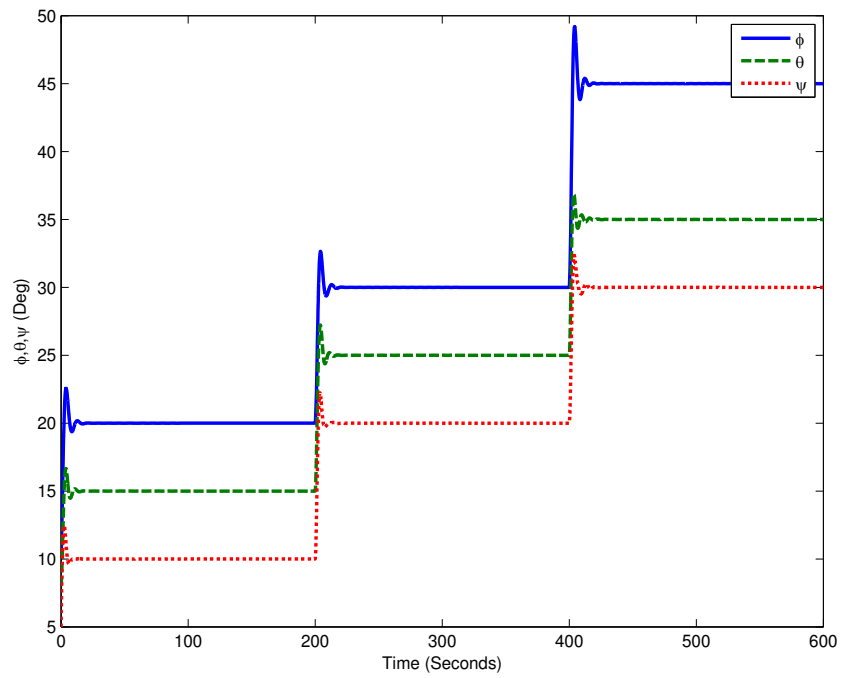


Figure 3.26: Case-IV attitude tracking

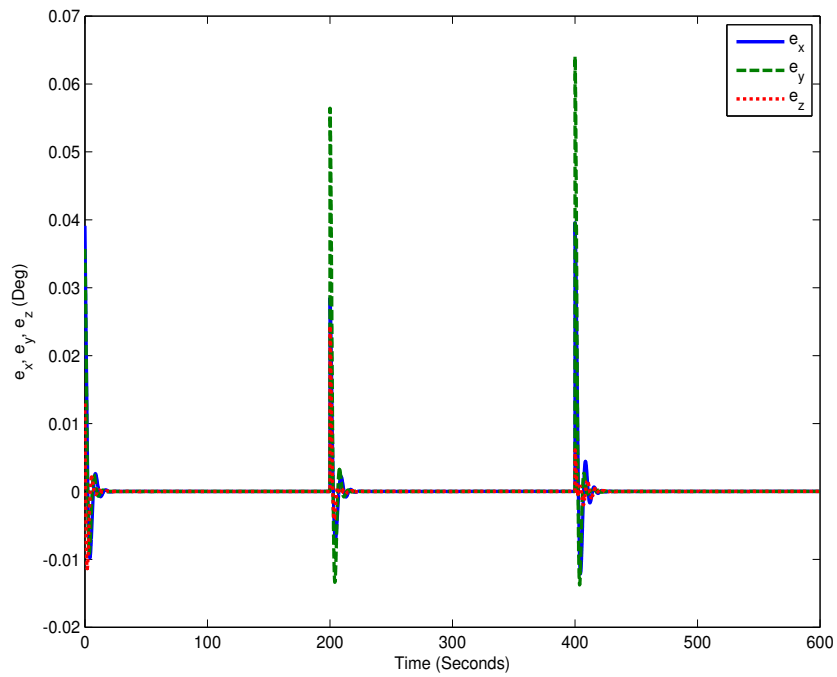


Figure 3.27: Case-IV attitude tracking error

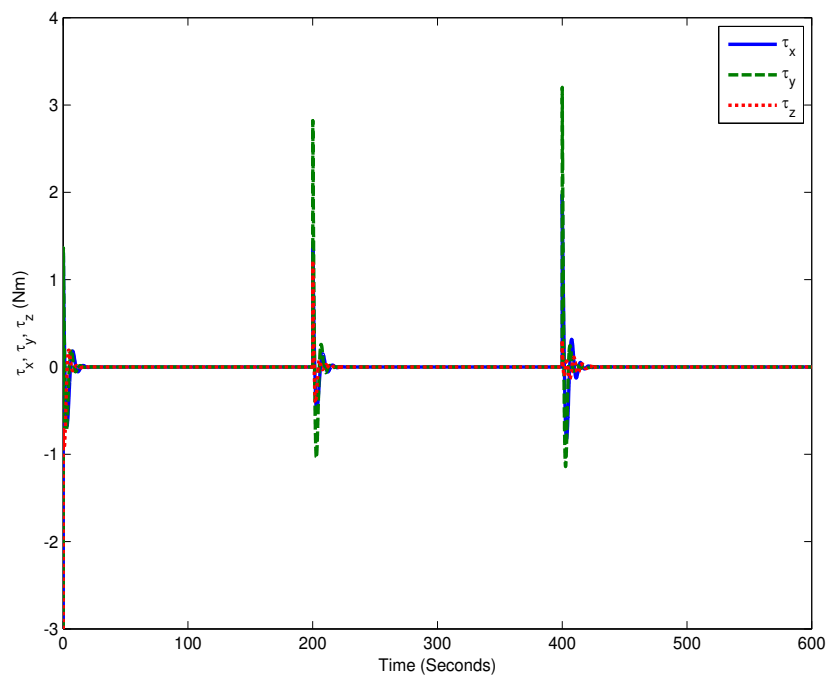


Figure 3.28: Case-IV attitude tracking control torque input

3.7 Output Feedback Controller Tuning using PSO

In this section, a recently introduced evolutionary algorithm based optimal design approach is presented. The output feedback control law proposed in Section 3.6 involves a total of nine parameters to be selected in the control law that drastically influences the performance of the controlled system. The fact that there is no straightforward correlation between these parameters and the performance of the system may impede its utilization. In this section, the use of PSO algorithm as a tool to infer the best parameters is presented. The PSO optimization is performed in time domain using a simple cost function which minimizes the absolute value of the tracking error while varying the controller gains. Simulation results are illustrated to show the effectiveness of the proposed approach.

PSO has been proposed and introduced in the literature not long ago [26]. This technique combines social psychology principles in socio-cognitive human agents and evolutionary computations. PSO has been motivated by the behavior of organisms, such as fish schooling and birds flocking. Generally, PSO is characterized as a simple concept, easy to implement, and computationally efficient. Unlike the other heuristic techniques, PSO has a flexible and well-balanced mechanism to enhance the global and local exploration abilities. Therefore, it has been extensively used in engineering as an efficient optimization tool as in [3], where the author uses it in an electrical engineering context to optimize the design of a power system stabilizer.

Similar to evolutionary algorithms, the PSO technique conducts searches using a population of particles, corresponding to individuals. Each particle represents a candidate solution to the problem at hand. In a PSO system, particles change their positions by flying around in a multidimensional search space until a relatively stationary position has been encountered, or until a desired requirement is achieved. There are numerous advantages of PSO over conventional methods including [3]:

- PSO inherently features parallel search which makes it less vulnerable to undesired solutions known as local minima.

- PSO does not require the cost function to be differentiable, and thus extends the optimization criteria formulation. Thanks to the relaxed performance index that gives information for guiding the search, PSO is relieved from conventional constraints resulting from conformity assumptions.
- PSO is a stochastic optimization method and thus utilizes probabilistic transition rules in contrast with deterministic rules. Stochastic exploration and communication of the swarm is a clear advantage for searching complicated and uncertain spaces.
- PSO has the ability to control the balance between global and local exploration of the search space unlike the other heuristics like Genetic Algorithm (GA). This alleviates premature convergence problems and enhances the search.
- PSO is computationally lighter than many evolutionary based optimization algorithms like GA. It has even been implemented in some real-time applications for process industry [38], [59] & [54].
- PSO has been used in parametric optimization of a flexible satellite controller in [23]. Additionally, it has been used in the parametric design of a radial basis function neural network based sliding mode controller for attitude tracking in [14] and it was shown that PSO provided strong global search ability and convergent performance.
- PSO gives consistent solutions regardless of the initial population selection. The optimal solution being not affected by the initial guess is a desired practical feature.

3.7.1 Preliminary

Before stating the algorithm it is important to understand the jargon used in the literature. For the thesis to be self-content we can recall some definitions [3]:

- A particle $X(t)$ is a temporary candidate solution. It is a real vector of dimension m where m is the number of parameters to be optimized. The j^{th} particle can be described as $X_j(t) = [x_{j1}, x_{j2} \dots x_{jm}]$, where x 's are the optimized parameters and x_{jk} is the position of the j^{th} particle with respect to the k^{th} dimension (i.e., the value of the k^{th} "optimized" parameter in the j^{th} candidate solution).
- A population represents a set of n particles at time t (i.e. $pop(t) = [X_1(t), X_2(t) \dots X_n(t)]^T$).
- A swarm is a population of moving particles that tends to cluster together while each particle seems to be moving in a random direction.
- Each particle is characterized by a velocity. The moving particles velocity $V(t)$ is a real vector of dimension m . At time t the j^{th} particle velocity $V_j(t)$ consists of $V_j(t) = [v_{j1}(t), v_{j2}(t) \dots v_{jm}(t)]$, where v_{jk} is the velocity of the j^{th} particle with respect to the k^{th} dimension.
- The inertia weight $w(t)$ is a parameter that controls the impact of the previous velocities on the current velocity. Hence, it influences the trade off between the global and local exploration abilities of the particles. For initial stages of the search process, a large inertia weight to enhance the global exploration is recommended, and for later stages, the inertia weight is reduced for better local exploration.
- The decrement function for decreasing the inertia weight given as $w(t) = dw(t-1)$, where d is a decrement constant smaller than but close to 1, is used in this work.
- Individual best $X^*(t)$, as a particle moves through the search space, it compares its fitness value at the current position to the best fitness value it has ever attained at any time up to the current time. The best position that is associated with the best fitness encountered so far is called the individual best $X^*(t)$. For each particle in the swarm, $X^*(t)$ can be determined and updated during the search. In a minimization problem with objective function J , the individual best of the j^{th}

particle $X_j^*(t)$ is determined so that $J(X_j^*(t)) \leq J(X_j(\tau)), \forall \tau \leq t$. For simplicity, define $J_j^* = J(X_j^*(t))$. For the j^{th} particle, individual best can be expressed as $X_j^*(t) = [x_{j1}^*, x_{j2}^* \dots x_{jm}^*]$.

- The global best $X^{**}(t)$ is the best position among all of the individual best positions achieved so far. Hence, the global best can be determined such that $J(X_j^{**}(t)) \leq J(X_j^*(t)), j = 1, 2 \dots n$. For simplicity, define $J^{**} = J(X^{**}(t))$.
- The stopping condition is the event that triggers the end of the optimization process. For our case the search will terminate either if the number of iterations since the last change of the best solution is greater than a prespecified number or the number of iterations reaches the maximum allowable limit or when the objective function is achieved.

The particle velocity in the k^{th} dimension is limited by some maximum value, v_k^{max} . This limit enhances the local exploration of the problem space. The maximum velocity in the k^{th} dimension is characterized by the range of the k^{th} optimized parameter and is given by:

$$v_k^{max} = \frac{x_k^{max} - x_k^{min}}{N} \quad (3.60)$$

where N is a chosen number of intervals in the k^{th} dimension.

3.7.2 PSO algorithm

In this section we can thus summarize the PSO algorithm [3]:

1. Initialization: at time $t = 0$ generate n random particles $\{X_j(0), j = 1, 2 \dots n\}$, where $x_{jk}(0)$ is generated by randomly selecting a value with uniform probability over the k^{th} optimized parameter search space $[x_k^{min}, x_k^{max}]$. Similarly, it is possible to generate randomly initial velocities of all particles $\{V_j(0), j = 1, 2 \dots n\}$, where $v_{jk}(0)$ is generated by randomly selecting a value with uniform probability over the

k^{th} dimension $[-v_k^{max}, v_k^{max}]$. Each particle in the initial population is evaluated using the objective function J . For each particle, set $X_j^*(0) = X_j(0)$ and $J_j^* = J_j$, $j = 1, 2 \dots n$. Search for the best value of the objective function J_{best} . Once this is found set the particle associated with J_{best} as the global $X^{**}(0)$ with an objective function of J^{**} . Set the initial value of the inertia weight $w(0)$.

2. Time increment: update time by $t = t + 1$.
3. Weight update: Update the inertia weight according to $w(t) = dw(t - 1)$.
4. Velocity update: Using the global best and individual best, the j^{th} particle velocity in the k^{th} dimension is updated according to the following equation:

$$\begin{aligned}
 v_{jk}(t) = & w(t)v_{jk}(t - 1) \\
 & + c_1 r_1 [x_{jk}^*(t - 1) - x_{jk}(t - 1)] \\
 & + c_2 r_2 [x_{jk}^{**}(t - 1) - x_{jk}(t - 1)]
 \end{aligned}
 \tag{3.61}$$

where c_1 and c_2 are positive constants and r_1 and r_2 are uniformly distributed random numbers in $[0, 1]$. Check the velocity limits. If the velocity violated its limit, it must be set at its proper limit. It is worth mentioning that the second term represents the cognitive part of PSO where the particle changes its velocity based on its own thinking and memory. The third term represents the social part of PSO where the particle changes its velocity based on the psychological adaptation of knowledge.

5. Position update: Based on the updated velocities, each particle changes its position according to the following equation:

$$x_{jk}(t) = v_{jk}(t) + x_{jk}(t - 1) \quad (3.61)$$

6. Individual best update: each particle is evaluated according to updated position. If $J_j < J_j^*$, $j = 1, 2 \dots n$ then update individual best by $X_j^*(t) = X_j(t)$ and $J_j^* = J_j$, otherwise go to the following step.
7. Global best update: Search for the minimum value J_{min} among J_j^* , where min is the index of the particle with minimum objective function value, i.e. . If $J_{min} < J^{**}$ then update the global best as $X^{**} = X_{min}(t)$, and $J^{**} = J_{min}$, otherwise go to next step.
8. End check: If one of the stopping criteria is satisfied, then stop, else go to step 2.

The loss function intuitively suggested for optimizing the parameters s_p, s_d & α of the controller is defined as follows:

$$\min_{s_p, s_d, \alpha} J = \min_{s_p, s_d, \alpha} \int_0^{t_f} |q_d(t) - q(t)| dt \quad (3.62)$$

where $q_d(t)$ is the reference signal and $q(t)$ is the output signal.

3.7.3 Parameter Determination and Simulation Results

The PSO algorithm was run several times showing consistent results despite the random choice of the initial solution. However, though minor fluctuations in the final value for the loss function have been observed. Table 3.3 summarizes the parameters that were finally selected for the PSO algorithm showing the particles (P), generations (G), inertia weight (w_0) and decreasing factor (d). It is common practice to start with relatively large values for the inertia weight so as to enhance the exploration capability and then to limit it in order to favor local search.

Table 3.3: Parameters for PSO algorithm

P	G	w_0	d
30	100	0.8	0.8

The initial conditions were taken as

$$\begin{bmatrix} q_1(0) = -0.3 \\ q_2(0) = -0.4 \\ q_3(0) = 0.2 \end{bmatrix} \quad (3.63)$$

$$\begin{bmatrix} \omega_1(0) = 0.2 \\ \omega_2(0) = 0.2 \\ \omega_3(0) = 0.2 \end{bmatrix} \text{ rad/sec} \quad (3.64)$$

The inertia matrix for the spacecraft model is selected to be

$$h = \begin{pmatrix} 20 & 1.2 & 0.9 \\ 1.2 & 17 & 1.4 \\ 0.9 & 1.4 & 15 \end{pmatrix} \text{ kgm}^2 \quad (3.65)$$

The optimal values of the controller parameters were found to be

$s_p = 42.5455$, $s_d = 121.8785$, & $\alpha = 61.7203$ with an associated cost of $J = 47.8649$. Fig. 3.29 shows the learning curve of the PSO algorithm where we notice that convergence is attained after 130 generations and that there is relatively minor cost difference after 100 iterations.

The gains in Table. 3.1 were selected by trial and error, ranging from very small values shown in case-I to considerably large values as seen in case-III. However, from the simulations results in Section 3.6.2 it can be inferred that the minimum time to achieve zero steady state error was in case-III which was approximately 25 seconds whereas in the case of PSO based tuning steady state is achieved in 12 seconds. Figs. (3.30 & 3.31) shows the step response and the respective error of the stabilized non-linear plant,

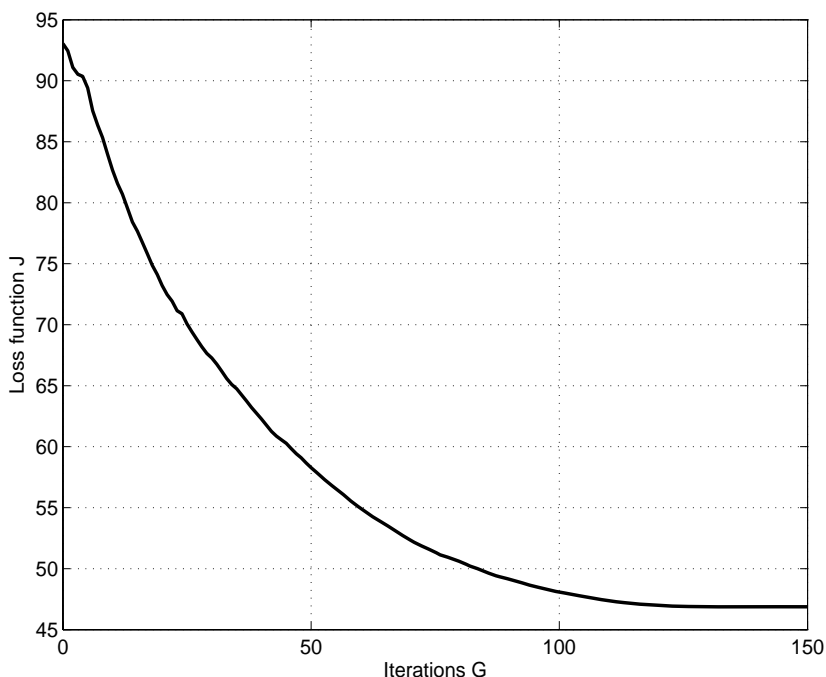


Figure 3.29: Learning curve of PSO algorithm

Fig. 3.32 shows the respective angular velocity plot and Fig. 3.33 shows the required controller effort for the plant stabilization. Figs. (3.30 & 3.32) show that the attitude and the angular velocity plot start with their assumed initial conditions and reach a steady state value in 12 seconds.

3.8 H_∞ Controllers Design of Spacecraft Attitude

In this section, we analyze two robust control approaches namely H_∞ Loop-shaping and H_∞ Mixed sensitivity approaches for controlling the spacecraft attitude and compare their results to the proposed output feedback approach presented in Section 3.6. The linearized spacecraft attitude model in terms of Euler's equation and MRP's was presented in Section 2.10 of Chapter 2 given as

$$G_{mrp} = \left[\begin{array}{c|c} A_{mrp} & B_{mrp} \\ \hline C_{mrp} & D_{mrp} \end{array} \right] \quad (3.66)$$

where A_{mrp} , B_{mrp} , C_{mrp} and D_{mrp} are stated in (2.29-2.31).

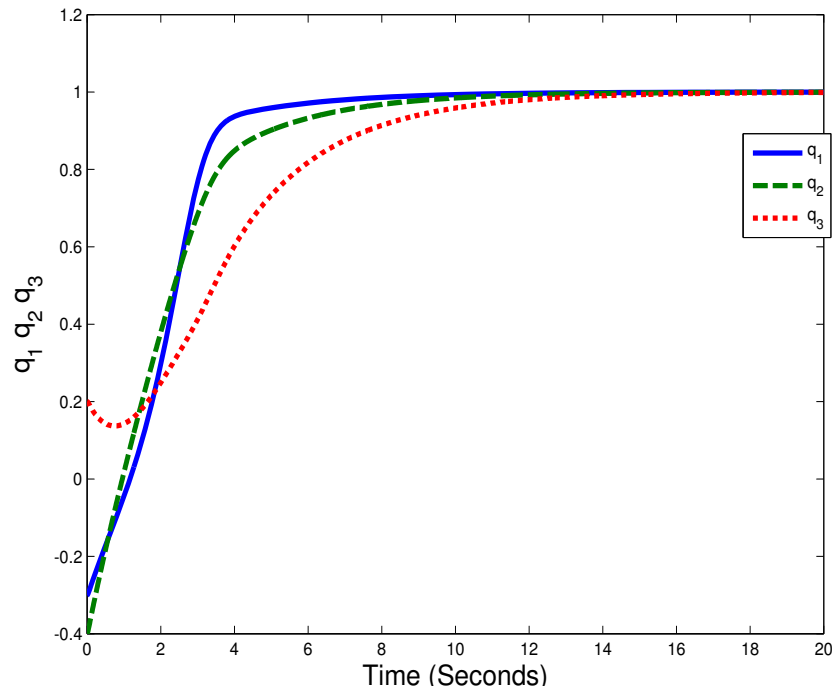


Figure 3.30: Step response of the stabilized N.L. plant

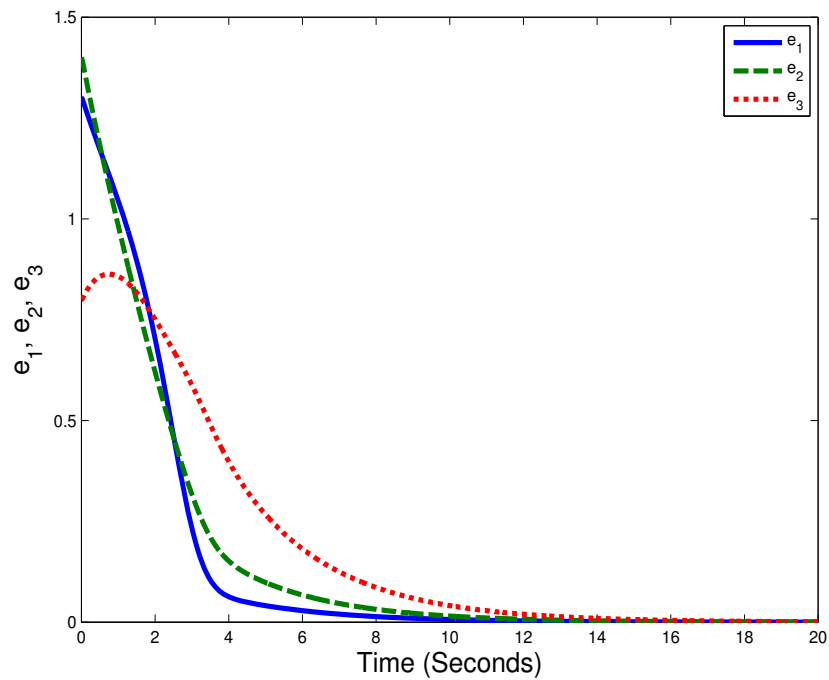


Figure 3.31: Step response error

3.8.1 H_∞ Loop-Shaping Controller Design

The H_∞ Loop Shaping Design Procedure (LSDP) was proposed by [33]. In this procedure we shape the open loop response of the plant. Since, we are dealing with a MIMO

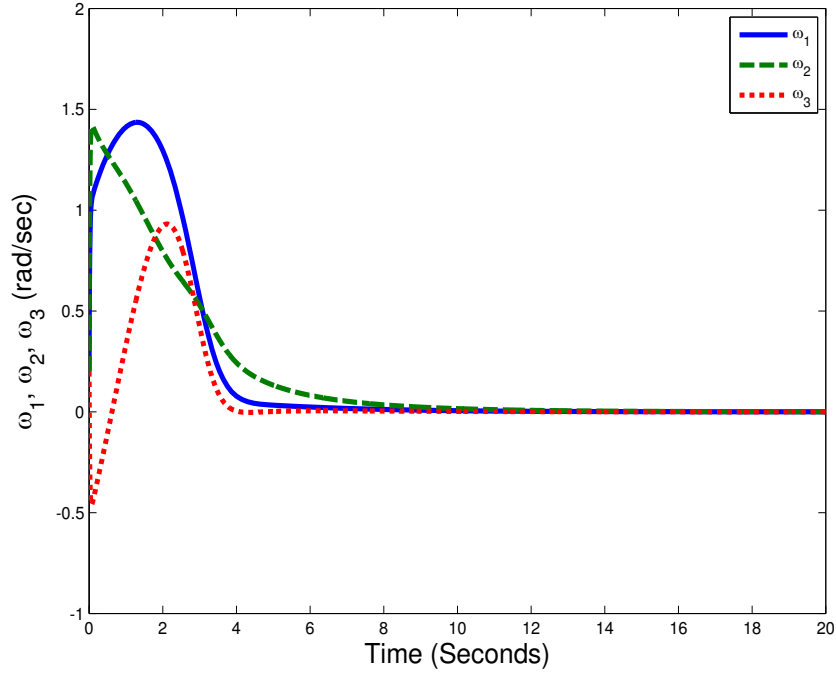


Figure 3.32: Angular velocity plot

system, the singular values of the plant are preferred over the eigenvalues as they give better information about the gains of the plant and the plant directions [50]. In the loop-shaping procedure the plant is augmented with pre and post-compensators to give a desired shape to the singular values of the open loop frequency response of the system. The loop-shaping design procedure for the linearized plant stated in (3.66) is carried out in the following steps.

- 1) Using a pre-compensator, W_1 as depicted in Fig. 3.34 the singular values of the nominal system, G_{mrp} are modified to give a desired loop-shape. We choose the desired loop-shape such that the singular values of the open loop gain have a gain cross-over frequency of 0.7 rad/second [47]. W_1 is a MIMO stable minimum phase shaping pre-filter. The shaped plant is $G_s = G_{mrp}W_1$.
- 2) A feedback controller, K_s is synthesized using normalized co-prime factorization of the shaped plant, G_s to compute an optimal loop-shaping controller, $K_{LS} = W_1K_s$.
- 3) The synthesized controller, K_{LS} is of 19th order and satisfies the desired loop shaping requirement and is tested on the linear as well as the nonlinear system with a step input. The simulation results are illustrated in Section 3.8.3.

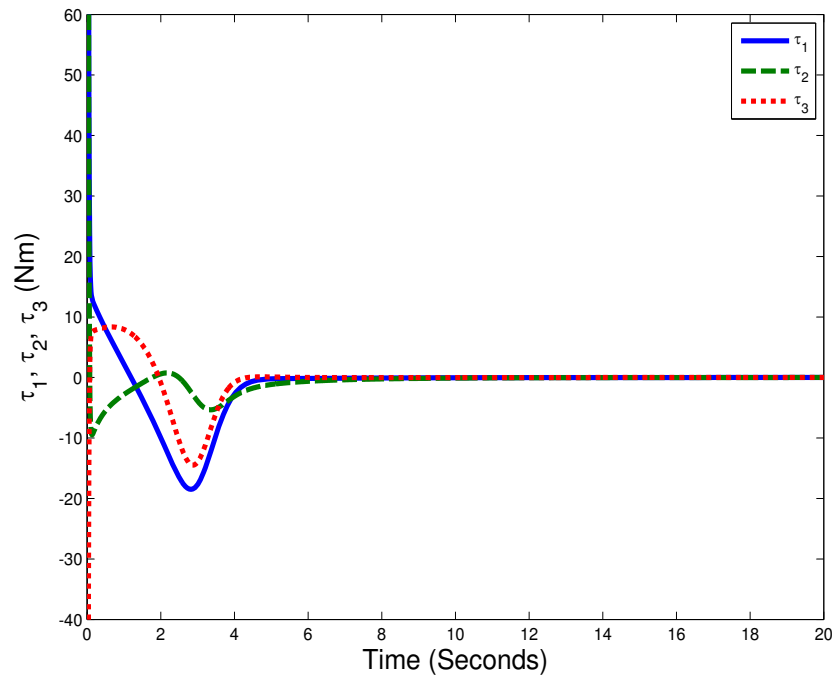
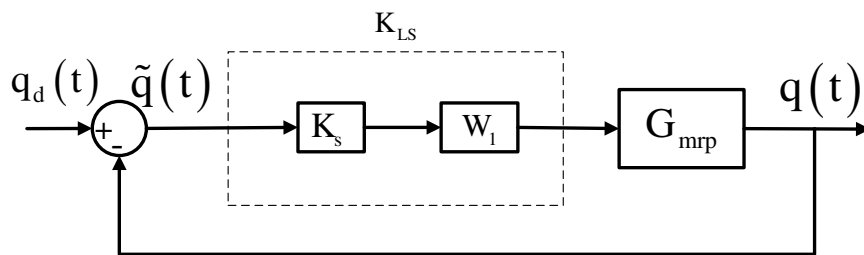


Figure 3.33: Control torque input

Figure 3.34: H_∞ Loop shaping controller design

3.8.2 H_∞ Mixed Sensitivity Controller Design

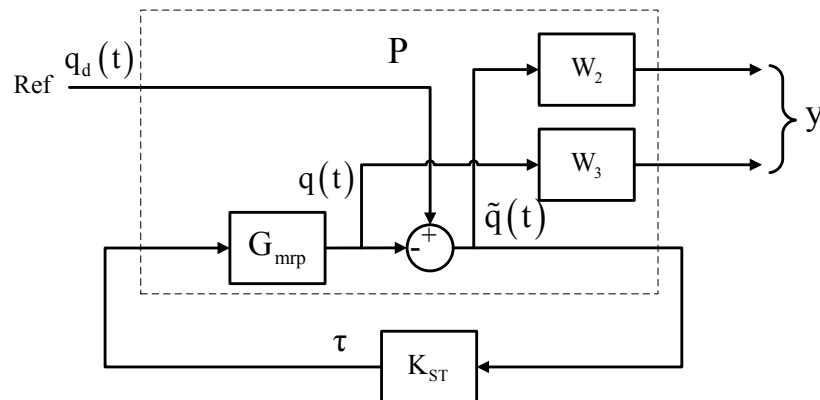


Figure 3.35: S/T Mixed sensitivity controller design

In the H_∞ mixed sensitivity approach an optimal controller, K_{ST} is synthesized for the plant, G_{mrp} by adding weighting functions to the sensitivity transfer function, $\mathbb{S} \triangleq (I + G_{mrp}K_{ST})^{-1}$ and the complementary sensitivity transfer function, $\mathbb{T} \triangleq (I + G_{mrp}K_{ST})^{-1}G_{mrp}K_{ST}$ of the closed-loop system. These weights contain the design goals and the extended plant is denoted by P as shown in Fig. 3.35. The weighting function W_2 has the control error $\tilde{q}(t) = \mathbb{S}q_d(t)$ as the input and, similarly the input to the weighting function, W_3 is the measurement $q(t) = \mathbb{T}q_d(t)$. The extended plant is given as follows [50]:

$$P = \begin{pmatrix} W_2 & -W_2G \\ 0 & W_3G \\ I & -G \end{pmatrix} \quad (3.67)$$

The closed-loop transfer function of the extended plant is given as follows:

$$T_{y,q_d} \triangleq \begin{bmatrix} W_2\mathbb{S} \\ W_3\mathbb{T} \end{bmatrix} \quad (3.68)$$

This approach of using a combination of sensitivity, \mathbb{S} and complementary sensitivity, \mathbb{T} is called a stacking approach and has the advantage of specifying a lower bound given by $W_2\mathbb{S}$ and an upper bound specified by $W_3\mathbb{T}$ [50]. The mixed sensitivity approach results in the following overall specifications:

$$\|N\|_\infty = \max_{\omega} \bar{\sigma}(N(j\omega)); N = \begin{bmatrix} W_2\mathbb{S} \\ W_3\mathbb{T} \end{bmatrix} \quad (3.69)$$

$\bar{\sigma}(N(j\omega))$ is the maximum singular value at each frequency ω . The weighting functions are chosen to be

$$W_2 = \frac{\frac{s}{M} + \omega_o}{s + \omega_o A} \quad (3.70)$$

$$W_3 = \frac{s + \frac{\omega_o}{M}}{As + \omega_o} \quad (3.71)$$

where

$\omega_o = 0.70$ rad/sec is the desired closed-loop bandwidth

$A = 10^{-3}$ is the desired disturbance attenuation inside the bandwidth and

$M = 1.5$ is the desired bound on $\|S\|_\infty$ and $\|T\|_\infty$. The optimal controller, K_{ST} resulting from (3.69) is of 12th order. The controller is tested on the linear and nonlinear system and the simulation results are illustrated in Section 3.8.3.

3.8.3 Simulation Results

H_∞ Loop Shaping Results

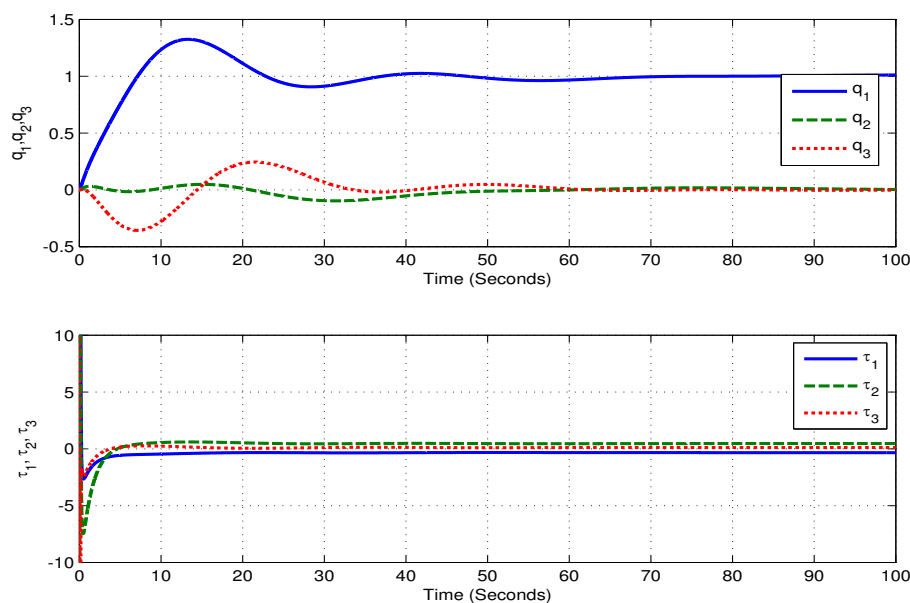


Figure 3.36: Channel-1 step response and control torque input of linear plant using LSDP

The H_∞ loop-shaping controller, K_{LS} is designed such that the open-loop singular value frequency response of the loop gain $L \triangleq G_{mrp}K_{LS}$ has a gain cross over frequency of 0.7 rad/sec [47]. The synthesized controller K_{LS} is of 19th order. The closed-loop system is excited with a step input for channel-1 in order to visualize the inter-axis coupling from other channels which are not excited with a reference signal. Fig. 3.36

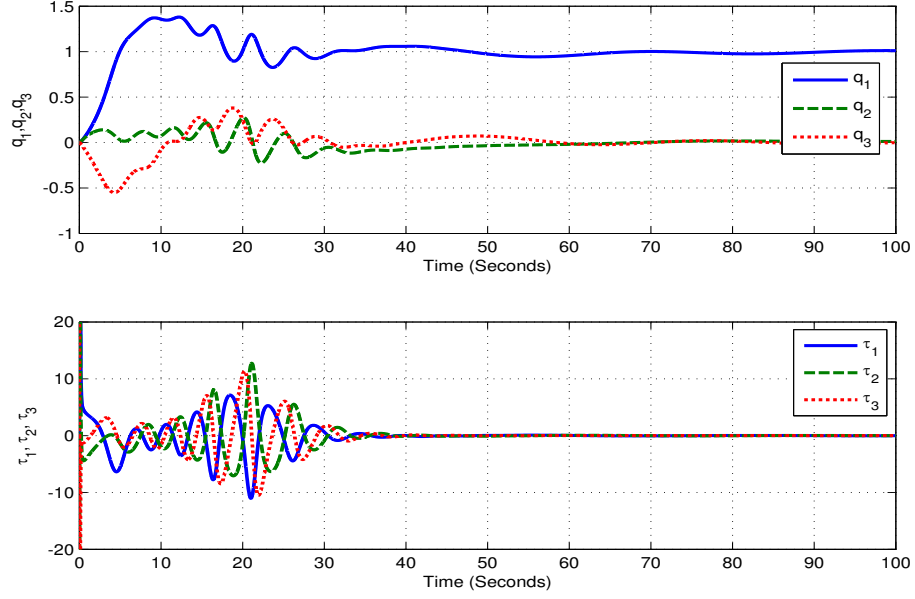


Figure 3.37: Channel-1 step response and control torque input of nonlinear plant using LSDP

and 3.37 shows the closed-loop attitude stabilization and the required control signal for the linear plant and the nonlinear plant using the LSDP based controller. In both the cases the control signal is limited to ± 50 Nm. The loop shaping accuracy, (γ_{ls}) achieved in this case was $\gamma_{ls} = 1.4772$. $\gamma_{ls} \geq 1$ where $\gamma_{ls} = 1$ for a perfect match. The inter-axis coupling in closed-loop is considerably stronger which is evident from both the linear and nonlinear responses of q_2 and q_3 which do not attain a steady state value of 0 till 60 seconds when their respective reference inputs are i.e. $q_{d2} = q_{d3} = 0$. The LSDP results illustrate that both the linear as well as nonlinear plant can be stabilized with this approach. The closed-loop poles in the case of the linear plant were found to be as follows.

$$\begin{aligned}
 & -4096.34 \pm i53.15, -4098.90, -4097.71, -4093.08, -4094.28, -24.46, -9.04, \\
 & -4096 \pm i0.4186, -4096, -4096 \pm 0.005, -4095.99, \\
 & -0.065 \pm i0.2153, -0.0272 \pm 0.063, -0.0256 \pm 0.0589, -0.0655, -0.053, -0.75, -0.75, -0.75
 \end{aligned} \tag{3.72}$$

However, the order of the loop-shaping controller is much larger than the output feedback controller.

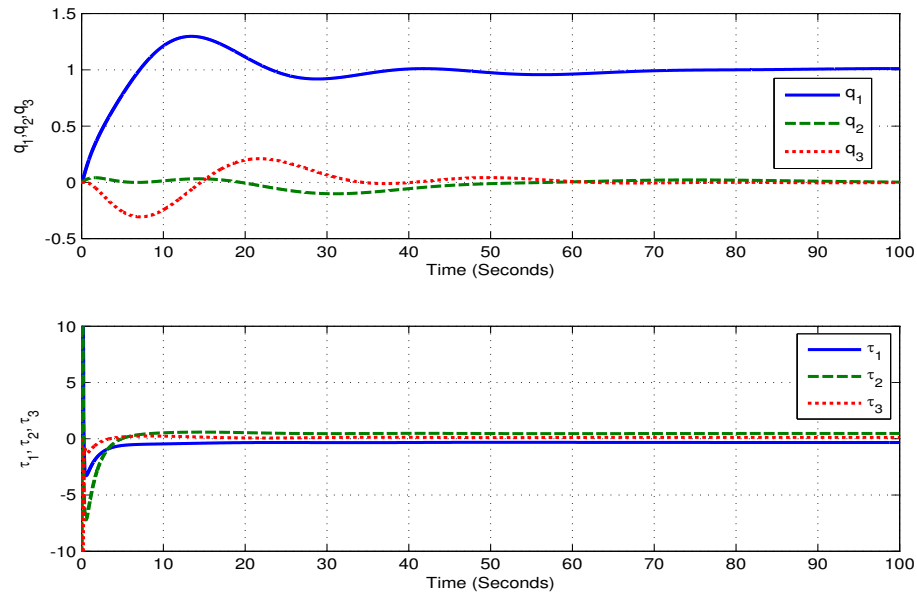
H_∞ Mixed Sensitivity Results

Figure 3.38: Channel-1 step response and control torque input of linear plant using mixed sensitivity approach

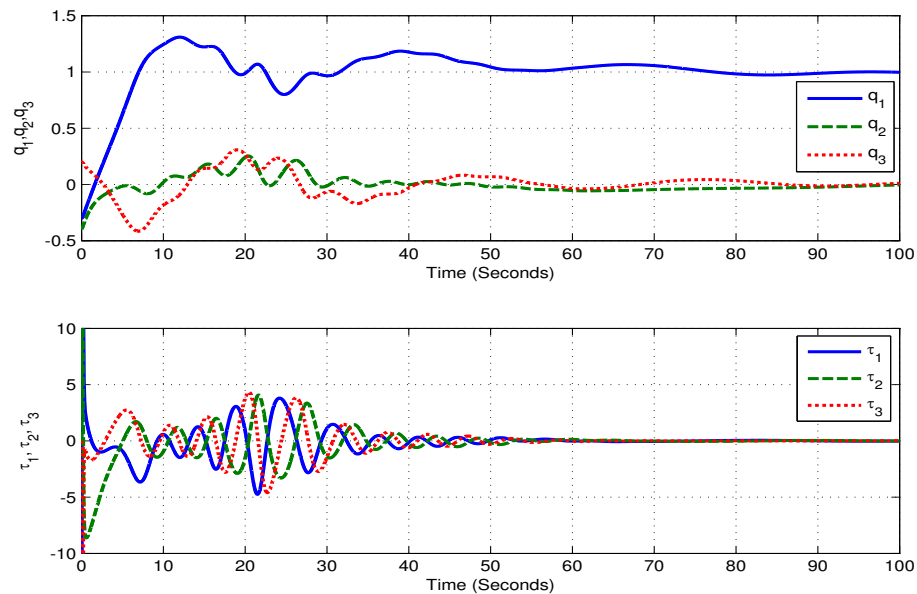


Figure 3.39: Channel-1 step response and control torque input of nonlinear plant using mixed sensitivity approach

In the H_∞ mixed sensitivity approach the designed controller, K_{ST} is of 12^{th} order. The closed-loop system is excited with a step input for channel-1 in order to visualize the inter-axis coupling from other channels which are not excited with a reference signal.

Fig. 3.38 and 3.39 shows the closed-loop attitude stabilization and the required control signal for the linear plant and the nonlinear plant using the mixed sensitivity approach. In both the cases the control signal is limited to ± 50 Nm. The closed-loop H_∞ norm described in (3.69) is found to be $\|N\|_\infty = 1.2645$. The inter-axis coupling in closed-loop is considerably stronger which is evident from both the linear and nonlinear responses of q_2 and q_3 which do not attain a steady state value of 0 till 60 seconds when their respective reference inputs are zero i.e. $q_{d2} = q_{d3} = 0$. The desired bound on \mathbb{S}_∞ and \mathbb{T}_∞ was defined as $M = 1.5$ and was found to be $\mathbb{S}_\infty = 1.062$ and $\mathbb{S}_\infty = 1.121$. The inter-axis coupling in closed-loop is considerably stronger and can be visualized from both the linear and nonlinear responses of q_2 and q_3 which do not attain a steady state value of 0 when their respective inputs are zero i.e. $q_{d2} = q_{d3} = 0$. Similar to the case of LSDP, the mixed sensitivity approach results illustrate that both the linear as well as nonlinear plant can be stabilized with this approach. The closed-loop poles in the case of the linear plant were found to be as follows.

$$\begin{aligned} & -673.79, -658.81, -636.08, -292.13, -236.33, -188.79, -166.09, -18.03, -7.169, \\ & -0.722, -0.697, -0.684, -0.0655 \pm i0.2153, -0.0264 \pm -0.0611, -0.0655, -0.053 \end{aligned} \quad (3.73)$$

However, the order of the mixed sensitivity controller is much larger than the output feedback controller. The proposed output feedback controller shown to stabilize the nonlinear plant given in (2.20-2.21) is tested on the linearized plant shown in (3.66). The controller gains are selected based on the PSO optimization presented in Section 3.7. Fig. 3.40 shows the linearized plant step response and the required controller effort with a saturation of ± 50 Nm. It can be inferred that the output feedback approach stabilizes both the linear and nonlinear plant in a very similar way whereas attitude stabilization is comparatively poorer in the robust control approaches for the nonlinear case. These are enunciated as follows:

The linear and nonlinear plant stabilization results based on loop-shaping and mixed

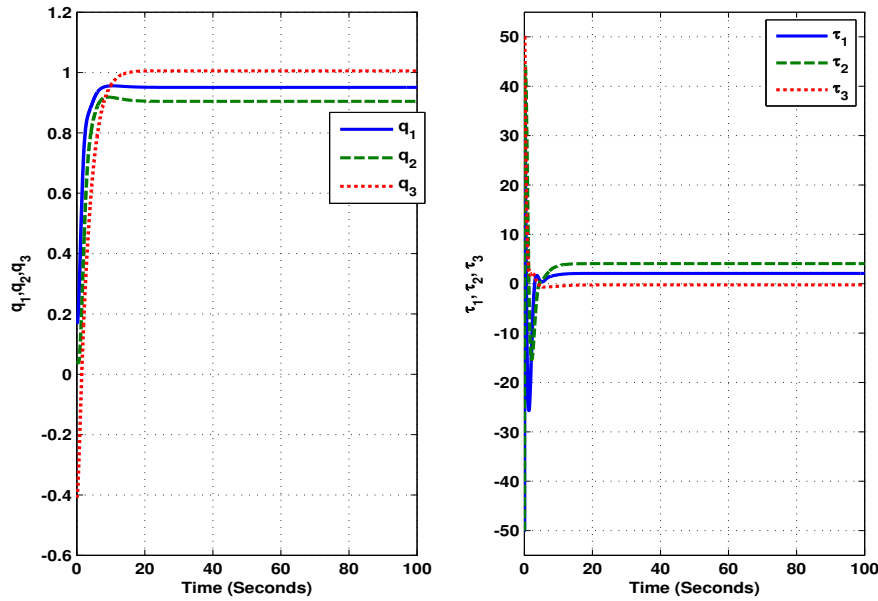


Figure 3.40: Linearized plant step response and control torque input with saturation of ± 50 Nm using output feedback control law

sensitivity approaches illustrate the following facts in comparison to the Lyapunov based output feedback approach presented in Section 3.6.

1. Both loop-shaping and mixed sensitivity approaches stabilize the linearized plant with a higher controller effort in comparison to the proposed output feedback approach presented in Section 3.6.
2. The robust control techniques synthesized for the linearized plant show poor stabilization results for the nonlinear case.
3. The output feedback approach shows good stabilization results for both the linear as well as the nonlinear case.
4. The order of the output feedback controller is small compared to the higher order controllers (Loop-shaping & mixed sensitivity) which also results in less controller effort.

Therefore, the output feedback approach globally asymptotically stabilizes the nonlinear as well as the linearized spacecraft attitude model defined in terms of the Euler's

equation of rotational dynamics and MRP's and shows satisfactory results in comparison to the existing robust control approaches.

3.9 Output Feedback Control in Quaternion Formulation

In this section the Quaternion based nonlinear spacecraft attitude model presented in Section 2.9.2 is stabilized using the previously proposed output feedback control law. The attitude defined in terms of Quaternions are assumed to be the only measurable quantity and angular velocity is not measured. This approach is similar to the one presented in Section 3.6. However Quaternion are used instead of MRP. The output feedback control law is shown to globally stabilize the nonlinear Quaternion based attitude model in the sense of Lyapunov by proposing a new candidate Lyapunov function. Simulation results are illustrated to demonstrate the attitude stabilization and time varying attitude acquisition of the nonlinear model.

3.9.1 Output Feedback Control Law

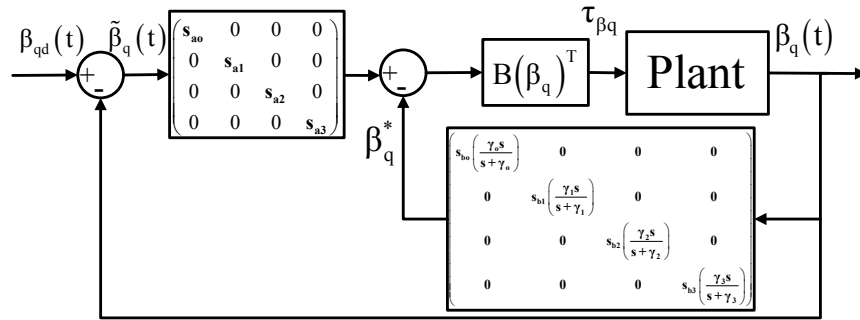


Figure 3.41: Quaternion based attitude stabilization using output feedback

The closed-loop system for the output feedback control law in Quaternion formulation is shown in Fig. 3.41 and the control law is given as follows:

$$\tau_{\beta_q} \triangleq [B(\beta_q)]^T (s_a \tilde{\beta}_q - \beta_q^*) \quad (3.74)$$

where

$$s_a = \text{diag}(s_{ao}, s_{a1}, s_{a2}, s_{a3}) \quad (3.75)$$

$$\beta_q^* = \text{diag}(\beta_{qo}^*, \beta_{q1}^*, \beta_{q2}^*, \beta_{q3}^*) \quad (3.76)$$

β_q^* is defined as follows, for $i = o, 1, 2, 3$.

$$\beta_{qi}^* = s_{bi} \frac{\gamma_i s}{s + \gamma_i} \quad (3.77)$$

$$\beta_{qi}^* s + \gamma_i \beta_{qi}^* = s_{bi} \gamma_i s \beta_{qi} \quad (3.78)$$

Taking inverse Laplace transforms of (3.78) we get

$$\dot{\beta}_{qi}^* + \gamma_i \beta_{qi}^* = s_{bi} \gamma_i \dot{\beta}_{qi} \quad (3.79)$$

$$\beta_{qi}^* = s_{bi} \dot{\beta}_{qi} - \frac{1}{\gamma_i} \dot{\beta}_{qi}^* \quad (3.80)$$

The design parameters in the control scheme are s_a in (3.75) and s_b and γ are defined as follows:

$$s_b = \text{diag}(s_{bo}, s_{b1}, s_{b2}, s_{b3}) \quad (3.81)$$

$$\gamma = \text{diag}(\gamma_o, \gamma_1, \gamma_2, \gamma_3) \quad (3.82)$$

To facilitate the subsequent control formulation, the nonlinear spacecraft attitude model defined in terms of Euler's equation of rotational dynamics and the Quaternion described in (2.14 & 2.21) are combined to form the following second order nonlinear dynamic equation of the Hamiltonian form, [52]. The detailed derivation can be found

in Section C.1.1 of Appendix C and can be stated as follows:

$$M^* \ddot{\beta}_q + N^* \dot{\beta}_q = \xi^T \tau_{\beta q} \quad (3.83)$$

where

$$M^* \triangleq \xi^T J \xi \quad (3.84)$$

$$N^* \triangleq -M^* \dot{B} \xi - \xi^T S(J \xi \dot{\beta}_q) \xi$$

The nonlinear dynamic equation in (3.83) shares similar properties with the rigid-link robot manipulator dynamics. Specifically, the inertia matrix M^* is positive definite and symmetric, and can be bounded as follows [66] & [52].

$$j_1 \|x\|^2 \leq x^T M^*(\beta_q) x \leq j_2 (\|\beta_q\|) \|x\|^2, \forall x \in \mathbb{R}^3 \quad (3.85)$$

where j_1 is a positive constant, and $j_2(\|\beta_q\|)$ is a positive non decreasing function. The matrices M^* and N^* satisfy the following skew-symmetric relationship [51], [66] and [52]

$$x^T \left(\frac{1}{2} \dot{M}^* - N^* \right) x = 0 \quad (3.86)$$

The derivation of (3.86) can be found in [17].

3.9.2 Stability Analysis

The control law described by (3.74) ensures the global asymptotic stability as delineated by the following theorem.

Theorem IV: *For the nonlinear system given in (2.14 & 2.21), the control scheme in (3.74) makes the closed-loop system stable and the attitude tracking error, $\tilde{\beta}_q(t)$ converges to zero.*

Proof: Consider the following positive function

$$V_6(\beta_q^*, \dot{\beta}_q, \tilde{\beta}_q) = \frac{1}{2} \left[\dot{\beta}_q^T M^* \dot{\beta}_q + \tilde{\beta}_q^T s_a \tilde{\beta}_q + \beta_q^{*T} (s_b \gamma)^{-1} \beta_q^* \right] \quad (3.87)$$

The positive definite function, V_6 is composed of the mechanical energy given by $\frac{1}{2}[\dot{\beta}_q^T M^* \dot{\beta}_q]$ and the gains discussed in (3.75, 3.81 & 3.82). The time derivative of the function, V_6 in (3.87) can be written as follows:

$$\begin{aligned} \dot{V}_6 &= \frac{1}{2}[\dot{\beta}_q^T M^* \ddot{\beta}_q + \dot{\beta}_q^T \dot{M}^* \dot{\beta}_q + \ddot{\beta}_q^T M^* \dot{\beta}_q] + \frac{1}{2}[\dot{\tilde{\beta}}_q^T s_a \dot{\tilde{\beta}}_q \\ &\quad + \dot{\tilde{\beta}}_q^T s_a \tilde{\beta}_q] + \frac{1}{2} \left[\beta_q^{*T} (s_b \gamma)^{-1} \dot{\beta}_q^* + \dot{\beta}_q^{*T} (s_b \gamma)^{-1} \beta_q^* \right] \end{aligned} \quad (3.88)$$

$$\dot{V}_6 = \dot{\beta}_q^T M^* \ddot{\beta}_q + \frac{1}{2} \dot{\beta}_q^T \dot{M}^* \dot{\beta}_q + \dot{\tilde{\beta}}_q^T s_a \tilde{\beta}_q + \beta_q^{*T} (s_b \gamma)^{-1} \dot{\beta}_q^* \quad (3.89)$$

$$\dot{V}_6 = \dot{\beta}_q^T (-N^* \dot{\beta}_q + \xi^T \tau_{\beta q}) + \frac{1}{2} \dot{\beta}_q^T \dot{M}^* \dot{\beta}_q + \dot{\tilde{\beta}}_q^T s_a \tilde{\beta}_q + \beta_q^{*T} (s_b \gamma)^{-1} \dot{\beta}_q^* \quad (3.90)$$

$$\dot{V}_6 = \dot{\beta}_q^T \left(\frac{1}{2} \dot{M}^* - N^* \right) \dot{\beta}_q + \dot{\beta}_q^T \xi^T \tau_{\beta q} + \dot{\tilde{\beta}}_q^T s_a \tilde{\beta}_q + \beta_q^{*T} (s_b \gamma)^{-1} \dot{\beta}_q^* \quad (3.91)$$

By the property of skew symmetry from (3.86), (3.91) can be written as follows

$$\dot{V}_6 = \dot{\beta}_q^T \xi^T \tau_{\beta q} + \dot{\tilde{\beta}}_q^T s_a \tilde{\beta}_q + \beta_q^{*T} (s_b \gamma)^{-1} \dot{\beta}_q^* \quad (3.92)$$

Then substituting the control signal from (3.74) in (3.92)

$$\dot{V}_6 = \dot{\beta}_q^T \xi^T B^T (s_a \tilde{\beta}_q - \beta_q^*) + \dot{\tilde{\beta}}_q^T s_a \tilde{\beta}_q + \beta_q^{*T} (s_b \gamma)^{-1} \dot{\beta}_q^* \quad (3.93)$$

$$\dot{V}_6 = \dot{\beta}_q^T s_a \tilde{\beta}_q - \dot{\beta}_q^T \beta_q^* + \dot{\tilde{\beta}}_q^T s_a \tilde{\beta}_q + \beta_q^{*T} (s_b \gamma)^{-1} \dot{\beta}_q^* \quad (3.94)$$

From $\xi^T B^T = I$, $\dot{\tilde{\beta}}_q = -\dot{\beta}_q$, we can get

$$\dot{V}_6 = -\dot{\beta}_q^T \beta_q^* + \beta_q^{*T} (s_b \gamma)^{-1} \dot{\beta}_q^* \quad (3.95)$$

Substituting $\dot{\beta}_{qi}^*$ from (3.80) in (3.95) we get

$$\dot{V}_6 = -\dot{\beta}_q^T \beta_q^* + \beta_q^{*T} (s_b \gamma)^{-1} (s_b \gamma \dot{\beta}_q - \gamma \beta_q^*) \quad (3.96)$$

$$\dot{V}_6 = -\beta_q^{*T} (s_b \gamma)^{-1} \gamma \beta_q^* \leq 0 \quad (3.97)$$

The time derivative of the positive definite function, V_6 is negative semi-definite by invoking the invariant set theorem [52]. Therefore, it can be stated that the Quaternion based nonlinear spacecraft attitude model can be stabilized by the output feedback control law in (3.74). The advantage of using this scheme is that the plant stabilization can be achieved by selecting a total of twelve positive gains in the feedback and feed-forward path of the closed loop system where the feedback consists of the plant output alone.

3.9.3 Simulation Results

The demonstration of the proposed scheme is illustrated with simulation results presented in this section. The mathematical model of spacecraft attitude given by (2.14 & 2.22) is simulated with (3.74) as the control input and the inertia matrix is given by (2.32). The initial conditions are taken from [7] and are described as follows

$$\begin{bmatrix} \omega_1(0) = 11.45 \\ \omega_2(0) = 11.45 \\ \omega_3(0) = 11.45 \end{bmatrix} \text{ Deg/sec} \quad (3.98)$$

$$\begin{bmatrix} \phi = 10 \\ \theta = 8 \\ \psi = 5 \end{bmatrix} \text{ Deg} \quad (3.99)$$

which corresponds to the following quaternions.

$$\begin{aligned}
 \beta_{q_0} &= 0.9931 \\
 \beta_{q_1} &= 0.08383 \\
 \beta_{q_2} &= 0.07322 \\
 \beta_{q_3} &= 0.03727
 \end{aligned} \tag{3.100}$$

The reference attitude is selected to be time varying and is expressed in terms of roll, (ϕ), pitch, (θ) and yaw, (ψ) angles as follows:

$$[\phi_1, \theta_1, \psi_1 = 20^\circ, 15^\circ, 10^\circ]^T \text{ for time } t = (0 - 100) \text{ sec}$$

$$[\phi_2, \theta_2, \psi_2 = 30^\circ, 25^\circ, 20^\circ]^T \text{ for time } t = (100 - 200) \text{ sec}$$

$$[\phi_3, \theta_3, \psi_3 = 45^\circ, 35^\circ, 30^\circ]^T \text{ for time } t = (200 - 300) \text{ sec}$$

The selection of the twelve positive gains stated in (3.75, 3.81 & 3.82) can be any positive values as far as convergence is concerned, as shown in Theorem IV in Section 3.9.2. Since there are no specific design requirements with respect to each individual channel in this example, we choose for simplicity the same values for the controllers on the four channels which are as follows:

$$\begin{aligned}
 s_a &= \text{diag}(42, 42, 42) \\
 s_b &= \text{diag}(121, 121, 121) \\
 \gamma &= \text{diag}(61, 61, 61)
 \end{aligned} \tag{3.101}$$

Fig. 3.42 shows the desired attitude (roll, pitch and yaw angles) namely, (ϕ_d, θ_d, ψ_d), measured attitude namely, (ϕ, θ, ψ) and attitude tracking error namely (ϕ_e, θ_e, ψ_e). The required controller effort is shown in Fig 3.43. The results illustrate the fact that the output feedback controller shows good tracking results with a maximum control torque of ± 50 Nm. However the plot is scaled to ± 10 Nm for clarity.

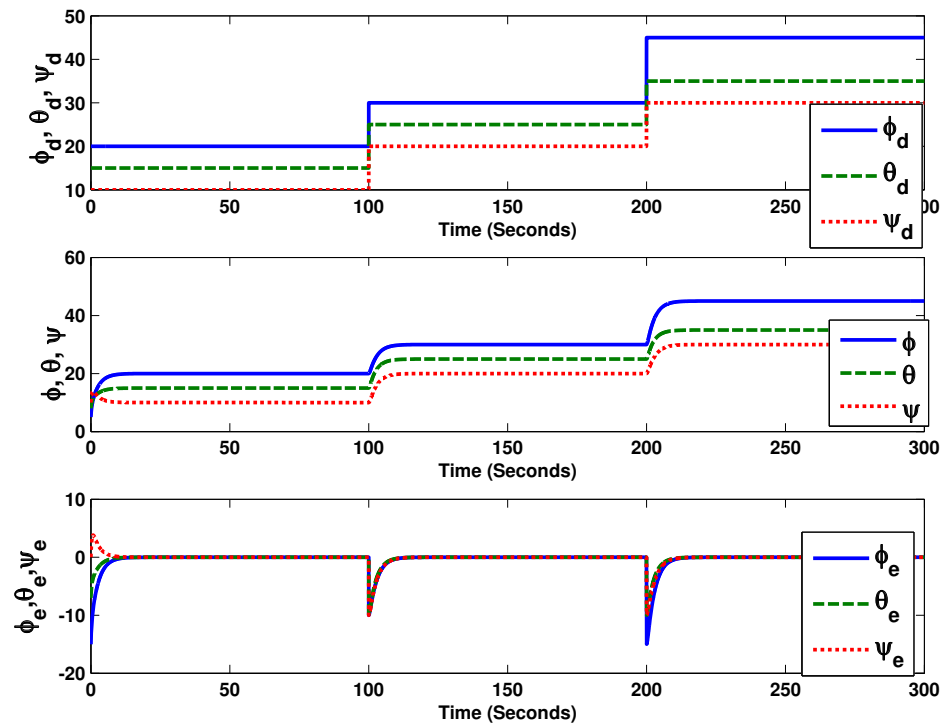


Figure 3.42: Quaternion based time varying attitude tracking

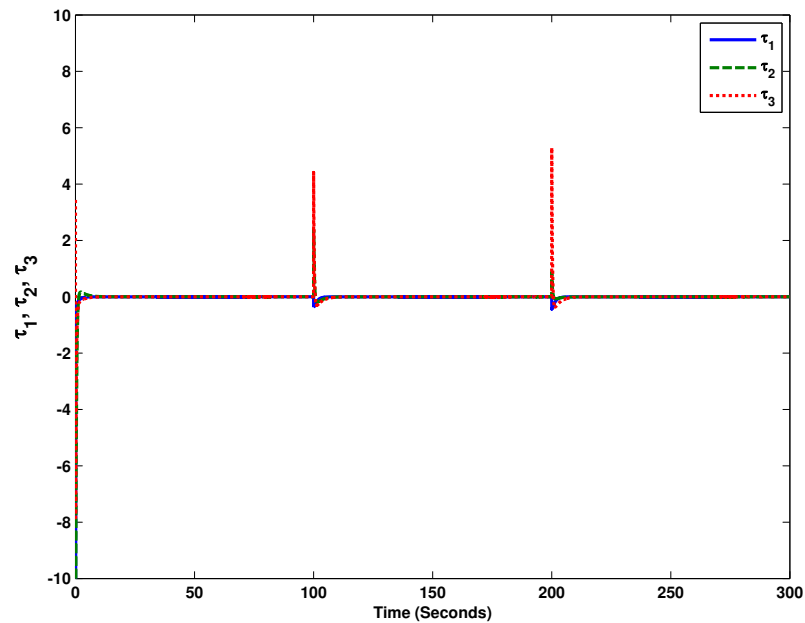


Figure 3.43: Quaternion based attitude tracking control torque

3.10 Conclusions

In this chapter, we have addressed the issue of attitude stabilization and control of a rigid spacecraft model. The nonlinear plant (attitude model) is defined using the Euler's equation of rotational dynamics and the kinematic differential equation represented by MRP. A new globally asymptotically stabilizing output feedback control law was proposed. The stability was proved by Lyapunov's theorem with a new Lyapunov candidate function. The proposed control scheme was shown to possess the robustness and simplicity of a PD controller which does not require attitude rate measurements, angular velocity measurements or direct use of differentiators as a necessary measurement in control structure design discussed in the literature. Furthermore, the control scheme does not require any information about the body principal moments of inertia and is therefore robust with respect to system parametric uncertainty. This was shown by case studies in which the inertia values are changed and still the closed-loop system is stable, while keeping the controller gains fixed. The simulation results illustrated the robust performance and zero tracking error of the overall closed loop demonstrating the effectiveness of the proposed approach.

The control law involved the selection of nine parameters which drastically influence the performance of the controlled system. Particle swarm optimization algorithm was used as a tool to infer the best parameters using a cost function which minimized the absolute value of the tracking error while varying the controller parameters. Then two robust control approaches namely H_∞ loop shaping and H_∞ mixed sensitivity were used to design controllers for the linearized attitude model. Simulations were performed on the linear and nonlinear plants. The simulation results illustrated that both the robust controllers take a longer time to stabilize the linearized plant and showed poor results when tested on the nonlinear case. The order of the synthesized controllers were also very large when compared with the proposed output feedback controller which illustrated good stabilization results for both the linear as well as the nonlinear case and required comparatively lesser controller effort.

A total of nine gains are required to be tuned in the output feedback control law. This was reduced to six in a modified approach. Global asymptotic stability is proved for the modified approach by a new candidate Lyapunov function and simulation results are illustrated to signify its effectiveness. The modified approach demonstrated similar results to the output feedback approach. In addition to nonlinear plant stabilization the modified approach is also shown to achieve time varying attitude tracking expressed in terms of roll, pitch and yaw angles.

A similar output feedback stabilization approach was then presented using Quaternion formulation. As before the global asymptotic stability was proved using a candidate Lyapunov function. Simulation results were shown to illustrate the effectiveness of the proposed approach when Quaternion are used instead of MRP. The approach successfully achieved time varying attitude tracking with considerably lesser controller effort and comparatively smaller controller order than the synthesized robust controllers with only the attitude as an available measurement.

3.10.1 Extension to Chapter 4

The nonlinear spacecraft attitude model discussed in Section 2.9.2 of Chapter 2 in terms of Euler's equation of rotational dynamics and Euler's parameters is further intensified by including actuator (reaction wheel) dynamics, nonlinear coupling terms, inertia tensors and the angular velocity terms neglected in the dynamics formulation in [44]. The derived nonlinear coupled dynamic system is cascaded with a Quaternion based kinematic model as shown in Section 2.9.2 to form an intricate yet realistic Large Space Telescope (LST) attitude model. A state feedback control structure is shown to stabilize the attitude of the LST model and track and a time varying attitude reference expressed in terms of roll, pitch and yaw angles.

3.10.2 Extension to Chapter 5

The linearized spacecraft attitude model stated in Section 2.10 of Chapter 2 is analyzed as a case study in predicting channel vulnerability to actuator degradations. The output feedback control law proposed in this chapter is shown to stabilize the linearized attitude model and the least/most vulnerable channel to an actuator degradation in the closed-loop spacecraft system is predicted by proposing interaction indices namely, (*RDI*) and (*i.i.i.*).

Chapter 4

Attitude Stabilization and Control of a Large Space Telescope Model

4.1 Introduction

In this chapter, a case study is presented on the attitude stabilization and control of a LST model. The LST model was developed by the National Aeronautics and Space Administration (NASA) under the direction of the George C. Marshall Space Flight Center (MSFC), Huntsville, Alabama. It was designed as a general purpose facility, capable of utilizing a wide range of scientific instruments expecting to contribute significantly to studies relevant to the origin and structure of the universe, the study of energy processes that occur in galactic nuclei, the study of early stages of stellar and solar systems, and observation of such highly evolved objects as supernova remnants and white dwarfs. It would weigh between 9,000 and 11,000 kg and have a length of 12 to 16 m and a diameter of 3.6 to 4 m. The basic LST elements are shown in Fig. 4.1, taken from a NASA technical report [44], are the Optical Telescope Assembly (OTA), the Scientific Instruments (SI), and the Support Systems Module (SSM). The most important optical element in the OTA is a diffraction-limited primary mirror approximately 3 m in diameter. The potential scientific instruments include a diffraction-limited camera, a low and a high dispersion spectrographs. All support systems such as control actuators, electronics, the

power unit, and the data transmission assembly are combined in the SSM. Solar panels supply the electrical power to the LST. The spacecraft will orbit earth at an altitude of 600 to 800 km at an inclination of 28.5 degrees. Further details are given in [2].

The aim of this chapter is to derive the nonlinear fully coupled dynamic equations of motion for the LST model by taking into account the nonlinear coupling terms, inertia tensors and the angular velocity terms neglected in [44]. The derived nonlinear, coupled dynamic system will be combined with a Quaternion based kinematic model to form a nonlinear attitude model of the LST system with three reaction wheels as actuators.

A state feedback control law is designed in this chapter to stabilize and achieve time varying attitude tracking. Simulation results are illustrated to demonstrate that the state feedback control law is able to achieve time varying attitude tracking in the presence of environmental disturbances (gravity gradient, magnetic, aerodynamic & solar pressure) and actuator failures at specific intervals of time.

In Section 4.2 the LST model is described. The equations of motion are discussed in Section 4.3. In Section 4.4, we derive the nonlinear fully coupled dynamic equations of motion. The reaction wheels are discussed in Section 4.5. The attitude model design and the control law description is given in Section 4.6. Simulation results are illustrated in Section 4.7 and the chapter concludes in Section 4.8 with some remarks for possible future research in this direction.

4.2 LST Model Description

The basic elements of LST are shown in Fig. 4.2 taken from [44] which primarily consists of the OTA, SI and the SSM. The LST model has a nearly cylindrical, beam like shape. The principal axes frame S , with its origin at the center of mass, is defined as follows [44]: The x_s axis (roll-axis) corresponds to the telescope axis, the y_s axis (pitch-axis) is located along the solar wing axis and the z_s axis (yaw-axis) completes the orthogonal frame.

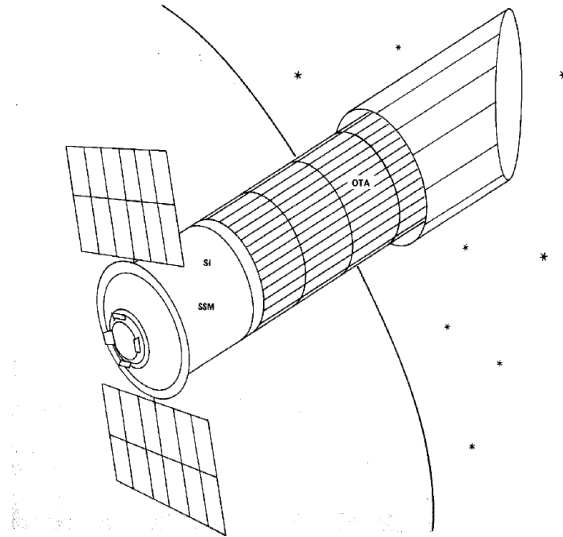


Figure 4.1: LST spacecraft configuration [44]

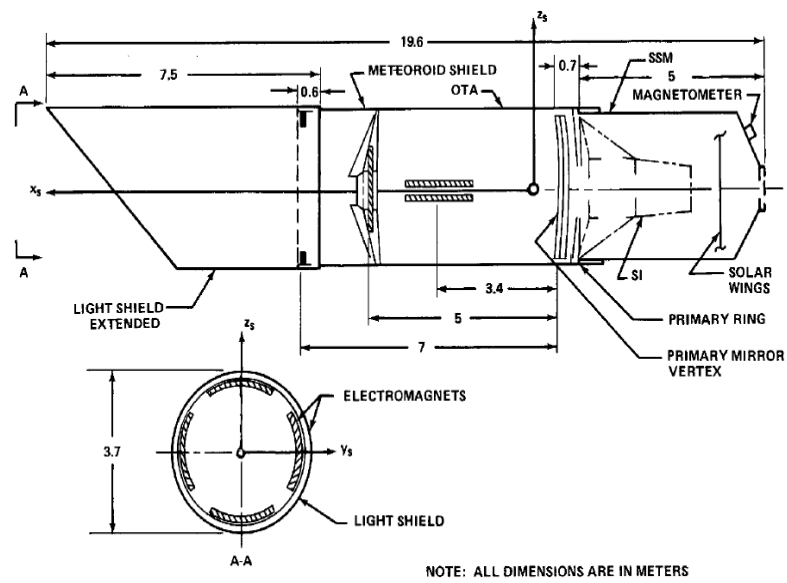


Figure 4.2: Basic elements of LST [44]

The LST is assumed to be a rigid body. The inertia matrix I of the LST is given by

$$I = \begin{pmatrix} I_x & 0 & 0 \\ 0 & I_y & 0 \\ 0 & 0 & I_z \end{pmatrix} \quad (4.1)$$

where $I_x = 14,656 \text{ kgm}^2$, $I_y = 91,772 \text{ kgm}^2$ and $I_z = 95,027 \text{ kgm}^2$ in the on-orbit configuration with extended light shield and solar wings. The corresponding mass totals 9,380 kg. Inside the SSM there are three symmetric reaction wheels mounted orthogonally and parallel to the x_s , y_s and z_s axes as shown in Fig. 4.3 wherein rw-1, rw-2 and rw-3 are the reaction wheels. rw-1 is mounted parallel to the roll axis, rw-2 is mounted parallel to the pitch axis about the solar arrays and rw-3 is mounted parallel to the yaw axis. The reaction wheels have the following inertia tensors.

$$I_1 = \begin{pmatrix} I_{1x} & 0 & 0 \\ 0 & I_{1y} & 0 \\ 0 & 0 & I_{1y} \end{pmatrix}, I_2 = \begin{pmatrix} I_{2z} & 0 & 0 \\ 0 & I_{2y} & 0 \\ 0 & 0 & I_{2z} \end{pmatrix}, I_3 = \begin{pmatrix} I_{3x} & 0 & 0 \\ 0 & I_{3x} & 0 \\ 0 & 0 & I_{3z} \end{pmatrix} \quad (4.2)$$

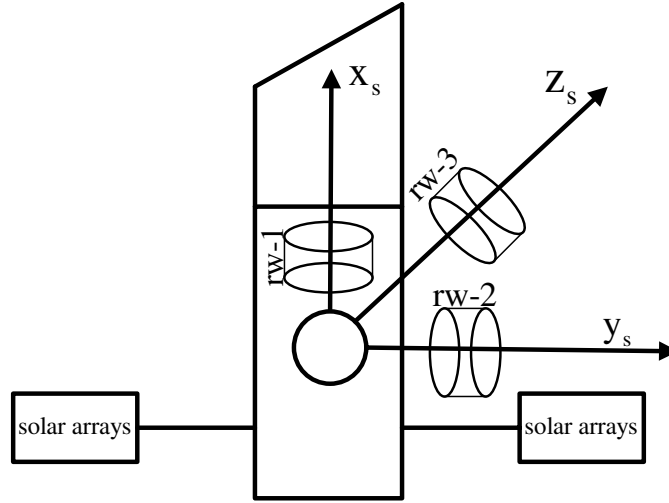


Figure 4.3: Reaction wheel configuration of LST model

The roll, pitch and yaw angles of the LST are denoted as ϕ, θ & ψ and are related to their respective angular velocities as follows:

$$\begin{pmatrix} \omega_x = \dot{\phi} \\ \omega_y = \dot{\theta} \\ \omega_z = \dot{\psi} \end{pmatrix} \quad (4.3)$$

where ω_x, ω_y and ω_z are the angular velocities about the x_s, y_s and z_s axes. Similarly the

angular velocities of the three reaction wheels can be expressed in terms of components as follows:

$$\begin{pmatrix} \omega_{xr} \\ 0 \\ 0 \end{pmatrix}, \begin{pmatrix} 0 \\ \omega_{yr} \\ 0 \end{pmatrix}, \begin{pmatrix} 0 \\ 0 \\ \omega_{zr} \end{pmatrix} \quad (4.4)$$

The internal torque (control torque) produced by the reaction wheels can be written as follows:

$$\begin{pmatrix} M_{1x} \\ M_{1y} \\ M_{1z} \end{pmatrix}, \begin{pmatrix} M_{2x} \\ M_{2y} \\ M_{2z} \end{pmatrix}, \begin{pmatrix} M_{3x} \\ M_{3y} \\ M_{3z} \end{pmatrix} \quad (4.5)$$

The external torques (disturbances) acting on the LST about its three orthogonal axes are denoted as M_x , M_y & M_z . The dynamic equations of the LST model are presented in section 4.3.

4.3 LST Model Equations of Motion

In this section the equations of motion for LST model and the three reaction wheels serving as actuators are stated [48].

The dynamic equations for the LST model are as follows:

$$I_x \dot{\omega}_x + \omega_y \omega_z (I_z - I_y) + I_{3z} \omega_{zr} \omega_y - I_{2y} \omega_{yr} \omega_z + I_{1x} \dot{\omega}_{xr} = M_x \quad (4.6)$$

$$I_y \dot{\omega}_y + \omega_x \omega_z (I_x - I_z) + I_{1x} \omega_{xr} \omega_z - I_{3z} \omega_{zr} \omega_x + I_{2y} \dot{\omega}_{yr} = M_y \quad (4.7)$$

$$I_z \dot{\omega}_z + \omega_x \omega_y (I_y - I_x) + I_{2y} \omega_{yr} \omega_x - I_{1x} \omega_{xr} \omega_y + I_{3z} \dot{\omega}_{zr} = M_z \quad (4.8)$$

The dynamic equations for the reaction wheel mounted parallel to the x_s axis are:

$$I_{1x} \dot{\omega}_x + I_{1x} \dot{\omega}_{xr} = M_{1x} \quad (4.9)$$

$$I_{1y}\dot{\omega}_y + (I_{1x} - I_{1y})\omega_y\omega_z + I_{1x}\omega_{xr}\omega_z = M_{1y} \quad (4.10)$$

$$I_{1y}\dot{\omega}_z + (I_{1y} - I_{1x})\omega_x\omega_y - I_{1x}\omega_{xr}\omega_y = M_{1z} \quad (4.11)$$

The dynamic equations for the reaction wheel mounted parallel to the y_s axis are:

$$I_{2z}\dot{\omega}_x + (I_{2y} - I_{2z})\omega_x\omega_z + I_{2y}\omega_{yr}\omega_x = M_{2x} \quad (4.12)$$

$$I_{2y}\dot{\omega}_y + I_{2y}\dot{\omega}_{yr} = M_{2y} \quad (4.13)$$

$$I_{2z}\dot{\omega}_z + (I_{2z} - I_{2y})\omega_y\omega_z - I_{2y}\omega_{yr}\omega_z = M_{2z} \quad (4.14)$$

The dynamic equations for the reaction wheel mounted parallel to the z_s axis are:

$$I_{3x}\dot{\omega}_x + (I_{3x} - I_{3z})\omega_x\omega_y + I_{3z}\omega_{zr}\omega_y = M_{3x} \quad (4.15)$$

$$I_{3x}\dot{\omega}_y + (I_{3z} - I_{3x})\omega_x\omega_z + I_{3z}\omega_{zr}\omega_x = M_{3y} \quad (4.16)$$

$$I_{3z}\dot{\omega}_z + I_{3z}\dot{\omega}_{zr} = M_{3z} \quad (4.17)$$

For simplification, [48] and [44] assumed that the reaction wheels are small, so that $I_{1x} \ll I_x$, $I_{2y} \ll I_y$, $I_{3z} \ll I_z$ and they have one degree of freedom only. Then the equations (4.6-4.17) can be simplified to

$$I_x\dot{\omega}_x + \omega_y\omega_z(I_z - I_y) + I_{1x}\dot{\omega}_{xr} = M_x \quad (4.18)$$

$$I_y \dot{\omega}_y + \omega_x \omega_z (I_x - I_z) + I_{2y} \dot{\omega}_{yr} = M_y \quad (4.19)$$

$$I_z \dot{\omega}_z + \omega_x \omega_y (I_y - I_x) + I_{3z} \dot{\omega}_{zr} = M_z \quad (4.20)$$

$$I_{1x} \dot{\omega}_x + I_{1x} \dot{\omega}_{xr} = M_{1x} \quad (4.21)$$

$$I_{2y} \dot{\omega}_y + I_{2y} \dot{\omega}_{yr} = M_{2y} \quad (4.22)$$

$$I_{3z} \dot{\omega}_z + I_{3z} \dot{\omega}_{zr} = M_{3z} \quad (4.23)$$

Substituting (4.21 in 4.18), (4.22 in 4.19) & (4.23 in 4.20), we get the following three equations describing the motions along the individual axes and their interconnections [48]

$$\begin{aligned} I_x \dot{\omega}_x + \omega_y \omega_z (I_z - I_y) &= (M_x - M_{1x}) \\ I_y \dot{\omega}_y + \omega_x \omega_z (I_x - I_z) &= (M_y - M_{2y}) \\ I_z \dot{\omega}_z + \omega_x \omega_y (I_y - I_x) &= (M_z - M_{3z}) \end{aligned} \quad (4.24)$$

(4.24) can be further simplified as follows:

$$\dot{\omega}_x = \frac{(M_x - M_{1x}) - \omega_y \omega_z (I_z - I_y)}{I_x} \quad (4.25)$$

$$\dot{\omega}_y = \frac{(M_y - M_{2y}) - \omega_x \omega_z (I_x - I_z)}{I_y} \quad (4.26)$$

$$\dot{\omega}_z = \frac{(M_z - M_{3z}) - \omega_x \omega_y (I_y - I_x)}{I_z} \quad (4.27)$$

The LST model discussed in this section is linear [44], [48] and it ignores the nonlinear

coupling phenomena and may not be an entirely satisfactory description of the LST model as stated by [48]. In the next section we derive the fully coupled equations of motion for the LST model including the three reaction wheels. The nonlinear coupling terms, inertia and the angular velocity terms neglected in (4.24) will be accounted in the forthcoming derivation. The attitude of the coupled and decoupled LST model is controlled. Single channel attitude stabilization is illustrated in order to visualize the inter-axis coupling and is demonstrated in the simulation results section.

4.4 Derivation of Coupled Equations for LST Model

The LST model dynamics stated in (4.6-4.8) can be viewed as the dynamics about each axis with the influence of reaction wheel dynamics about all the axes. This can be expressed about each axis of the LST as follows:

Dynamics about x_s axis + Reaction wheel dynamics about x_s, y_s and z_s axes = External torque about x_s axis (M_x)

Dynamics about y_s axis + Reaction wheel dynamics about x_s, y_s and z_s axes = External torque about y_s axis (M_y)

Dynamics about z_s axis + Reaction wheel dynamics about x_s, y_s and z_s axes = External torque about z_s axis (M_z)

The reaction wheel dynamics about x_s, y_s and z_s from (4.9, 4.14 & 4.15) can be re-arranged and substituted in x_s axis dynamic equation stated in (4.6). In a similar way, the reaction wheel dynamics about x_s, y_s and z_s from (4.10, 4.13 & 4.16) are re-arranged and substituted in y_s axis dynamic equation stated in (4.7) and the reaction wheel dynamics about x_s, y_s and z_s from (4.11, 4.12 & 4.17) are re-arranged and substituted in z_s axis dynamic equation stated in (4.8).

$$\dot{\omega}_x(I_x - I_{3x} - I_{1x}) - \omega_x \omega_y (I_{3x} - I_{3z}) + \omega_y \omega_z (I_z - I_y - I_{2z} + I_{2y}) - I_{2z} \dot{\omega}_z = M_x - M_{1x} - M_{3x} - M_{2z} \quad (4.28)$$

$$\dot{\omega}_y(I_y - I_{1y} + I_{3x} - I_{2y}) + \omega_x \omega_z(I_x - I_z + I_{3z} - I_{3x}) - \omega_y \omega_z(I_{1x} - I_{1y}) = M_y - M_{1y} + M_{3y} - M_{2y} \quad (4.29)$$

$$-I_{2z} \dot{\omega}_x + \dot{\omega}_z(I_z - I_{1y} - I_{3z}) + \omega_x \omega_y(I_y - I_x - I_{1y} + I_{1x}) - \omega_x \omega_z(I_{2y} - I_{2z}) = M_z - M_{2x} - M_{1z} - M_{3z} \quad (4.30)$$

Inter substitution of (4.28 & 4.30) and simplifying (4.28-4.30), we get the following:

$$\begin{aligned} \dot{\omega}_x = & -I_{2z}^{-1} \Delta^{-1} \omega_x \omega_y (I_z I_{3x} - I_z I_{3z} - I_{1y} I_{3x} + I_{1y} I_{3z} - I_{3z} I_{3x} + I_{3z}^2) + \\ & -I_{2z}^{-1} \Delta^{-1} \omega_y \omega_z (-I_z^2 + I_z I_y + I_z I_{2z} - I_z I_{2y} + I_{1y} I_z - I_{1y} I_y) \\ & -I_{2z}^{-1} \Delta^{-1} \omega_y \omega_z (-I_{1y} I_{2z} + I_{1y} I_{2y} + I_{3z} I_z - I_{3z} I_y - I_{3z} I_{2z} + I_{3z} I_{2y}) \\ & -I_{2z}^{-1} \Delta^{-1} I_z (M_x - M_{1x} - M_{3x} - M_{2z}) \\ & -I_{2z}^{-1} \Delta^{-1} I_{1y} (-M_x + M_{1x} + M_{3x} + M_{2z}) \\ & -I_{2z}^{-1} \Delta^{-1} I_{3z} (-M_x + M_{1x} + M_{3x} + M_{2z}) \\ & \Delta^{-1} \omega_x \omega_y (I_y - I_x - I_{1y} + I_{1x}) \\ & \Delta^{-1} \omega_x \omega_z (-I_{2y} + I_{2z}) \\ & \Delta^{-1} (-M_z + M_{2x} + M_{1z} + M_{3z}) \end{aligned} \quad (4.31)$$

$$\dot{\omega}_y = \frac{M_y - M_{1y} + M_{3y} - M_{2y} - \omega_x \omega_z (I_x - I_z + I_{3z} - I_{3x}) + \omega_y \omega_z (I_{1x} - I_{1y})}{(I_y - I_{1y} + I_{3x} - I_{2y})} \quad (4.32)$$

$$\begin{aligned}
\dot{\omega}_z = & -I_{2z}^{-1}\Delta^{-1}\omega_x\omega_y(-I_xI_y + I_x^2 + I_xI_{1y} - I_xI_{1x} + I_{3x}I_y - I_{3x}I_x) \\
& -I_{2z}^{-1}\Delta^{-1}\omega_x\omega_y(I_{3x}I_{1y} + I_{3x}I_{1x} + I_{1x}I_y - I_{1x}I_x - I_{1x}I_{1y} + I_{1x}^2) \\
& -I_{2z}^{-1}\Delta^{-1}\omega_x\omega_z(I_xI_{2y} - I_xI_{2z} - I_{3x}I_{2y} + I_{3x}I_{2z} - I_{1x}I_{2y} + I_{1x}I_{2z}) \\
& -I_{2z}^{-1}\Delta^{-1}I_x(M_z - M_{2x} - M_{1z} - M_{3z}) \\
& -I_{2z}^{-1}\Delta^{-1}I_{3x}(-M_z + M_{2x} + M_{1z} + M_{3z}) \\
& -I_{2z}^{-1}\Delta^{-1}I_{1x}(-M_z + M_{2x} + M_{1z} + M_{3z}) \\
& \Delta^{-1}\omega_x\omega_y(-I_{3x} + I_{3z}) \\
& \Delta^{-1}\omega_y\omega_z(I_z - I_y - I_{2z} + I_{2y}) \\
& \Delta^{-1}(-M_x + M_{1x} + M_{3x} + M_{2z}) \tag{4.33}
\end{aligned}$$

where

$$\Delta = I_{2z} + I_{2z}^{-1}[-I_zI_x + I_zI_{3x} + I_zI_{1x} + I_{1y}I_x - I_{1y}I_{3x} - I_{1y}I_{1x} + I_{3z}I_x - I_{3z}I_{3x} - I_{3z}I_{1x}] \tag{4.34}$$

(4.31-4.33) are the coupled nonlinear dynamic equations of the LST model with reaction wheels as actuators in contrast to the linear decoupled equations described earlier in (4.25-4.27).

4.5 LST Reaction Wheels

Reaction wheels are used as actuators when accurate and time optimal attitude control is mandatory. In [47] it is stated that the choice of reaction wheel depends on the performance to be achieved by the satellite's attitude control system. Some of the basic technical features required from a reaction wheel for the desired performance to be achieved are maximum achievable torque, maximum momentum capacity, low torque

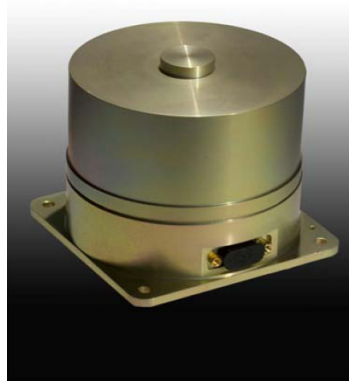


Figure 4.4: Reaction wheel [1]

noise and low coulomb friction torques [47]. Some of the drawbacks of the reaction wheels are relatively small effective torque and the possibility of reaction wheel saturation [43]. Fig. 4.4 shows a reaction wheel manufactured by SSBV Space and Ground Systems, UK [1]. Let x, y & z be three mutually perpendicular axes, m be the mass in (kilogram), h be the height and $l = w$ be the length and width of the reaction wheel shown in Fig. 4.4. The reaction wheel rotates about its x - axis and its moment of inertia about x, y & z axes can be calculated as follows:

$$I_{1x} = \frac{mr^2}{2}$$

$$I_{1y} = I_{1z} = \frac{1}{12}(3r^2 + h^2) \quad (4.35)$$

where $r = \frac{l}{2} = \frac{w}{2}$. The technical specifications of the reaction wheel shown in Fig. 4.4 are given in appendix D. Its physical characteristics will be used in calculating the moment of inertia of the reaction wheel for the LST model and are given as follows:

$$\begin{aligned} \text{Mass} &= 1.550kg \\ \text{Length=width} &= 102mm \\ \text{height} &= 105mm \end{aligned} \quad (4.36)$$

The axial and transverse inertias of the LST reaction wheel are calculated using the

relationship stated in (4.35) and the physical characteristics in (4.36) and are given as follows:

$$\begin{aligned} I_{1x} &= 0.002 \text{ kgm}^2 \\ I_{1y} &= I_{1z} = 0.0016 \text{ kgm}^2 \end{aligned} \quad (4.37)$$

4.6 Attitude Stabilization and Tracking of LST Model

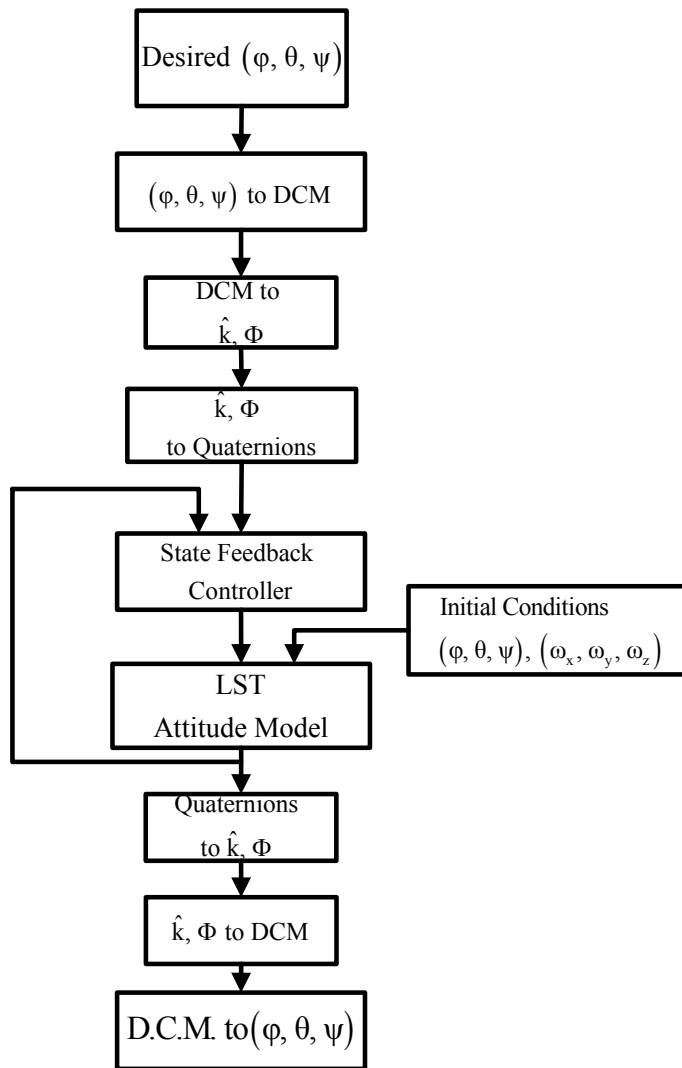


Figure 4.5: LST model attitude tracking control system

In this section the derived nonlinear coupled dynamic equations of LST given in (4.31-4.33) are cascaded with the kinematic differential equations in terms of Quaternion formulation discussed in Section 2.5 of Chapter 2. The attitude tracking control system

for the LST Model is shown in Fig. 4.5. The desired attitude is time varying and is expressed in terms of roll, pitch and yaw angles in degrees. The Euler angles are transformed to the DCM using (3-2-1) Euler angle sequence wherein the z, y & x axis are rotated about an angle of ψ, θ & ϕ degrees. The resulting DCM is given by the following relationship:

$$DCM = \begin{pmatrix} c\theta c\psi & c\theta s\psi & -s\theta \\ s\phi s\theta c\psi - c\phi s\psi & s\phi s\theta s\psi + c\phi c\psi & s\phi c\theta \\ c\phi s\theta c\psi + s\phi s\psi & c\phi s\theta s\psi - s\phi c\psi & c\phi c\theta \end{pmatrix} \quad (4.38)$$

where the notation $c = \cos$ and $s = \sin$ of the angles ϕ, θ & ψ . The Euler eigenangle, Φ and Euler eigenaxis, \hat{k} is calculated from the DCM using the following relationship.

$$\Phi = \cos^{-1} \left(\frac{1}{2} (C_{11} + C_{22} + C_{33} - 1) \right) \quad (4.39)$$

$$\hat{k} = \begin{pmatrix} k_1 \\ k_2 \\ k_3 \end{pmatrix} = \frac{1}{2\sin\Phi} \begin{pmatrix} C_{23} - C_{32} \\ C_{31} - C_{13} \\ C_{12} - C_{21} \end{pmatrix} \quad (4.40)$$

where $C_{i,j}$ is the i_{th} row and j_{th} column element of the DCM. The Quaternions, β_q are calculated from the Euler eigenangle, Φ and Euler eigenaxis, \hat{k} using the following relationship.

$$\beta_q = \begin{pmatrix} \beta_{q1} \\ \beta_{q2} \\ \beta_{q3} \\ \beta_{q0} \end{pmatrix} = \begin{pmatrix} k_1 \sin(\frac{\Phi}{2}) \\ k_2 \sin(\frac{\Phi}{2}) \\ k_3 \sin(\frac{\Phi}{2}) \\ \cos(\frac{\Phi}{2}) \end{pmatrix} \quad (4.41)$$

The kinematic differential equations of motion in terms of Quaternion's was stated

in (2.14) and is mentioned below [42]:

$$\begin{pmatrix} \dot{\beta}_{q0} \\ \dot{\beta}_{q1} \\ \dot{\beta}_{q2} \\ \dot{\beta}_{q3} \end{pmatrix} = \begin{pmatrix} \beta_{q0} & -\beta_{q1} & -\beta_{q2} & -\beta_{q3} \\ \beta_{q1} & \beta_{q0} & -\beta_{q3} & \beta_{q2} \\ \beta_{q2} & \beta_{q3} & \beta_{q0} & -\beta_{q1} \\ \beta_{q3} & -\beta_{q2} & \beta_{q1} & \beta_{q0} \end{pmatrix} \begin{pmatrix} 0 \\ \omega_x \\ \omega_y \\ \omega_z \end{pmatrix} \quad (4.42)$$

where $[\omega_x \ \omega_y \ \omega_z]^T$ is the angular velocity of the LST model in a body-fixed frame.

4.6.1 Attitude Model Design

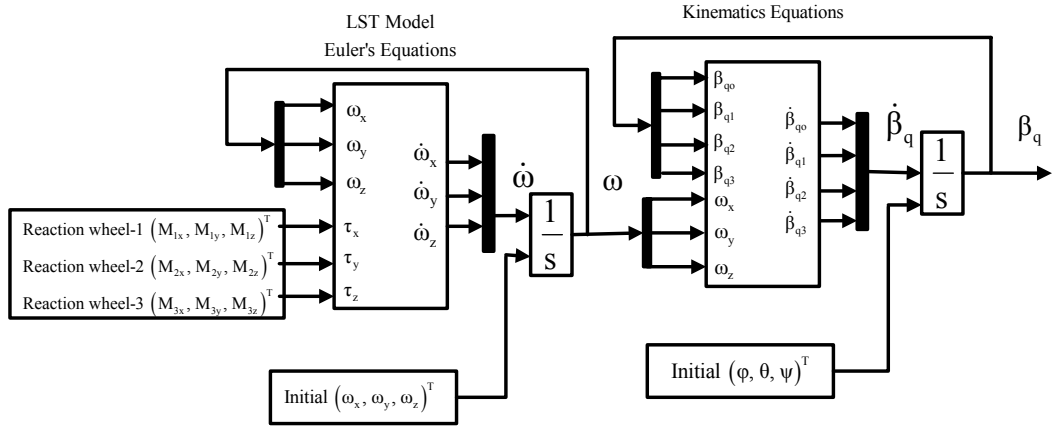


Figure 4.6: Attitude model design in simulink

The attitude model consisting of the Euler's equations, (4.31-4.33) and the kinematic equations, (4.42) is modeled in simulink as shown in Fig. 4.6. The attitude model consists of two integrators blocks. The first block calculates the angular velocity vector, ω with initial conditions specified in degrees/second. The second integrator calculates the attitude of the LST model with initial attitude specified in terms of roll, pitch and yaw angles expressed in degrees. The control torque is added in the Euler's equations block and the kinematics equations block calculates the plant output.

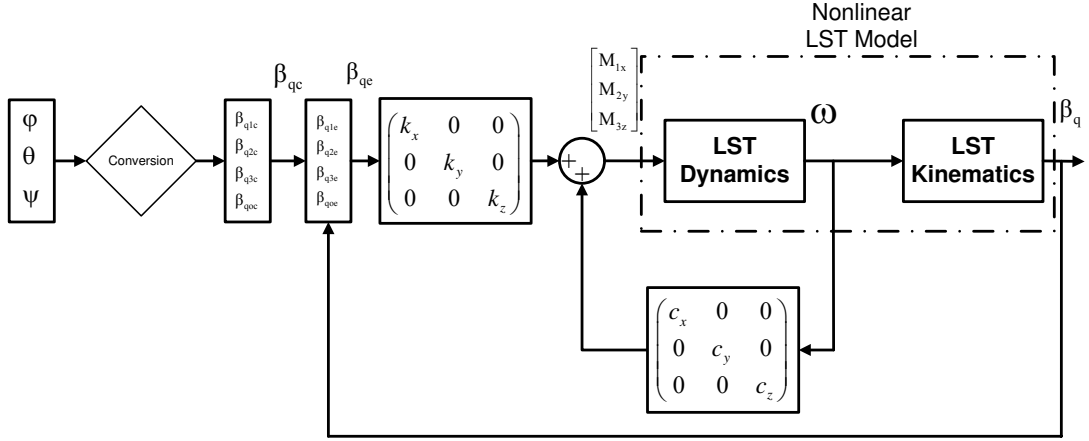


Figure 4.7: LST model attitude stabilization

4.6.2 State Feedback Controller

A state feedback control structure is shown to stabilize the attitude of the formulated nonlinear LST model as depicted in Fig. 4.7. The control law requires the angular velocity vector and the attitude error vector in terms of Quaternions in computing the control law. The angular velocity vector is given by

$$\omega \triangleq \begin{pmatrix} \omega_x \\ \omega_y \\ \omega_z \end{pmatrix} \quad (4.43)$$

where ω_x , ω_y and ω_z are the angular velocities about the x_s , y_s and z_s axes of the LST model. The attitude error Quaternion vector is computed using the current attitude quaternions, $(\beta_{q1}, \beta_{q2}, \beta_{q3}, \beta_{qo})$ stated in (4.41) and the desired attitude quaternions given by

$$\beta_{qc} \triangleq \begin{pmatrix} \beta_{q1c} \\ \beta_{q2c} \\ \beta_{q3c} \\ \beta_{qoc} \end{pmatrix} \quad (4.44)$$

The attitude error Quaternion vector is given in [62] as follows:

$$\begin{bmatrix} \beta_{q1e} \\ \beta_{q2e} \\ \beta_{q3e} \\ \beta_{q0e} \end{bmatrix} = \begin{bmatrix} \beta_{q0c} & \beta_{q3c} & -\beta_{q2c} & -\beta_{q1c} \\ -\beta_{q3c} & \beta_{q0c} & \beta_{q1c} & -\beta_{q2c} \\ \beta_{q2c} & -\beta_{q1c} & \beta_{q0c} & -\beta_{q3c} \\ \beta_{q1c} & \beta_{q2c} & \beta_{q3c} & \beta_{0c} \end{bmatrix} \begin{bmatrix} \beta_{q1} \\ \beta_{q2} \\ \beta_{q3} \\ \beta_{q0} \end{bmatrix} \quad (4.45)$$

The state feedback control law to stabilize the attitude of the nonlinear LST model can be stated as follows:

$$\begin{pmatrix} M_{1x} \\ M_{2y} \\ M_{3z} \end{pmatrix} = \underbrace{\begin{pmatrix} k_x & 0 & 0 \\ 0 & k_y & 0 \\ 0 & 0 & k_z \end{pmatrix}}_k \begin{pmatrix} \beta_{q1e} \\ \beta_{q2e} \\ \beta_{q3e} \end{pmatrix} + \underbrace{\begin{pmatrix} c_x & 0 & 0 \\ 0 & c_y & 0 \\ 0 & 0 & c_z \end{pmatrix}}_c \begin{pmatrix} \omega_x \\ \omega_y \\ \omega_z \end{pmatrix} \quad (4.46)$$

where the control law involves two feedback loops, namely, inner and outer. The inner loop comprises of angular velocity feedback with a positive definite gain matrix c . The outer loop feeds back the measured attitude in terms of quaternions. The attitude error Quaternion vector computed in (4.45) is multiplied with a positive definite gain matrix k .

4.7 Simulation Results

4.7.1 Initial Conditions

The following initial conditions stated in [42] are chosen for the simulation of the LST attitude model given in (4.31-4.33 & 4.42) and the control law given in (4.46).

$$\begin{bmatrix} \omega_x = 11.45 \\ \omega_y = 11.45 \\ \omega_z = 11.45 \end{bmatrix} \text{Deg/sec} \quad (4.47)$$

$$\begin{aligned}
\phi &= 10^\circ \\
\theta &= 8^\circ \\
\psi &= 5^\circ
\end{aligned} \tag{4.48}$$

The inertia matrix, (I) of the LST is given as follows [44]:

$$I = \begin{pmatrix} 14656 & 0 & 0 \\ 0 & 91772 & 0 \\ 0 & 0 & 95027 \end{pmatrix} (kgm^2) \tag{4.49}$$

The axial and transverse inertia of the reaction wheels discussed in section 4.5 were calculated in (4.37) and are given as follows:

$$I_1 = \begin{pmatrix} 0.002 & 0 & 0 \\ 0 & 0.0016 & 0 \\ 0 & 0 & 0.0016 \end{pmatrix} \tag{4.50}$$

$$I_2 = \begin{pmatrix} 0.0016 & 0 & 0 \\ 0 & 0.002 & 0 \\ 0 & 0 & 0.0016 \end{pmatrix} \tag{4.51}$$

$$I_3 = \begin{pmatrix} 0.0016 & 0 & 0 \\ 0 & 0.0016 & 0 \\ 0 & 0 & 0.002 \end{pmatrix} \tag{4.52}$$

The external torques (disturbances) acting on the LST depend on the external environment in space. The maximum values of the respective external torques are given in [2] and are mentioned below:

Gravity gradient 0.2200 N-m

Magnetic 0.0500 N-m

Aerodynamic 0.0001 N-m

Solar pressure 0.0004 N-m

The total external disturbance acting on the LST model is taken to be $M_x=M_y=M_z=0.2705$ N-m.

4.7.2 Attitude Tracking

The desired attitude is selected in terms of Euler angles as follows:

$$\begin{aligned}\phi &= 20^\circ \\ \theta &= 15^\circ \\ \psi &= 10^\circ\end{aligned}\tag{4.53}$$

The selection of the two gain matrices namely, k & c in (4.46) has to be positive definite and are selected by trial and error. We choose for simplicity the same values for the controllers on the three channels to be as follows:

$$k = \text{diag}(50, 50, 50) 10^3\tag{4.54}$$

$$c = \text{diag}(80, 80, 80) 10^3\tag{4.55}$$

The transverse torques produced by the reaction wheels are very small when compared to the axial torques i.e. $M_{1y}, M_{1z} \ll M_{1x}$, $M_{2x}, M_{2z} \ll M_{2y}$ & $M_{3x}, M_{3y} \ll M_{3z}$ and are neglected in [44]. In this simulation, the transverse torques are taken into consideration and are chosen to be 5% of the axial value as shown below:

$$\begin{aligned}
M_{1y} &= M_{1z} = 5\%M_{1x} \\
M_{2x} &= M_{2z} = 5\%M_{2y} \\
M_{3x} &= M_{3y} = 5\%M_{3z}
\end{aligned} \tag{4.56}$$

Fig. 4.8 shows the attitude tracking of the coupled and decoupled LST model. The required controller effort for both the models is shown in Fig. 4.9. The control signal is limited to ± 2000 Nm. The attitude error Quaternions are shown in Fig. 4.10. The attitude tracking, controller effort and the tracking error plots shows the small but significant amount of coupling present in the coupled LST model. Fig. 4.8 shows the overshoot in attitude tracking for the coupled model and is slightly higher than the decoupled case. Fig. 4.9 illustrates a slightly higher controller effort for the coupled LST compared to the decoupled case, although the control signal is bounded between ± 2000 Nm. In a similar manner the peak value of the tracking error is higher for the coupled case when compared to the decoupled model and is evident from Fig. 4.10.

Fig. 4.11 shows the roll axis stabilization and control for the coupled and decoupled LST model wherein the objective is to achieve attitude tracking about the roll axis i.e. ($\phi = 20^\circ$). The pitch and yaw attitude remain the same as specified in the initial conditions stated in (4.48). The purpose of such an illustration is to visualize the inter-axis coupling and how a specific channel output is achieved in spite of the interactions from other channels. The control signal is limited to ± 2000 Nm and the required controller effort is shown in Fig. 4.12. The attitude error Quaternion in this case is shown in Fig. 4.13. Figs. 4.11-4.13 illustrate that there is a significant amount of coupling in the LST model and is slightly more in the coupled case when compared with the decoupled model. Although pitch and yaw reference is unchanged from their initial values, they vary a lot before settling back to their initial values of $\theta = 8^\circ$ and $\psi = 5^\circ$. Steady state values for θ and ψ in the decoupled case is achieved at approximately 35 seconds whereas in the coupled case steady state is achieved in 37 seconds. The peak value of the second channel control signal (M_{2y}), exceeds 1000 Nm in the coupled case while in the decoupled case it is less than 1000 Nm. A similar response is observed for the

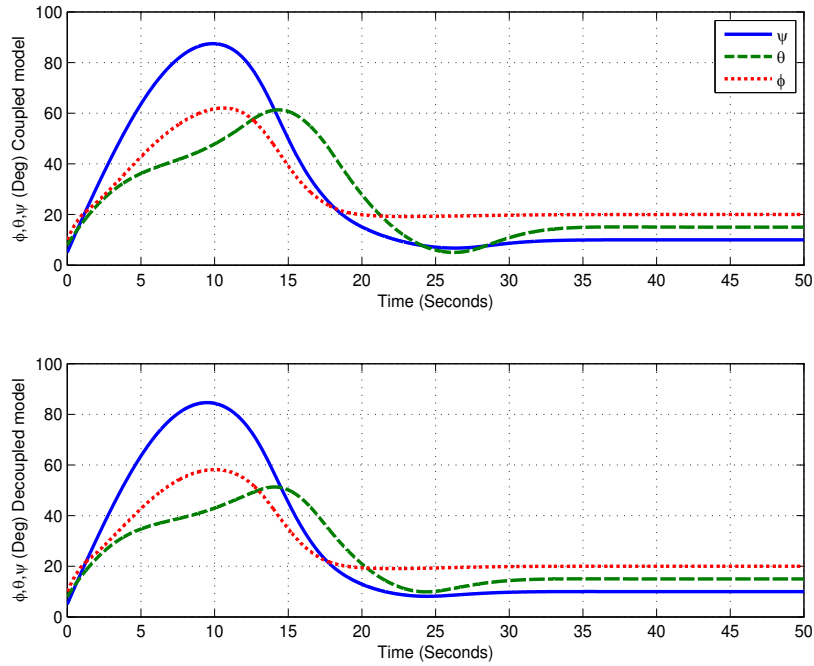


Figure 4.8: Attitude tracking of coupled and decoupled LST model

negative peak value of the first channel control signal (M_{1x}). Similarly, from Fig. 4.13 the error in coupled case takes a longer time to go zero while it is less in the decoupled case. These facts explain the significance of the coupling terms involved in the coupled model.

4.8 Conclusions and Future Work

In this chapter, a case study was presented on a LST model developed by NASA [2] & [44]. The LST model considered by [44] is linear and decoupled. We have attempted to derive a fully coupled nonlinear dynamic model fitted with three reaction wheels as actuators. In doing so, we took into account the nonlinear coupling terms, the inertia tensors and the angular velocity terms neglected in [44]. The derived LST model dynamic equation was cascaded with a Quaternion based kinematic model and simulated using a state feedback control law proposed in [62] to achieve time varying attitude tracking. Simulation results have been illustrated demonstrating the stabilization and control of the coupled and decoupled LST model. Single channel attitude stabilization is

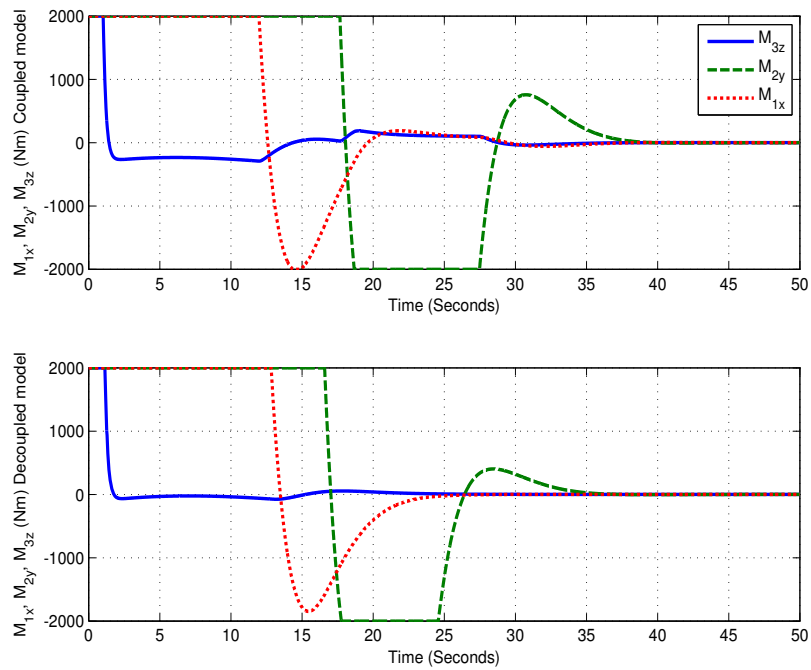


Figure 4.9: Attitude tracking control torque input for coupled and decoupled LST model

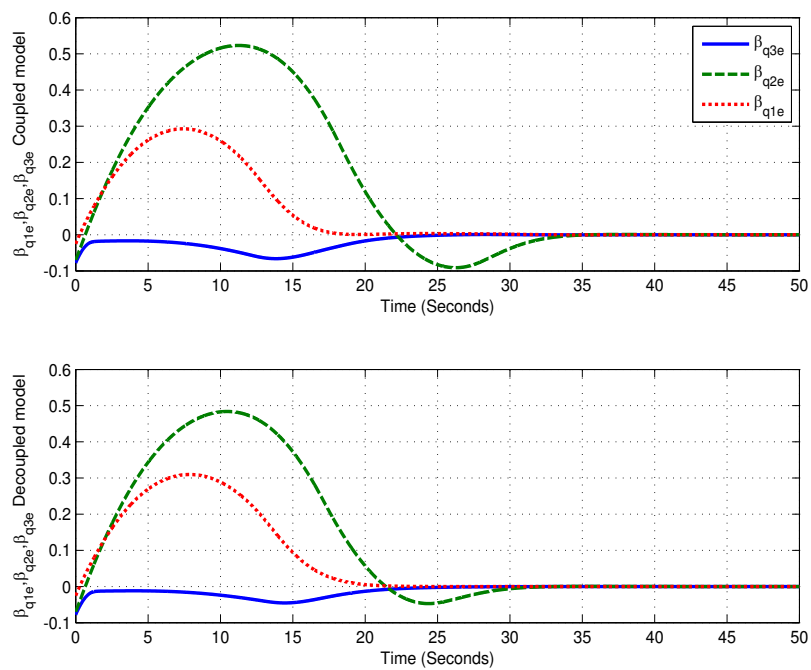


Figure 4.10: Attitude error quaternions of coupled and decoupled LST model

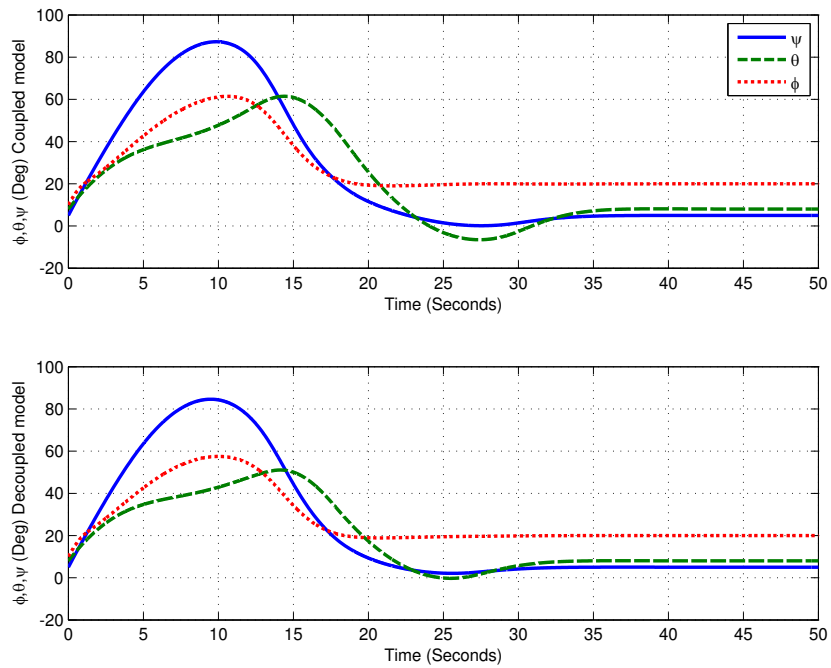


Figure 4.11: Roll axis stabilization and control of coupled and decoupled LST model

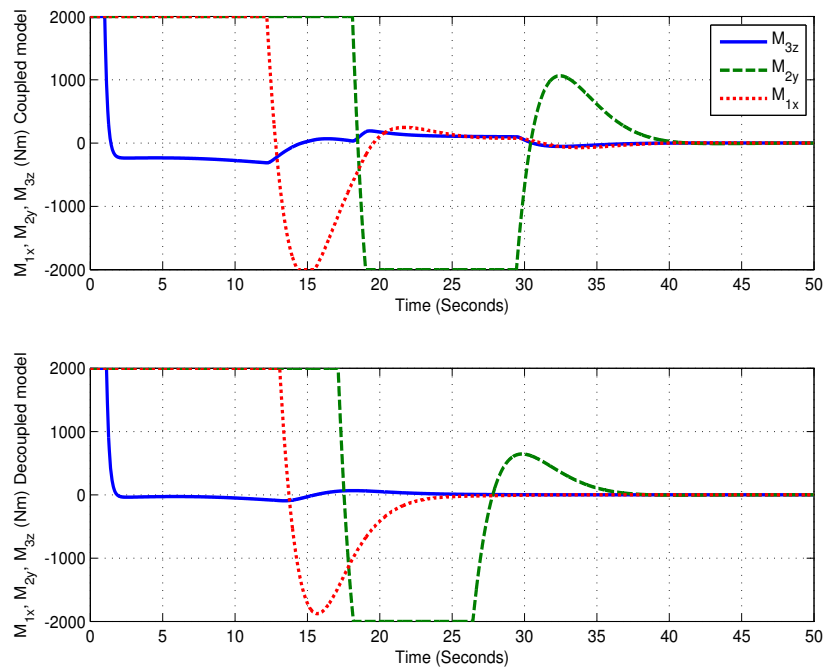


Figure 4.12: Roll axis stabilization control torque input for coupled and decoupled LST model

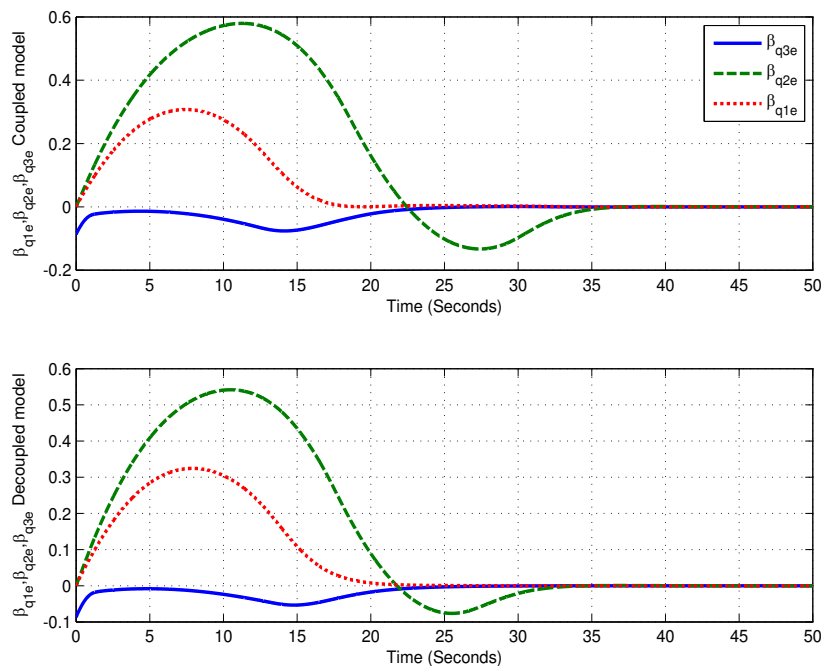


Figure 4.13: Roll axis stabilization error for coupled and decoupled LST model

illustrated in order to visualize the inter-axis coupling. It was verified from simulations that the state feedback control law is able to achieve time varying attitude tracking in the presence of environmental disturbances such as (gravity gradient, magnetic, aerodynamic & solar pressure) and actuator failures at specific intervals of time. The state feedback control parameters have been selected at random in this case study. The use of optimal algorithms to infer the best controller parameters can be a possible extension in the future. A Lyapunov stability analysis can be performed which ensures global asymptotic stability of the LST model using the state feedback approach.

Chapter 5

Study of MIMO Subsystem

Interactions for Better Performance and Fault Tolerance

5.1 Introduction

A MIMO system comprises of more than one input and output and is generally categorized into two types, namely, decoupled and coupled. In a decoupled MIMO system, an individual input mainly affects an individual output whereas in a coupled system multiple inputs affects a single output. Coupled systems are more difficult to control in comparison to decoupled systems because of the channel interactions. MIMO systems can either be controlled by a centralized control structure or by a set of Single-Input-Single-Output (SISO) decentralized controllers. Decentralized control is preferred over the centralized control for the following reasons [39]:

- Decentralized control has a simple design and can be easily implemented.
- Each loop can be independently tuned with fewer tuning parameters compared to centralized controllers.

On the contrary, centralized controllers are more complex and lack integrity which is a key property in decentralized control and ensures that the closed-loop system remains stable as the subsystem controllers are brought in and out of service [50]. There are two key steps involved in the successful design of a decentralized controller, namely, loop configuration and controller tuning [27]. Loop configuration is defined as pairing the manipulated variables and the controlled variables to achieve minimum interactions among loops so that the resulting multivariable control system mostly resembles a collection of SISO counterparts and the subsequent controller tuning can be largely facilitated by SISO design techniques [68]. Hence the main objective in selecting an appropriate loop configuration is to result in a multivariable plant close to being diagonally dominant. In order to have such a loop configuration, we need to have some information about the subsystem interactions. The concept of Relative Gain Array (RGA) was first introduced by Bristol in 1966 [11]. The RGA is an empirical measure of interaction and has found widespread acceptance in the control community because of its simplicity. In order to overcome its limitations many extensions and generalizations like, the Niederlinski Index (NI) [36], Dynamic Relative Gain Array (DRGA) [65], Effective Relative Gain Array (ERGA) [68], Partial Relative Gain Array (PRGA) [21], Relative Interaction Array (RIA) [69] and Effective Relative Energy Array (EREA) [35] have been proposed. These generalized forms of RGA have outlined their set of rules which can be followed to form a loop configuration resulting in the most decoupled system. As the decoupled system would be least interactive, its controller design would be much easier when compared to its most interactive counter part.

However, the choice of best loop configuration when an input channel is prone to actuator degradation has not been explicitly addressed in the literature. While decentralized control aims to decouple a MIMO system such that there are minimum interactions among its subsystems by choosing an appropriate loop configuration depending on interactive measures such as (RGA, NI, RIA, ERGA & EREA), the "opposite" case can prove to be useful when there are actuator degradations. In such a case the subsystem

interactions can aid the degraded channel for a better performance of the whole system. In this chapter such an actuator degradation problem is considered along the line of system configuration. A new approach for structure configuration of MIMO systems in both open and closed-loop is presented. A simple interaction measure based on H_∞ norm of the MIMO subsystems is defined namely, the (*RDI*). The *RDI* helps in understanding the effect of one input on an output. Simple guidelines are given which are effective in configuring an open and closed-loop system towards coupling and decoupling. The effectiveness of the *RDI* is verified by simulation results and a performance measure given in terms of RMSE. The *RDI* is further extended to the (*i.i.i.*) which helps in investigating how the overall system output would be affected by actuator degradation which occurs on each individual input channels. Applications of *RDI* and *i.i.i.* are analyzed and compared with the use of RGA, NI, RIA, ERGA & EREA in examples. In literature, the concept of system configuration has been addressed by existing interaction measures stated earlier and their effectiveness was mainly demonstrated by examples on distillation columns. In this chapter, *RDI* and its associated guidelines are tested on similar examples to verify the effectiveness of the approach and compare it with existing interaction measures. *i.i.i.* has been shown to predict the channel vulnerability to actuator failure based on the inherent plant interaction for the spacecraft attitude model discussed in chapter 3.

In the next section the existing interaction measures and their guidelines are first introduced and their decoupling measures are illustrated with examples.

5.2 Existing Interaction Measures

In this section we give an overview of RGA. Some important properties, drawbacks of RGA and its extensions to overcome the drawbacks are outlined. It is worthwhile to mention that RGA and its subsequent analysis are transfer function based. The extension of RGA based on the state space model can be found in [27].

5.2.1 Relative Gain Array

Consider a multivariable system with " n " inputs and " n " outputs described by the following transfer function matrix

$$G(s) = \begin{bmatrix} g_{11}(s) & g_{12}(s) & \dots & g_{1n}(s) \\ g_{21}(s) & g_{22}(s) & \dots & g_{2n}(s) \\ \dots & \dots & \dots & \dots \\ g_{n1}(s) & g_{n2}(s) & \dots & g_{nn}(s) \end{bmatrix} \quad (5.1)$$

The relative gain for a selected pair of input-output variables is defined as the ratio of the open loop dc-gain of that pair, with all other loops open, to their open loop gain when all other loops in the system are closed

$$\lambda_{i,j} = \frac{(\partial y_i / \partial u_j)_{\text{all loops open}}}{(\partial y_i / \partial u_j)_{\text{all other loops closed except for loop } y_i - u_j}} \quad (5.2)$$

where y_i is the i^{th} controlled variable and u_j is the j^{th} manipulated variable.

The RGA is then defined as follows:

$$\Lambda(G) = G \otimes G^{-T} = \begin{bmatrix} \lambda_{11} & \lambda_{12} & \dots & \lambda_{1n} \\ \lambda_{21} & \lambda_{22} & \dots & \lambda_{2n} \\ \dots & \dots & \dots & \dots \\ \lambda_{n1} & \lambda_{n2} & \dots & \lambda_{nn} \end{bmatrix} \quad (5.3)$$

where the operator " \otimes " is the Hadamard product and G^{-T} represents the transpose of the inverse of G .

Example 5.2.1 Consider the following multivariable system [24]

$$G_1(s) = \begin{bmatrix} \frac{-2e^{-s}}{10s+1} & \frac{1.5e^{-s}}{s+1} & \frac{e^{-s}}{s+1} \\ \frac{1.5e^{-s}}{s+1} & \frac{e^{-s}}{s+1} & \frac{-2e^{-s}}{10s+1} \\ \frac{e^{-s}}{s+1} & \frac{-2e^{-s}}{10s+1} & \frac{1.5e^{-s}}{s+1} \end{bmatrix} \quad (5.4)$$

The corresponding RGA is

$$\Lambda(G_1(s)) = \begin{bmatrix} -0.9302 & 1.1860 & 0.7442 \\ 1.1860 & 0.7442 & -0.9302 \\ 0.7442 & -0.9302 & 1.1860 \end{bmatrix} \quad (5.5)$$

The RGA matrix for the multivariable system in (5.4) is shown in (5.5). The RGA possesses the following main properties [11]:

1. Summation of the rows and columns of the RGA are equal to unity
2. It is independent of input/output scaling
3. $\lambda_{i,j}$ is independent of how the $n-1$ loops are paired
4. Any permutation of rows and columns in the system transfer function matrix $G(s)$ leads to the same permutation in the RGA
5. If the transfer function matrix $G(s)$ is triangular or diagonal, the RGA will be an identity matrix

5.2.2 Implications of RGA

The values of λ_{ij} can cover all possible numbers from $-\infty$ to $+\infty$. They can be classified into six different categories as follows:

1. $\lambda_{i,j} = 1$
2. $\lambda_{i,j} = 0$
3. $\lambda_{i,j} = \pm\infty$
4. $\lambda_{i,j} < 0$
5. $0 < \lambda_{i,j} < 1$
6. $\lambda_{i,j} > 1$

A discussion of each category with its properties and implications can be found in [31] & [27]. The role of RGA as an indicator of sensitivity to uncertainty is dealt with in [50]. The most desirable value of λ is 1, which indicates that the open loop and the closed loop gains in (5.2) are the same and there is no interaction from other subsystems. A general square system with " n " inputs and " n " outputs will have $n!$ loop configurations. The system described in Example 5.2.1 will have six different loop configurations and their respective RGA values are shown in Table 5.1

Table 5.1: Loop configurations and their respective RGA

Loop Configurations	RGA
$u_1 - y_1, u_2 - y_2, u_3 - y_3$	diag(-0.9302, 0.7442, 1.1860)
$u_1 - y_1, u_2 - y_3, u_3 - y_2$	diag(-0.9302, -0.9302, -0.9302)
$u_1 - y_2, u_2 - y_1, u_3 - y_3$	diag(1.1860, 1.1860, 1.1860)
$u_1 - y_2, u_2 - y_3, u_3 - y_1$	diag(1.1860, -0.9302, 0.7442)
$u_1 - y_3, u_2 - y_1, u_3 - y_2$	diag(0.7442, 1.1860, -0.9302)
$u_1 - y_3, u_2 - y_2, u_3 - y_1$	diag(0.7442, 0.7442, 0.7442)

It can be observed from Table 5.1 that the possible choice of loop configurations which are close to being decoupled are $u_1 - y_2, u_2 - y_1, u_3 - y_3$ and $u_1 - y_3, u_2 - y_2, u_3 - y_1$ as they satisfy the RGA based pairing rule of closeness to 1. However, several pairs may

satisfy the RGA guideline and one may run into ambiguity as in the present case. To resolve this issue an intuitive measure of the overall interaction was suggested in [70] given as follows:

$$\min \sum |\lambda_{i,j}^k - 1| \quad (5.6)$$

where $\lambda_{i,j}^k$ denotes the paired RGA elements corresponding to the k^{th} loop configuration. Therefore in the case of several pairing alternatives proposed by the RGA, the overall measure given in (5.6) can be used for identifying the pairing with minimum overall interaction. However, as the distance of the RGA elements from 1 does not quantify the amount of interaction, this measure is found to be inadequate under some circumstances and inherits the same limitations from the RGA [69] & [27]. The concept of RIA was introduced to overcome these shortcomings in [69] and will be discussed next.

5.2.3 Relative Interaction Array

The RIA is defined as follows [69]:

$$\phi_{i,j} = \frac{1}{\lambda_{ij}} - 1 \quad (5.7)$$

and also

$$\lambda_{i,j} = \frac{1}{\phi_{ij} + 1} \quad (5.8)$$

Hence in matrix form RIA can be defined as follows

$$\Phi(G) = \begin{bmatrix} \phi_{11} & \phi_{12} & \dots & \phi_{1n} \\ \phi_{21} & \phi_{22} & \dots & \phi_{2n} \\ \dots & \dots & \dots & \dots \\ \phi_{n1} & \phi_{n2} & \dots & \phi_{nn} \end{bmatrix} \quad (5.9)$$

The corresponding RIA matrix for the system described in (5.4) is given as follows

$$\Phi(G_1(s)) = \begin{bmatrix} -2.0750 & -0.1568 & 0.3437 \\ -0.1568 & 0.3437 & -2.0750 \\ 0.3437 & -2.0750 & -0.1568 \end{bmatrix} \quad (5.10)$$

The RIA matrix characterizes the following implications about loop interactions [69]:

1. $\phi_{ij} = 0$ implies that there is no interaction and $\lambda_{ij} = 1$
2. $\phi_{ij} > 0$ implies that interaction acts in the same direction as the interaction free system.
3. $\phi_{ij} > 1$ implies interaction dominates over interaction free system gain.
4. $\phi_{ij} < 0$ implies interaction acts in the reverse direction as interaction free system gain.
5. $\phi_{ij} < -1$ implies reverse interaction dominates over interaction free system gain

5.2.4 Niederlinski Index

Integrity is an important and desirable feature of a decentralized control system which ensures the closed-loop stability as the subsystem controllers are brought in and out of service [11]. Niederlinski, [36], in 1971 introduced a theorem for solving the integrity problem which is stated as follows [18]: *"The closed loop system consisting of the multivariable system in (5.1) and a multiloop control system is structurally monotonic unstable if and only if"*

$$NI \triangleq \frac{\det[G(0)]}{\prod_{i=1}^k G_{ii}(0)} < 0 \quad (5.11)$$

where 'k' is the total number of individual loops. The NI serves as an important stability rule which states that the loop should be configured in such a way that the corresponding NI is positive. In addition to the stability and integrity depending on its sign, NI has

been extended to measure the overall interaction by its size [70], which states that the loop should be configured in a such a way that the resulting NI is close to 1.

RGA-RIA-NI based pairing rules:

Based on the properties of RGA, RIA and NI the following points are crucial for a decoupled loop configuration:

- Configure the system loop with corresponding RGA close to one, [11].
- RGA elements must be positive.
- Large RGA elements are not appropriate for loop configuration [49].
- NI must be positive and close to one, [18] & [70].
- Configure the system loop such that all the RIA elements are close to zero, [69].
- All the RIA elements should be greater than -1 and the elements close to -1 should be avoided, [69].

For ease of notation the loop configurations will be denoted as follows:

$$u_1 - y_1, u_2 - y_2, u_3 - y_3 \equiv uy_{123}$$

$$u_1 - y_1, u_2 - y_3, u_3 - y_2 \equiv uy_{132}$$

$$u_1 - y_2, u_2 - y_1, u_3 - y_3 \equiv uy_{213}$$

$$u_1 - y_2, u_2 - y_3, u_3 - y_1 \equiv uy_{231}$$

$$u_1 - y_3, u_2 - y_1, u_3 - y_2 \equiv uy_{312}$$

$$u_1 - y_3, u_2 - y_2, u_3 - y_1 \equiv uy_{321}$$

The RIA and NI values for the six different loop configurations of the MIMO system in (5.4) are shown in Table 5.2.

Following the RGA-RIA-NI based rules $uy_{123}, uy_{132}, uy_{231}$ & uy_{312} are not recommended and only two loop configurations, namely, uy_{213} & uy_{321} can be selected. Similar to the RGA, two pairing candidates satisfy the pairing rules. In order to choose the best

Table 5.2: Loop configurations and their respective RIA, NI & $\Phi_{min}(G_1(s))$

Loop Configurations	RIA	NI	$\Phi_{min}(G)$
uy_{123}	diag(-2.0750, 0.3437, -0.1568)	1.7917	2.5755
uy_{132}	diag(-2.0750, -2.0750, -2.0750)	-0.6719	6.2250
uy_{213}	diag(-0.1568, -0.1568, -0.1568)	1.5926	0.4704
uy_{231}	diag(-0.1568, -2.0750, 0.3437)	1.7917	2.5755
uy_{312}	diag(0.3437, -0.1568, -2.0750)	1.7917	2.5755
uy_{321}	diag(0.3437, 0.3437, 0.3437)	5.3750	1.0311

pair for a decoupled loop configuration an overall interaction measure based on RIA is proposed in [69] given as follows:

$$\Phi_{min}(G) = \min \sum |\phi_{ij}^k| \quad (5.12)$$

where ϕ_{ij}^k denotes the paired RIA elements corresponding to the k^{th} loop configuration. This interaction measure identifies the pairing with the minimum overall interaction. (5.12) can also be expressed in terms of its respective RGA elements as follows.

$$\min \sum \left| \frac{1}{\lambda_{ij}^k} - 1 \right| \quad (5.13)$$

Hence the following statement can be added to the RGA-RIA-NI set of rules [69].

- Configure the system loop for which, $\Phi_{min}(G)$ is minimum

From Table 5.2, it can be inferred that the loop configuration corresponding to uy_{213} is the most decoupled system as it has the least overall interaction based on RIA in addition to satisfying the RGA-RIA-NI set of rules. The RIA and NI measures do not provide much insight about the subsystem interactions than the RGA, although they provide valuable alternative points. This is mainly due to the fact that RGA, RIA and NI analyze the system at steady state, but otherwise the interactions may vary at

different operating frequencies. To address this issue the concept of Dynamic Relative Gain Array (DRGA) was introduced by Witcher & McAvoy [65] in 1977. It is basically an extension of RGA [11] defined as follows:

$$DRGA(G) = G(j\omega) \otimes G(j\omega)^{-T} \quad (5.14)$$

The DRGA is a computationally involved approach which overcomes the limitations of the static RGA by considering the effects of the system dynamics. However, RGA is independent of controller design, but these features are lost in DRGA which depends on the controller structure [12] & [58]. To combine the advantages of both RGA and DRGA and overcome their deficiencies the concept of ERGA was proposed by Xiong et al in 2005 [68] and will be discussed in the following section.

5.2.5 Effective Relative Gain Array

ERGA is an extension of RGA, wherein two factors are considered namely, the steady state gain and the response speed or the system bandwidth. ERGA utilizes both these information in providing a measure of the subsystems interaction. The steady state gain reflects the effect of the manipulated variable u_j on the controlled variable y_i and the response speed accounts for the sensitivity of y_i to u_j indicating the interaction rejection ability of the plant. The notable feature of ERGA is that it is controller independent and suggests a loop configuration with minimal interaction within the interested frequency range both statically and dynamically and is defined as follows [68]:

$$\zeta_{i,j} = \frac{e_{i,j}}{\hat{e}_{i,j}} \quad (5.15)$$

where $e_{i,j}$ is the effective gain for a particular transfer function when all other loops are open, given by

$$e_{i,j} = \underbrace{g_{i,j}(0)}_{\text{steady state gain}} \underbrace{\int_0^{\omega_{B, i,j}} |g_{i,j}^0(j\omega)| d\omega}_{\text{response speed}} \quad (5.16)$$

where $\omega_{B, i,j}$ for $i, j = 1, 2, \dots, n$ are the bandwidth of the transfer function $g_{ij}^0(j\omega)$. The bandwidth of a transfer function are the frequencies from which the steady state gain is attenuated more than 3 dB i.e.

$$g_{i,j}(j\omega_{B, i,j}) = \frac{g_{i,j}(0)}{\sqrt{2}} \quad (5.17)$$

To simplify the calculation the integration of e_{ij} is approximated by a rectangular area and e_{ij} is given by [68]:

$$e_{i,j} \approx g_{i,j}(0)\omega_{B, i,j} \text{ for } i, j = 1, 2, \dots, n \quad (5.18)$$

$\hat{e}_{i,j}$ is the effective gain between the controlled variable y_i and the manipulated variable u_j when all other loops are closed.

In terms of matrix the effective gain can be expressed as follows:

$$E = G(0) \otimes \Omega \quad (5.19)$$

where

$$G(0) = \begin{bmatrix} g_{11}(0) & g_{12}(0) & \dots & g_{1n}(0) \\ g_{21}(0) & g_{22}(0) & \dots & g_{2n}(0) \\ \dots & \dots & \dots & \dots \\ g_{n1}(0) & g_{n2}(0) & \dots & g_{nn}(0) \end{bmatrix} \quad (5.20)$$

and

$$\Omega = \begin{bmatrix} \omega_{B,11} & \omega_{B,12} & \cdots & \omega_{B,1n} \\ \omega_{B,21} & \omega_{B,22} & \cdots & \omega_{B,2n} \\ \cdots & \cdots & \cdots & \cdots \\ \omega_{B,n1} & \omega_{B,n2} & \cdots & \omega_{B,nn} \end{bmatrix} \quad (5.21)$$

Finally, in terms of matrix the ERGA is given by

$$\Upsilon(G) = E \otimes E^{-T} = \begin{bmatrix} \zeta_{11} & \zeta_{12} & \cdots & \zeta_{1n} \\ \zeta_{21} & \zeta_{22} & \cdots & \zeta_{11} \\ \cdots & \cdots & \cdots & \cdots \\ \zeta_{n1} & \zeta_{n2} & \cdots & \zeta_{nn} \end{bmatrix} \quad (5.22)$$

As both RGA and ERGA use relative gains, the properties and implications of RGA discussed earlier can be extended to ERGA. Similar to the RGA-RIA-NI based pairing rules the ERGA-NI based pairing rules can be summarized as follows [68]:

ERGA-NI based pairing rules

1. Configure the system loop with corresponding ERGA elements closest to one and are positive.
2. Large ERGA elements should be avoided.
3. NI must be positive.

The corresponding ERGA matrix for the system described in (5.4) is given as follows:

$$\Upsilon(G_1(s)) = \begin{bmatrix} 0.0554 & 0.6977 & 0.2468 \\ 0.6977 & 0.2468 & 0.0554 \\ 0.2468 & 0.0554 & 0.6977 \end{bmatrix} \quad (5.23)$$

From the above ERGA matrix for the system in (5.4), the loop configuration corresponding to uy_{213} satisfies the ERGA-NI set of rules, primarily the rule of being closest to 1 [68] and suggests uy_{213} as the most decoupled loop configuration. In the next section

another measure of interaction called the Effective Relative Energy Array is discussed which complements ERGA.

5.2.6 Effective Relative Energy Array

EREA is an extension of ERGA proposed by Naini et al [35] in 2009. Similar to the case of ERGA both the steady state gain and response speed are utilized in calculating subsystem interactions of a coupled system. The effective energy of a particular transfer function is defined as follows [35]:

$$ef_{i,j} = |g_{i,j}(0)|g_{i,j}(0)\omega_{B, i,j} \quad (5.24)$$

where $\omega_{B, i,j}$ for $i, j = 1, 2, \dots, n$ are the bandwidth of the transfer function $g_{i,j}^0(j\omega)$. The effective energy matrix is calculated as follows:

$$F = |G(0)| \otimes G(0) \otimes \Omega \quad (5.25)$$

where

$$|G(0)| = \begin{bmatrix} |g_{11}(0)| & |g_{12}(0)| & \dots & |g_{1n}(0)| \\ |g_{21}(0)| & |g_{22}(0)| & \dots & |g_{2n}(0)| \\ \dots & \dots & \dots & \dots \\ |g_{n1}(0)| & |g_{n2}(0)| & \dots & |g_{nn}(0)| \end{bmatrix} \quad (5.26)$$

and Ω is the bandwidth matrix defined in (5.21)

In terms of matrix the EREA is given as follows

$$\Upsilon(G) = F \otimes F^{-T} \quad (5.27)$$

The EREA matrix also possesses the important property of rows and columns summing to one. Similar to the cases of RGA-RIA-NI and ERGA-NI, EREA-NI based loop configuration rules have been proposed in [35] and are discussed below:

EREA-NI based pairing rules

1. Configure the system loop with corresponding EREA elements closest to one and are positive.
2. Large EREA elements should be avoided.
3. NI must be positive.

The corresponding EREA matrix for the system described in (5.4) is given as follows:

$$\Upsilon(G_1(s)) = \begin{bmatrix} 0.0556 & 0.8179 & 0.1264 \\ 0.8179 & 0.1264 & 0.0556 \\ 0.1264 & 0.0556 & 0.8179 \end{bmatrix} \quad (5.28)$$

From the above EREA matrix for the system in (5.4), the loop configuration corresponding to uy_{213} satisfies the EREA-NI set of rules, primarily the rule of being closest to one [35] and suggests uy_{213} as the most decoupled loop configuration.

Therefore, ERGA and EREA pairing rules complement each other and in certain cases EREA measure can provide valuable insight and suggest an acceptable loop configuration while ERGA may guide us to an improper loop configuration. This has been demonstrated with an example in [35].

Based on the existing interaction measures and their guidelines, one can configure a system towards more coupling by following the "counter" pairing rules of RGA, RIA, NI, ERGA & EREA discussed before. In this case the input-output pair should be chosen such that:

1. RGA, NI, ERGA & EREA are farthest from one or negative.
2. RIA is close to -1 or farthest from zero.

Table 5.3: Existing interaction measures for $G_2(s)$

$$\text{RGA: } \Lambda(G_2(s)) = \begin{bmatrix} -0.2010 & 1.2024 & -0.0014 \\ 1.5941 & -0.3623 & -0.2318 \\ -0.3931 & 0.1599 & 1.2332 \end{bmatrix}$$

$$NI_{uy_{123}} = -4.0544, \quad NI_{uy_{132}} = 21.8937, \quad NI_{uy_{213}} = 0.6757$$

$$NI_{uy_{231}} = -3.6039, \quad NI_{uy_{312}} = 8.7575, \quad NI_{uy_{321}} = -8.6494$$

$$\text{RIA: } \Phi(G_2(s)) = \begin{bmatrix} -5.9759 & -0.1683 & -701.6000 \\ -0.3727 & -3.7604 & -5.3140 \\ -3.5439 & 5.2554 & -0.1891 \end{bmatrix}$$

$$\Phi_{uy_{213}} \equiv \Phi_{\min}(G_2(s)) = 0.7301$$

$$\text{ERGA: } \Upsilon(G_2(s)) = \begin{pmatrix} 0.0053 & 0.6855 & 0.3092 \\ -0.1257 & 0.3277 & 0.7980 \\ 1.1204 & -0.0132 & -0.1072 \end{pmatrix}$$

$$\text{EREA: } \Upsilon(G_2(s)) = \begin{pmatrix} 0.0184 & 0.5852 & 0.3965 \\ -1.8893 & 0.4302 & 2.4591 \\ 2.8709 & -0.0154 & -1.8556 \end{pmatrix}$$

Example 5.2.2 Consider a transfer function model, $G_2(s)$ given by [41]

$$\begin{bmatrix} y_1 \\ y_2 \\ y_3 \end{bmatrix} = G_2(s) \begin{bmatrix} u_1 \\ u_2 \\ u_3 \end{bmatrix} \quad (5.29)$$

where

$$G_2(s) = \begin{bmatrix} \frac{0.4}{(s+1)^2} & \frac{4(s+3)}{(s+5)(s+2)} & \frac{-2}{s+4} \\ \frac{2}{(s+2)(s+1)} & \frac{2}{(s+2)^2} & \frac{1}{(s+2)} \\ \frac{6(-s+1)}{(s+5)(s+4)} & \frac{4}{(s+3)^2} & \frac{8}{(s+2)(s+5)} \end{bmatrix} \quad (5.30)$$

Table 5.3 shows the existing interaction measures for the MIMO system in (5.29).

The RGA-NI-RIA pairing rules suggest uy_{213} as being close to decoupled [27] & [41].

The ERGA-EREA pairing rules suggest pairing uy_{231} but their corresponding NI is negative. [41] have used the approach of Participation Matrix (PM) in suggesting uy_{213} as the most decoupled pair. The system structure towards coupling cannot be accurately known from the existing measures following the "opposite" rules and can be any one from the six possible pairs. A system configured towards coupling and decoupling can be accurately known by its simulation and assessing its response in terms of a performance measure to be defined in the next section.

5.3 RMSE based Performance Measure

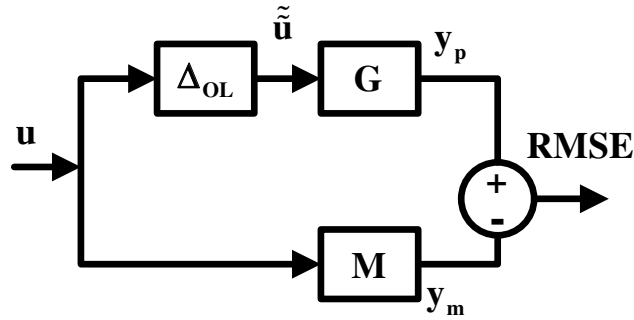


Figure 5.1: RMSE based plant-model performance measure in open-loop

In this section a performance measure is defined which illustrates the decoupled and coupled system configuration based on the simulation of the system and its model. RMSE is used as a performance measure in identifying the system configured towards decoupling and coupling. Fig. 5.1 shows the plant (G) and its model (M). Actuator degradation is considered in this work. Hence, when there is no actuator degradation, $M = G$ in the simulation.

Δ_{OL} is the input effectiveness matrix given as follows:

$$\Delta_{OL} = \begin{pmatrix} \delta_{ol1} & 0 & 0 & 0 \\ 0 & \delta_{ol2} & 0 & 0 \\ 0 & 0 & \dots & 0 \\ 0 & 0 & 0 & \delta_{oln} \end{pmatrix} \quad (5.31)$$

Table 5.4: RMSE for different system configurations and Δ_{OL} for $G_2(s)$

System configuration	RMSE	$\Delta_{OL} = \text{diag}[0 \ 1 \ 1]$	$\Delta_{OL} = \text{diag}[1 \ 0 \ 1]$	$\Delta_{OL} = \text{diag}[1 \ 1 \ 0]$
e_{uy123}		0.3940	1.1918	0.4969
		0.9875	0.4950	0.4962
		0.2979	0.1467	0.7932
e_{uy132}		0.3940	0.4969	1.1918
		0.9875	0.4962	0.4950
		0.2979	0.7932	0.1467
e_{uy213}		1.1918	0.3940	0.4969
		0.4950	0.9875	0.4962
		0.1467	0.2979	0.7932
e_{uy231}		1.1918	0.4969	0.3940
		0.4950	0.4962	0.9875
		0.1467	0.7932	0.2979
e_{uy312}		0.4969	0.3940	1.1918
		0.4962	0.9875	0.4950
		0.7932	0.2979	0.1467
e_{uy321}		0.4969	1.1918	0.3940
		0.4962	0.4950	0.9875
		0.7932	0.1467	0.2979

$y_p = [y_{p1} \ y_{p2} \ \dots \ y_{pn}]^T$ is the plant output and $y_m = [y_{m1} \ y_{m2} \ \dots \ y_{mn}]^T$ is the model output. RMSE between the plant and its model is given by the following relation:

$$\begin{aligned}
e_1 &\triangleq \frac{1}{N} \sqrt{\sum_{i=1}^N (y_{p1}(i) - y_{m1}(i))^2} \\
e_2 &\triangleq \frac{1}{N} \sqrt{\sum_{i=1}^N [y_{p2}(i) - y_{m2}(i)]^2} \\
&\quad \vdots \\
e_n &\triangleq \frac{1}{N} \sqrt{\sum_{i=1}^N [y_{pn}(i) - y_{mn}(i)]^2}
\end{aligned} \tag{5.32}$$

$$e \triangleq [e_1, e_2, \dots, e_n]$$

where N is the number of sampling points.

When a system structure is closer to decoupling an output will largely depend on its respective input and be less affected from other inputs. A structure closer to coupling is affected from other inputs as well as its respective input. The actuator effectiveness array Δ_{OL} in (5.31) is selected such that only one input is faulty. For a system structure closer to decoupling the channel with faulty input will have the maximum error and the structure closer to coupling will have the minimum error given in (5.32).

Table 5.4 shows the RMSE values for the six possible loop configurations of the MIMO system described in (5.29) with the input effectiveness matrix defined in (5.31). It can be observed from Table 5.4 that for the system structure uy_{213} the RMSE for a channel is maximum in comparison to the other loop configurations, when its respective input is zero i.e., for the input-output pair uy_{213} , $e_1 = 1.1918$ when $u_1 = 0$, $e_2 = 0.9875$ when $u_2 = 0$ and $e_3 = 0.7932$ when $u_3 = 0$. Hence the RMSE based performance measure confirms the system structure uy_{213} as the most decoupled configuration. It should be recalled that the (RGA-NI-RIA) based pairing also recommends uy_{213} as the most decoupled configuration, whereas (ERGA-EREA) based pairing recommends uy_{231} as more towards decoupling. In order to find the system structure towards coupling,

we look for the channel with minimum RMSE value when its respective input is set to zero from Table 5.4. In this case the RMSE will be minimum because the output will depend more on other channel inputs rather than its corresponding input. The system structure uy_{132} has the minimum RMSE namely, $e_1 = 0.3940$, when $u_1 = 0$ and $e_3 = 0.1467$, when $u_3 = 0$. Although e_2 in uy_{132} is greater than e_2 in uy_{132} , i.e. $0.4962 > 0.4950$ but the difference is negligible when compared to e_3 in uy_{132} & uy_{123} , i.e. $0.1467 < 0.7932$. Hence in comparison the RMSE is minimum for uy_{132} when Δ_{OL} is varied. This illustrates that uy_{132} is the most coupled configuration. However this cannot be inferred from the existing measures using the "counter" pairing rules discussed previously.

5.4 H_∞ Norm based Interaction Index

In this section, a new index called as Relative Dependency Index (RDI), and RDI Array (RDIA), is introduced. The proposed index shows the relative dependency of an output upon an input of an open and closed-loop MIMO system. It is efficient in providing information in MIMO systems to help facilitate:

1. Decoupling in open-loop stable systems.
2. Decoupling in closed-loop systems.
3. Predicting channel vulnerability in case of actuator degradation for open and closed-loop systems.

5.4.1 Decoupling in Open-loop Stable System

Relative Dependency Index: The *RDI* for the MIMO system $G(s)$ in (5.1) is defined as follows, for the pair of i^{th} output and j^{th} input:

$$f_{i,j} \triangleq \frac{\|g_{i,j}(s)\|_\infty}{\|[g_{i,1}(s) \cdots g_{i,j-1}(s) g_{i,j+1}(s) \cdots g_{i,n}(s)]\|_\infty} \quad (5.33)$$

$f_{i,j} = \infty$, if $[g_{i,1}(s) \dots g_{i,j-1}(s) g_{i,j+1}(s) \dots g_{i,n}(s)]$ is a zero transfer function vector. $f_{i,j}$ shows the relative dependency of the i^{th} output upon the j^{th} input of a MIMO system. The constant matrix $f(G) \triangleq [f_{i,j}]$, for $i, j = 1, \dots, n$ is called *RDIA* of $G(s)$ in (5.1). With $f(G)$, structure configuration of $G(s)$ can be inferred. The following procedure can be followed in studying the open-loop interactions of the system.

Near-decoupling configuration procedure of an open-loop system

1. Calculate the *RDIA*, $f(G)$, for the MIMO system $G(s)$.
2. Select the largest element of $f(G)$ for the i^{th} row, say $f_{i,j}$.
3. Permute the i^{th} output and the j^{th} input to the first output and input, respectively.
4. Repeat the above steps over the bottom-right $(n-1) \times (n-1)$ sub-matrix of permuted $f(G)$.

Consider the MIMO system $G_2(s)$ in (5.29), an example taken from [41]. The *RDIA* for $G_2(s)$ defined in (5.33) is given as follows:

$$\text{RDIA : } f(G_2(s)) = \begin{pmatrix} 0.3077 & 1.8741 & 0.3953 \\ 1.4142 & 0.4472 & 0.4472 \\ 0.8406 & 0.1734 & 1.1687 \end{pmatrix} \quad (5.34)$$

The *RDIA* for $G_2(s)$ in (5.34) shows the relative dependency of i^{th} output upon the j^{th} input as follows:

1. y_1 predominantly depends on u_2 and less depends on u_1 .
2. y_2 predominantly depends on u_1 and less depends on both u_2 and u_3 .
3. y_3 predominantly depends on u_3 and less depends on u_2 .

Therefore, the near decoupling configuration procedure suggests uy_{213} system structure more towards decoupling

In order to verify the veracity of *RDIA*, it can be compared with the RMSE based performance measure shown in Table 5.4. Since y_1 largely depends on u_2 , the error e_1 in e_{uy123} will be maximum when $u_2 = 0$, i.e. ($1.1918 > 0.3940$ & 0.4969). In a similar manner from the *RDIA*, it is known that y_2 largely depends on u_1 , so the error e_2 in e_{uy123} will be maximum when $u_1 = 0$, i.e. ($0.9875 > 0.4950$ & 0.4962) and as y_3 mainly depends on u_3 , the error e_3 in e_{uy123} will be maximum when $u_3 = 0$, i.e. ($0.7932 > 0.2979$ & 0.1467). For the system configuration towards minimal input dependence, the following can be inferred from Table 5.4:

1. As y_1 minimally depends on u_1 and the error e_1 in e_{uy123} will be minimum when $u_1 = 0$, i.e. ($0.3940 < 1.1918$ & 0.4969).
2. As y_3 minimally depends on u_2 , so the error e_3 in e_{uy123} will be minimum when $u_2 = 0$, i.e. ($0.1467 < 0.2979$ & 0.7932).

Hence the RMSE based performance measure also shows that the system structure uy_{213} is decoupled.

The existing interaction measures (RGA, NI, RIA, ERGA & EREA) and its associated guidelines aiming to decouple a system or the "counter" guidelines leading to a coupled system structure are inconsistent in configuring the system structure and understanding the effect of j^{th} input upon the i^{th} output. The *RDI* and *RDIA* overcomes these limitations and is efficient in studying the MIMO system interactions. This is further demonstrated by the following examples.

Example 5.2.3 Consider the two-input-two-output linearized transfer function model of a two product distillation column given in [20] as follows:

$$\begin{bmatrix} y_d \\ y_e \end{bmatrix} = G_3(s) \begin{bmatrix} u_d \\ u_e \end{bmatrix} \quad (5.35)$$

where

$$G_3(s) = \begin{bmatrix} g_{dd}(s) & g_{de}(s) \\ g_{ed}(s) & g_{ee}(s) \end{bmatrix} \quad (5.36)$$

$$g_{dd}(s) = \frac{0.012441(s + 0.2247)(s + 0.07857)(s^2 + 1.14s + 2.355)(s^2 + 12.24s + 93.58)}{(s + 1.788)(s + 0.2536)(s + 0.07541)(s + 0.005154)(s^2 + 1.328s + 3.138)}$$

$$g_{de}(s) = \frac{0.013772(s - 32.12)(s + 1.587)(s + 0.2315)(s + 0.09287)(s^2 + 1.31s + 3.162)}{(s + 1.788)(s + 0.2536)(s + 0.07541)(s + 0.005154)(s^2 + 1.328s + 3.138)}$$

$$g_{ed}(s) = \frac{0.079012(s + 0.2082)(s + 0.07361)(s^2 - 3.578s + 4.237)(s^2 - 2.374s + 11.69)}{(s + 1.788)(s + 0.2536)(s + 0.07541)(s + 0.005154)(s^2 + 1.328s + 3.138)}$$

$$g_{ee}(s) = \frac{0.0055124(s - 181.3)(s + 1.229)(s + 0.2169)(s + 0.06691)(s^2 + 1.328s + 3.407)}{(s + 1.788)(s + 0.2536)(s + 0.07541)(s + 0.005154)(s^2 + 1.328s + 3.138)} \quad (5.37)$$

- y_d : distillate
- y_e : bottom product composition
- u_d : reflux flow
- u_e : boilup flow

The detailed nonlinear and linearized dynamic model of the distillation column can be found in [20]. The distillation column given in (5.35) has two possible structure configurations and for ease of notation will be denoted as follows:

$$\begin{aligned} u_d - y_d, u_e - y_e &\equiv uy_{de} \\ u_d - y_e, u_e - y_d &\equiv uy_{ed} \end{aligned} \quad (5.38)$$

Table 5.5 shows the existing interaction measures for the distillation column given in (5.35). In order to configure the system towards decoupling based on (RGA, RIA, ERGA & EREA), the corresponding interaction measures should be close to one and large interaction elements have to be avoided [49], [68] & [35]. This would lead to

Table 5.5: Existing interaction measures for $G_3(s)$

$$\text{RGA: } \Lambda(G_3(s)) = \begin{pmatrix} 36.8729 & -35.8729 \\ -35.8729 & 36.8729 \end{pmatrix}$$

$$NI_{uy_{de}} = 0.0271, \quad NI_{uy_{ed}} = -0.0279$$

$$\text{RIA: } \Phi(G_3(s)) = \begin{pmatrix} -0.9729 & -1.0279 \\ -1.0279 & -0.9729 \end{pmatrix}$$

$$\Phi_{uy_{de}} \equiv \Phi_{\min}(G_3(s)) = 1.9458$$

$$\text{ERGA: } \Upsilon(G_3(s)) = \begin{pmatrix} 34.1568 & -33.1568 \\ -33.1568 & 34.1568 \end{pmatrix}$$

$$\text{EREA: } \Upsilon(G_3(s)) = \begin{pmatrix} 17.9847 & -16.9847 \\ -16.9847 & 17.9847 \end{pmatrix}$$

a dubious situation as all the interaction measures have large elements for both the diagonal (uy_{de}) and off-diagonal (uy_{ed}) system structure in Table 5.5. However the NI and RIA based system structure with minimum overall interaction given in (5.12) would suggest uy_{de} as decoupled and uy_{ed} as the coupled system structure. The *RDIA* for $G_3(s)$ defined in (5.33) is given as follows:

$$\text{RDIA: } f(G_3(s)) = \begin{pmatrix} 1.0150 & 0.9852 \\ 0.9852 & 1.0126 \end{pmatrix} \quad (5.39)$$

The *RDIA* based system interaction guidelines points out the following:

1. y_d predominantly depends on u_d and less depends on u_e .
2. y_e predominantly depends on u_e and less depends on u_d .

Therefore the *RDIA* based near decoupling configuration procedure suggests uy_{de} as more towards decoupling.

The RMSE based performance measure for $G_3(s)$ in (5.35) is shown in Table 5.6. y_d largely depends on u_d and y_e largely depends on u_e . Therefore, the error e_1 in $e_{uy_{de}}$ will be maximum when $u_d = 0$, i.e. ($32.5251 > 31.5970$) and the error e_2 in $e_{uy_{de}}$ will be

Table 5.6: RMSE for system configurations of $G_3(s)$

System configuration	RMSE	$\Delta_{OL} = \text{diag}[0 \ 1]$	$\Delta_{OL} = \text{diag}[1 \ 0]$
$e_{uy_{de}}$		32.5251	31.5970
		40.1171	41.8090
$e_{uy_{ed}}$		31.5970	32.5251
		41.8090	40.1171

maximum when $u_e = 0$, i.e. ($41.8090 > 40.1171$). For the system configuration towards minimal input dependence, the following can be inferred from Table 5.6:

1. As y_d minimally depends on u_e , the error e_1 in $e_{uy_{de}}$ will be minimum when $u_e = 0$, i.e. ($31.5970 < 32.5251$).
2. As y_e minimally depends on u_d , the error e_2 in $e_{uy_{de}}$ will be minimum when $u_d = 0$, i.e. ($40.1171 < 41.8090$).

Hence the RMSE based performance measure also shows that the system structure uy_{de} is decoupled.

Example 5.2.4 Consider a transfer function model for a pilot scale, binary distillation column used to separate ethanol and water given by [13]

$$\begin{bmatrix} y_a \\ y_b \\ y_c \end{bmatrix} = G_4(s) \begin{bmatrix} u_a \\ u_b \\ u_c \end{bmatrix} \quad (5.40)$$

where

$$G_4(s) = \begin{bmatrix} \frac{0.66e^{-2.6s}}{6.7s + 1} & \frac{-0.61e^{-3.5s}}{8.64s + 1} & \frac{-0.0049e^{-s}}{9.06s + 1} \\ \frac{1.11e^{-6.5s}}{3.25s + 1} & \frac{-2.36e^{-3s}}{5s + 1} & \frac{-0.012e^{-1.2s}}{7.09s + 1} \\ \frac{-33.68e^{-9.2s}}{8.15s + 1} & \frac{46.2e^{-9.4s}}{10.9s + 1} & \frac{0.87(11.61s + 1)e^{-s}}{(3.89s + 1)(18.8s + 1)} \end{bmatrix} \quad (5.41)$$

where y_a is the overhead mol fraction of ethanol, y_b is the mol fraction of ethanol in the side stream, and y_c is temperature on Tray 19; u_a is the overhead reflux flow rate, u_b is side stream draw-off rate, and u_c is reboiler steam pressure. The detailed model of the distillation column can be found in [37]. Table 5.7 shows the existing interaction measures for the distillation column described in (5.40). The RGA, NI, RIA, ERGA and EREA pairing rules suggest the system structure uy_{123} as being close to decoupled [27] & [13]. The system structure towards coupling cannot be accurately known from the existing measures following the "opposite" rules described previously and would possibly be any one from ($uy_{132}/uy_{213}/uy_{231}/uy_{312}/uy_{321}$).

The *RDIA* for $G_4(s)$ defined in (5.33) is given as follows:

$$\text{RDIA : } f(G_4(s)) = \begin{pmatrix} 1.0819 & 0.9242 & 0.0055 \\ 0.4703 & 2.1260 & 0.0046 \\ 0.7289 & 1.3713 & 0.0152 \end{pmatrix} \quad (5.42)$$

The *RDIA* for $G_4(s)$ in 5.42 shows the relative dependency of i^{th} output upon the j^{th} input as follows:

1. y_a predominantly depends on u_a and less depends on u_c .
2. y_b predominantly depends on u_b and less depends on u_c .
3. y_c predominantly depends on u_b and less depends on u_c .

Table 5.7: Existing interaction measures for $G_4(s)$

$$\text{RGA: } \Lambda(G_4(s)) = \begin{bmatrix} 1.9454 & -0.6737 & -0.2718 \\ -0.6643 & 1.8991 & -0.2348 \\ -0.2811 & -0.2254 & 1.5065 \end{bmatrix}$$

$$NI_{uy123} = 0.3752, \quad NI_{uy132} = -1.3896, \quad NI_{uy213} = -0.8632$$

$$NI_{uy231} = 2.0625, \quad NI_{uy312} = 2.0235, \quad NI_{uy321} = -1.3055$$

$$\text{RIA: } \Phi(G_4(s)) = \begin{bmatrix} -0.4860 & -2.4844 & -4.6794 \\ -2.5053 & -0.4734 & -5.2598 \\ -4.5573 & -5.4361 & -0.3362 \end{bmatrix}$$

$$\Phi_{uy123} \equiv \Phi_{\min}(G_4) = 1.2956$$

$$\text{ERGA: } \Upsilon(G_4(s)) = \begin{pmatrix} 2.3338 & -1.1017 & -0.2321 \\ -0.8550 & 2.0366 & -0.1816 \\ -0.4788 & 0.0651 & 1.4138 \end{pmatrix}$$

$$\text{EREA: } \Upsilon(G_4(s)) = \begin{pmatrix} 1.3507 & -0.2851 & -0.0657 \\ -0.2621 & 1.3040 & -0.0420 \\ -0.0887 & -0.0190 & 1.1076 \end{pmatrix}$$

Table 5.8: RMSE for system configurations uy_{123} and Δ_{OL} for $G_4(s)$

System configuration	RMSE	$\Delta_{OL} = \text{diag}[0 \ 1 \ 1]$	$\Delta_{OL} = \text{diag}[1 \ 0 \ 1]$	$\Delta_{OL} = \text{diag}[1 \ 1 \ 0]$
		0.6260	0.5699	0.0046
e_{uy123}		1.0503	2.2537	0.0114
		30.5892	41.2788	0.8131

Table 5.8 shows the RMSE based performance measure for the system structure uy_{123} for all possible values of Δ_{OL} . From Table 5.8, it can be inferred that since y_a largely depends on u_a , the error e_1 in e_{uy123} will be maximum when $u_a = 0$, i.e. ($0.6260 > 0.5699$ & 0.0046). In a similar manner from the *RDIA* in (5.42), it is known that y_b largely depends on u_b , so the error e_2 in e_{uy123} will be maximum when $u_b = 0$, i.e. ($2.2537 > 1.0503$ & 0.0114) and as y_c mainly depends on u_b , the error e_3 in e_{uy123} will be maximum when $u_b = 0$, i.e. ($41.2788 > 30.5892$ & 0.8131). For the system configuration

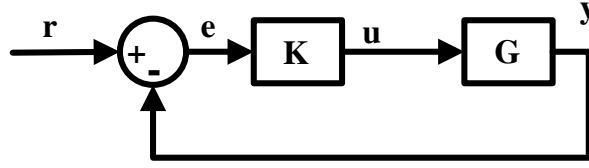


Figure 5.2: Multivariable output feedback control system

towards minimal input dependence, the following can be inferred from Table 5.8:

1. As y_a minimally depends on u_c and the error e_1 in $e_{uy_{123}}$ will be minimum when $u_c = 0$, i.e. $(0.0046 < 0.6260 \ \& \ 0.5699)$.
2. As y_b minimally depends on u_c , the error e_2 in $e_{uy_{123}}$ will be minimum when $u_c = 0$, i.e. $(0.0114 < 1.0503 \ \& \ 2.2537)$.
3. As y_c minimally depends on u_c , the error e_3 in $e_{uy_{123}}$ will be minimum when $u_c = 0$, i.e. $(0.8131 < 30.5892 \ \& \ 41.2788)$.

Therefore, the near decoupling configuration procedure suggests uy_{123} system structure more towards decoupling

5.4.2 Decoupling in Closed-loop System

The general block diagram of a multivariable output feedback control system is shown in Fig. 5.2, where G is given by (5.1), K is the multivariable stabilizing controller which can have a centralized or decentralized form. u is the control input, r is the reference input and e is the error signal. y is the closed-loop system output given by:

$$y = [(I_{n \times n} + GK)^{-1}GK]r = \bar{G}r = [\bar{g}_{i,j}]r \text{ for } i, j = 1, \dots, n \quad (5.43)$$

where $I_{n \times n} \triangleq \text{Diag}[1]_{n \times n}$

Then

$$m_{i,j} \triangleq \frac{\|\bar{g}_{i,j}(s)\|_\infty}{\|[\bar{g}_{i,1}(s) \cdots \bar{g}_{i,j-1}(s) \bar{g}_{i,j+1}(s) \cdots \bar{g}_{i,n}(s)]\|_\infty} \quad (5.44)$$

$m_{i,j} = \infty$, if $[\bar{g}_{i,1}(s) \dots \bar{g}_{i,j-1}(s) \bar{g}_{i,j+1}(s) \dots \bar{g}_{i,n}(s)]$ is a zero transfer function. $m_{i,j}$ shows the relative dependency of the i^{th} output upon the j^{th} input of a closed-loop MIMO system. The constant matrix $m(\bar{G}) \triangleq [m_{i,j}]$, for $i, j = 1, \dots, n$ is called the *RDIA* of $\bar{G}(s)$ in (5.43). With $m(\bar{G})$, structure configuration of $\bar{G}(s)$ can be inferred. The following procedure can be followed in studying the closed-loop interactions of the system.

Near-decoupling configuration procedure of a closed-loop system

1. Calculate the *RDIA*, $m(\bar{G})$, for the closed-loop MIMO system $\bar{G}(s)$.
2. Select the largest element of $m(\bar{G})$ for the i^{th} row, say $m_{i,j}$.
3. Permute the i^{th} output and the j^{th} input to the first output and input, respectively.
4. Repeat the above steps over the bottom-right $(n-1) \times (n-1)$ sub-matrix of permuted $m(\bar{G})$.

Example 5.2.5 Consider the methanol-water distillation column of Wood and Berry (1973) [67] given by:

$$\begin{bmatrix} x_D(s) \\ x_B(s) \end{bmatrix} = \underbrace{\begin{bmatrix} P_{11}(s) & P_{12}(s) \\ P_{21}(s) & P_{22}(s) \end{bmatrix}}_{P(s)} \begin{bmatrix} R(s) \\ S(s) \end{bmatrix} \quad (5.45)$$

where

$$\begin{aligned} P_{11}(s) &= \frac{12.8e^{-s}}{16.7s+1}, & P_{12}(s) &= \frac{-18.9e^{-3s}}{21s+1} \\ P_{21}(s) &= \frac{6.6e^{-7s}}{10.9s+1}, & P_{22}(s) &= \frac{-19.4e^{-3s}}{14.4s+1} \end{aligned} \quad (5.46)$$

The detailed dynamic model of the distillation column can be found in [67] and will be discussed briefly in this chapter.

- $x_D(s)$: overhead product composition
- $x_B(s)$: bottom product composition

- $P_{11}(s)$: direct process transfer function (tf), relating overhead composition to reflux flow
- $P_{12}(s)$: interacting process tf, relating overhead composition to steam flow
- $P_{21}(s)$: interacting process tf, relating overhead composition to steam flow
- $P_{22}(s)$: direct process tf, relating bottom composition to steam flow
- $R(s)$: reflux flow rate
- $S(s)$: steam flow rate

[22] in 1997 proposed two multi-loop Proportional-Integral (PI) controllers used to control the multivariable process $P(s)$ in (5.45) based on gain and phase margin specifications. The PI controller values were found to be [22]:

$$G_{c1}(s) = \text{diag} \left[0.57 \left(1 + \frac{1}{20.70s} \right), -0.11 \left(1 + \frac{1}{12.88s} \right) \right] \quad (5.47)$$

$$G_{c2}(s) = \text{diag} \left[0.38 \left(1 + \frac{1}{21.64s} \right), -0.07 \left(1 + \frac{1}{14.80s} \right) \right] \quad (5.48)$$

The closed-loop transfer function from the reference input to the system output for the multivariable process $P(s)$ in (5.45) with the PI controller $G_{c1}(s)$ and $G_{c2}(s)$ given in (5.47) and (5.48) can be written as follows:

$$\begin{bmatrix} x_D \\ x_B \end{bmatrix} = \tilde{P}_{ci} \begin{bmatrix} r_1 \\ r_2 \end{bmatrix} \quad (5.49)$$

where

$$\tilde{P}_{ci} \triangleq [(I + PG_{ci})^{-1}]PG_{ci} \text{ for } i = 1, 2 \quad (5.50)$$

For ease of notation the closed-loop structure configuration of (5.49) will be denoted as follows:

$$r_1 - x_D, r_2 - x_B \equiv xr_{DB}$$

$$r_1 - x_B, r_2 - x_D \equiv xr_{BD}$$

The *RDIA* for \tilde{P}_{ci} in (5.50) from (5.44) can be written as follows:

$$\text{RDIA : } m(\tilde{P}_{c1}) = \begin{bmatrix} 5.3104 & 0.1883 \\ 0.5586 & 1.7902 \end{bmatrix} \quad (5.51)$$

$$\text{RDIA : } m(\tilde{P}_{c2}) = \begin{bmatrix} 5.2735 & 0.1896 \\ 0.5259 & 1.9015 \end{bmatrix}$$

The *RDIA* for \tilde{P}_{c1} and \tilde{P}_{c2} in (5.51) shows the relative dependency of i^{th} output upon the j^{th} input as follows:

1. For both \tilde{P}_{c1} and \tilde{P}_{c2} , x_D predominantly depends on r_1 and x_B depends on r_2 and
2. x_D minimally depends on r_2 and x_B minimally depends on r_1 .

The *RDIA* based procedure for the closed-loop system P_{ci} in (5.49) suggests that for both the controllers G_{c1} and G_{c2} , xr_{DB} is close to being decoupled and xr_{BD} is close to being coupled. Similar to the case of open-loop, the veracity of *RDIA* for the closed-loop systems is verified with a performance measure which suggests the decoupled and coupled configuration based on the simulation of the closed-loop system and its respective model.

RMSE based performance for closed-loop systems

Fig. 5.3 shows the multivariable process discussed in (5.45) with the PI controllers, G_{c1} and G_{c2} in (5.47 & 5.48). $P_M = P$ is the model of the multivariable process. Δ_{CL} is the input effectiveness matrix given as follows:

$$\Delta_{CL} = \begin{pmatrix} \delta_{cl1} & 0 & 0 & 0 \\ 0 & \delta_{cl2} & 0 & 0 \\ 0 & 0 & \dots & 0 \\ 0 & 0 & 0 & \delta_{cln} \end{pmatrix} \quad (5.52)$$

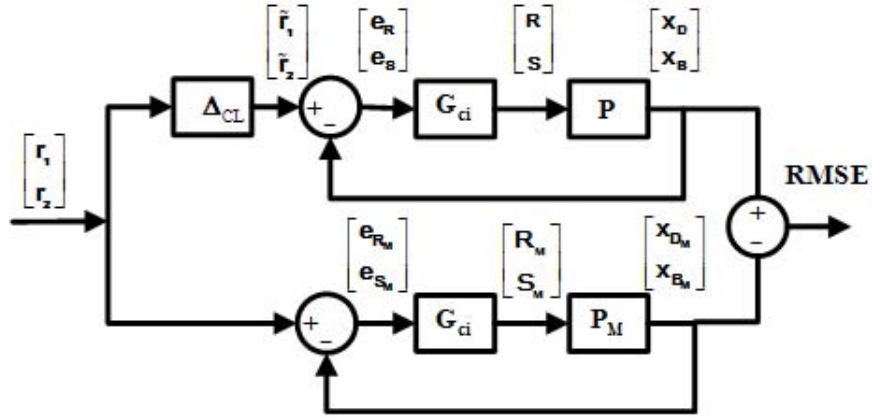


Figure 5.3: RMSE based plant-model performance measure in closed-loop

$[x_D \ x_B]^T$ is the plant output and $[x_{D_M} \ x_{B_M}]^T$ is the model output. $[r_1 \ r_2]^T$ is the reference input. RMSE between the plant and its model is given by the following relation:

$$e_D \triangleq \frac{1}{N} \sqrt{\sum_{i=1}^N (x_D(i) - x_{D_M}(i))^2} \quad (5.53)$$

$$e_B \triangleq \frac{1}{N} \sqrt{\sum_{i=1}^N (x_B(i) - x_{B_M}(i))^2}$$

where N is the number of sampling points.

As in the case of open-loop stable systems, the closed-loop system structure closer to decoupling will be less affected from other channel inputs, whereas a coupled structure is more influenced from other inputs. The input effectiveness array Δ_{CL} in (5.52) is selected such that one input is zero alternatively. For a closed-loop system structure closer to decoupling the channel with no input will have the maximum error and the structure closer to coupling will have the minimum error given in (5.53).

Tables (5.9 & 5.10) shows the RMSE values for the two loop configurations namely, $x_{r_{DB}}$ and $x_{r_{BD}}$ for the multivariable process described in (5.45) with the input effectiveness matrix defined in (5.52). It can be observed from tables (5.9 & 5.10) that for the system structure $x_{r_{DB}}$, e_D is maximum when $r_1 = 0$, i.e. $(0.9672 > 0.0271)$ and

Table 5.9: RMSE for system configurations of $\tilde{P}_{c1}(s)$

System configuration	RMSE	$\Delta_{CL} = \text{diag}[0 \ 1]$	$\Delta_{CL} = \text{diag}[1 \ 0]$
xr_{DB}		$e_D = 0.9672$ $e_B = 0.0314$	$e_D = 0.0271$ $e_B = 0.9344$
xr_{BD}		$e_D = 0.0271$ $e_B = 0.9344$	$e_D = 0.9672$ $e_B = 0.0314$

Table 5.10: RMSE for system configurations of $\tilde{P}_{c2}(s)$

System configuration	RMSE	$\Delta_{CL} = \text{diag}[0 \ 1]$	$\Delta_{CL} = \text{diag}[1 \ 0]$
xr_{DB}		$e_D = 0.9504$ $e_B = 0.0563$	$e_D = 0.0433$ $e_B = 0.8857$
xr_{BD}		$e_D = 0.0433$ $e_B = 0.8857$	$e_D = 0.9504$ $e_B = 0.0563$

(0.9504 > 0.0433) as x_D predominantly depends on r_1 and similarly e_B is maximum when $r_2 = 0$, i.e. (0.9344 > 0.0314) and (0.8857 > 0.0563) as x_B predominantly depends on r_2 . Hence this verifies that xr_{DB} is close to being decoupled. In a similar way e_D is minimum when $r_2 = 0$, i.e. (0.0271 < 0.9672) and (0.0433 < 0.9504) as x_D minimally depends on r_2 and similarly e_B is minimum when $r_1 = 0$, i.e. (0.0314 < 0.9344) and (0.0563 < 0.8857) as x_B minimally depends on r_1 . Hence this shows that xr_{BD} is close to being coupled. A similar analysis based on the existing interaction measures such as RGA, RIA, ERGA & EREA and their associated guidelines would give inconsistent results as they are based on open-loop stable systems and cannot be applied to a multivariable system in closed-loop. This inadequacy is overcome in RDI and $RDIA$ which is a simple and useful interaction measure and enables one to study closed-loop interactions of MIMO systems. The examples discussed so far illustrate the effective-

ness of RDI applied to distillation columns with the flexibility of input-output pairing or structure configuration. However this may not be possible in many dynamic systems. In such a case, the RDI becomes a useful tool in investigating a channel vulnerability to actuator faults and failures by identifying the least and most vulnerable channel to actuator failures and is discussed in the next section.

5.4.3 Predicting Channel Vulnerability in Case of Actuator Degradation for Open-loop Stable Systems

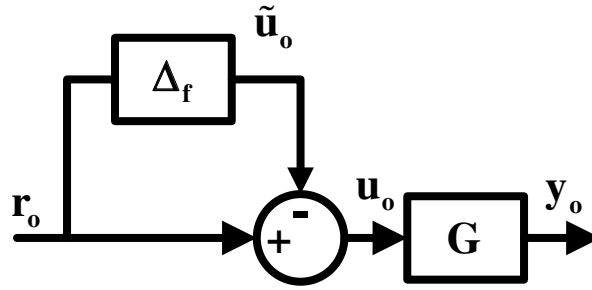


Figure 5.4: Open-loop stable MIMO system with actuator uncertainty

The general block diagram of an open-loop stable MIMO system with actuator uncertainty is shown in Fig. 5.4, where G is a stable MIMO system given by (5.1). u_o is the system input with actuator uncertainty Δ_f , incorporating the actuator degradation as follows:

$$\Delta_f = \begin{pmatrix} \delta_{f11} & 0 & 0 & 0 \\ 0 & \delta_{f22} & 0 & 0 \\ 0 & 0 & \dots & 0 \\ 0 & 0 & 0 & \delta_{fnn} \end{pmatrix} \quad (5.54)$$

where $0 \leq \delta_{fii} \leq 1$. $\delta_{fii} = 0$ and $\delta_{fii} = 1$ implies no and maximum actuator fault in the i^{th} channel. r_o is the reference input and y_o is the open-loop stable system output given by:

$$y_o = G(I - \Delta_f)r_o \quad (5.55)$$

The transfer function from the output y_o to the uncertain actuator input \tilde{u}_o can be written as follows:

$$y_o = G\tilde{u}_o = [\tilde{p}_{i,j}]\tilde{u}_o \text{ for } i, j = 1, \dots, n \quad (5.56)$$

$$\bar{q}_{i,j} \triangleq \frac{\|\tilde{p}_{i,j}(s)\|_\infty}{\|[\tilde{p}_{i,1}(s) \dots \tilde{p}_{i,j-1}(s) \tilde{p}_{i,j+1}(s) \dots \tilde{p}_{i,n}(s)]\|_\infty} \quad (5.57)$$

$\bar{q}_{i,j} = \infty$, if $[\tilde{p}_{i,1}(s) \dots \tilde{p}_{i,j-1}(s) \tilde{p}_{i,j+1}(s) \dots \tilde{p}_{i,n}(s)]$ is a zero transfer function. $\bar{q}_{i,j}$ shows the relative dependency of the i^{th} output upon the j^{th} actuator input. The constant matrix $\bar{q}(G) \triangleq [\bar{q}_{i,j}]$, for $i, j = 1, \dots, n$ is called the *RDIA* of $G(s)$ in (5.55).

In the case of actuator degradation consideration, we don't desire the system to be decoupled, otherwise one of the outputs will be totally or majorly lost. Rather, we want to spread out the dependency of the outputs over all the input channels. Hence, when one actuator fails, the outputs would be affected, but hopefully the effect would be reduced to minimum. In the scenario that one actuator is particularly vulnerable to faults/failures, the problem is which input channel should be selected for this actuator. For this purpose it is necessary to introduce another index, Input Impact Index (*i.i.i.*), which reflects how each actuator input influences the system outputs and is naturally based on *RDI*. Input impact index can be defined in different ways. The following is one of them.

Input Impact Index: The *i.i.i.* of the j^{th} input channel is defined as, for $j=1, \dots, n$.

$$\rho_{oj} \triangleq \max_{i=1, \dots, n} \{\bar{q}_{i,j}\} \quad (5.58)$$

With such defined input impact index and following a minmax approach, the input channel ϵ_o which would produce least impact on the system outputs in the case of actuator degradation could be selected as

$$\epsilon_o \triangleq \arg \min_{\{j=1,\dots,n\}} \{\rho_{oj}\} \quad (5.59)$$

The following procedure can be followed in studying the closed-loop interactions of the system from actuator to the system output.

***RDI-i.i.i.* based procedure for studying open-loop stable system interactions in case of actuator degradation**

1. Calculate the *RDIA*, $q(G)$, for the MIMO system $G(s)$ from (5.57).
2. Select the *i.i.i.* for each input channel as defined in (5.58)
3. The degraded channel should be selected with the input channel whose *i.i.i.* is minimum defined in (5.59)
4. In the case that more than one ρ 's reaching the minimum value, the second largest *RDI* in each corresponding columns should be compared and the least one among those is to be selected. And this procedure can be repeated accordingly.
5. If two columns of $\bar{q}(G)$ are same, then those two corresponding inputs will have same impact on the system output.

Consider the transfer function model, $G_4(s)$ from example 5.2.4 for a pilot scale, binary distillation column discussed in equations (5.40-5.41) taken from [13]. The *RDIA* for $G_4(s)$ can be calculated from (5.57) and is given as follows:

$$\text{RDIA : } \bar{q}(G_4(s)) = \begin{pmatrix} 1.0819 & 0.9242 & 0.0055 \\ 0.4703 & 2.1260 & 0.0046 \\ 0.7289 & 1.3713 & 0.0152 \end{pmatrix} \quad (5.60)$$

The *i.i.i.* for each input channel of $G_4(s)$ defined in (5.58) is given as follows:

$$\rho_{o1} = 1.0819, \rho_{o2} = 2.1260, \rho_{o3} = 0.0152 \quad (5.61)$$

Then from (5.59), the input channel that would produce the least impact on the system outputs in case of actuator degradation is given by the following equation.

$$\epsilon_o \triangleq \arg \min_{\{j=1,2,3\}} \{\rho_{oj}\} \quad (5.62)$$

It can be stated from (5.61-5.62) that the third input would produce the least impact on the system output in case of actuator degradation. The accuracy of *RDIA* and *i.i.i.* based procedure is verified with a performance measure based on the simulation of the open-loop system and its model.

RMSE based performance measure in case of actuator degradation for open-loop stable systems

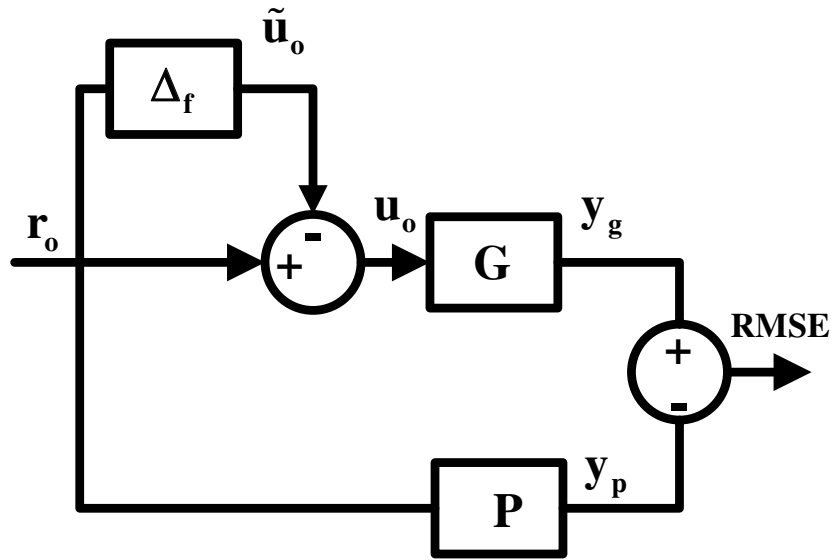


Figure 5.5: RMSE based performance measure in case of actuator degradation for open-loop stable systems

Fig. 5.5 shows an open-loop stable plant (G) and its model (P). Δ_f is the actuator uncertainty defined in (5.54). $y_g = [y_{g1} \ y_{g2} \ \dots \ y_{gn}]^T$ is the plant output and $y_p = [y_{p1} \ y_{p2} \ \dots \ y_{pn}]^T$ is the model output. RMSE between the plant affected from actuator degradation and its model (free from degradation) is given by the following relation:

$$e_{pg1} \triangleq \sqrt{((y_{g1}(i) - y_{p1}(i))^2 + \dots + (y_{gn}(i) - y_{pn}(i))^2)} \quad (5.63)$$

when $\Delta_f = \text{Diag}[0.9, 0, 0, \dots, 0]_{n \times n}$

$$e_{pg2} \triangleq \sqrt{((y_{g1}(i) - y_{p1}(i))^2 + \dots + (y_{gn}(i) - y_{pn}(i))^2)} \quad (5.64)$$

when $\Delta_f = \text{Diag}[0, 0.9, 0, \dots, 0]_{n \times n}$

$$e_{pgn} \triangleq \sqrt{((y_{g1}(i) - y_{p1}(i))^2 + \dots + (y_{gn}(i) - y_{pn}(i))^2)} \quad (5.65)$$

when $\Delta_f = \text{Diag}[0, 0, 0, \dots, 0.9]_{n \times n}$

where N is the number of sampling points.

In (5.63), e_{pg1} is the RMSE between the plant and its model when the first actuator degrades by 90%. In a similar manner e_{pgn} in (5.65) is the RMSE between the plant and its model when the " n^{th} " actuator degrades. Figs 5.6, 5.7 and 5.8 show the open-loop step response when the first, second and third actuators degrade by 90% respectively. The simulation is run for 200 seconds with a sampling time of 0.01 seconds and the actuators degrade at 100 seconds. The RMSE plot when the actuators in channels 1, 2 and 3 degrade is shown in Fig. 5.9. It can be inferred that the error is minimum when there is a degradation in channel-3 and the error is maximum when channel-2 actuator degrades. The average values of e_{pg1} , e_{pg2} and e_{pg3} in (5.63-5.65) can be calculated as follows

$$\begin{aligned} e_{p1} &\triangleq \text{mean}(e_{pg1}) \\ e_{p2} &\triangleq \text{mean}(e_{pg2}) \\ e_{p3} &\triangleq \text{mean}(e_{pg3}) \end{aligned} \quad (5.66)$$

The average values are found to be

$$\begin{aligned} e_{p1} &= 0.4643 \\ e_{p2} &= 0.6155 \\ e_{p3} &= 0.0127 \end{aligned} \quad (5.67)$$

From (5.67), the average RMSE values in order of magnitude can be written as follows, $e_{p3} < e_{p1} < e_{p2}$ which also suggests that an actuator fault in channel-3 produces a minimum impact on the overall open-loop system response and an actuator fault in

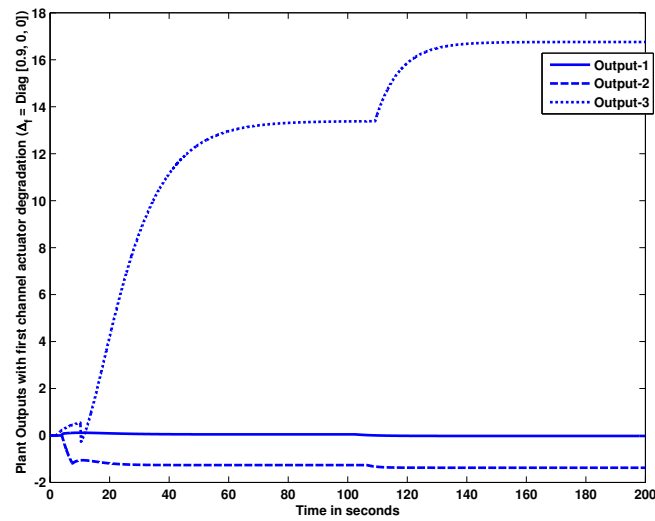


Figure 5.6: System response with channel-1 actuator degradation

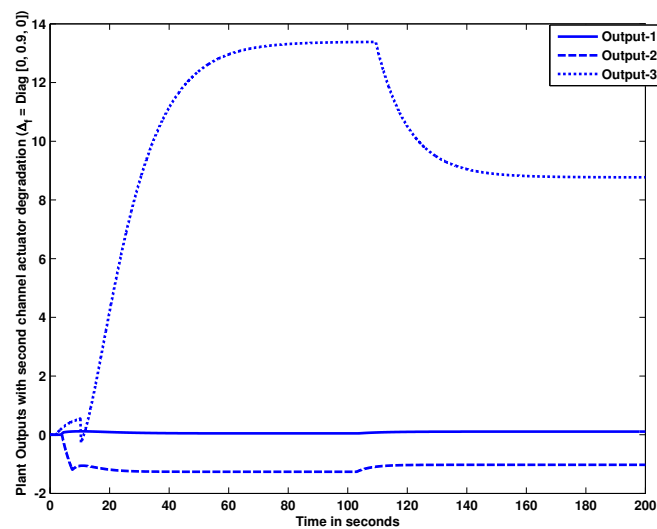


Figure 5.7: System response with channel-2 actuator degradation

channel-2 leads to a maximum performance degradation. Hence the $RDI-i.i.i.$ based guidelines can be effectively used as a tool in predicting a channel vulnerability in case of actuator degradation in open-loop stable systems. This approach can be extended to closed-loop systems as well and will be addressed in the next section.

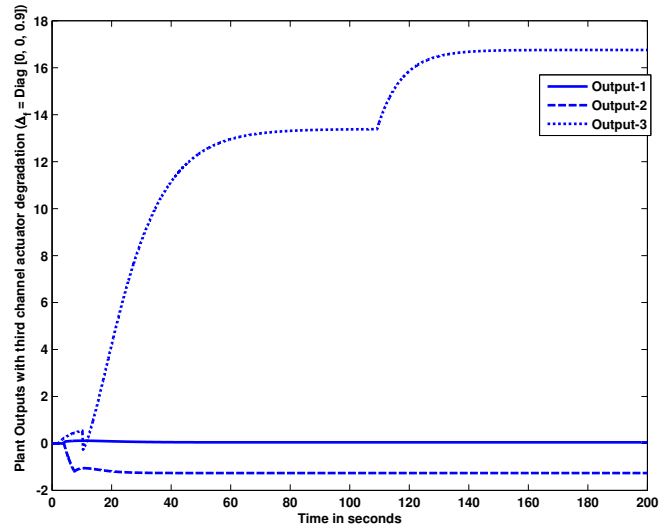


Figure 5.8: System response with channel-3 actuator degradation

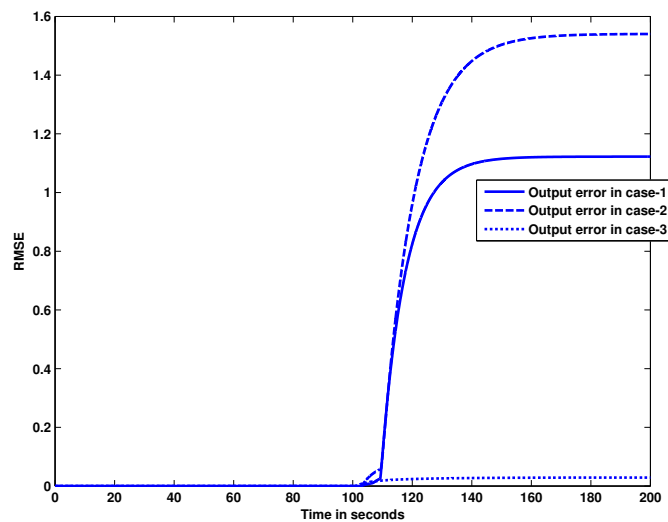


Figure 5.9: RMSE plot for actuator degradation in channels-1, 2 & 3

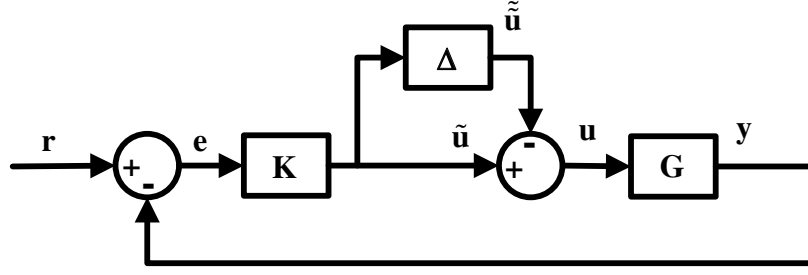


Figure 5.10: Multivariable output feedback control system with actuator uncertainty

5.4.4 Predicting Channel Vulnerability in Case of Actuator Degradation for Closed-loop Systems

The general block diagram of a multivariable output feedback control system with actuator uncertainty is shown in Fig. 5.10, where G is the stable or unstable MIMO system given by (5.1). K is the multivariable controller stabilizing G having a centralized or decentralized form. u is the control input with actuator uncertainty Δ , incorporating the actuator degradation as follows:

$$\Delta = \begin{pmatrix} \delta_{11} & 0 & 0 & 0 \\ 0 & \delta_{22} & 0 & 0 \\ 0 & 0 & \dots & 0 \\ 0 & 0 & 0 & \delta_{nn} \end{pmatrix} \quad (5.68)$$

where $0 \leq \delta_{ii} \leq 1$. $\delta_{ii} = 0$ and $\delta_{ii} = 1$ implies no and maximum actuator fault in the i^{th} channel. r and e are the reference input and error signal. y is the closed-loop system output given by:

$$y = (I + G(I - \Delta)K)^{-1}G(I - \Delta)Kr \quad (5.69)$$

The transfer function from the uncertain actuator input \tilde{u} to the output y can be written as follows:

$$y = [(I + GK)^{-1}G]\tilde{u} = \tilde{G}\tilde{u} = [\tilde{g}_{i,j}]\tilde{u} \text{ for } i, j = 1, \dots, n \quad (5.70)$$

$$h_{i,j} \triangleq \frac{\|\tilde{g}_{i,j}(s)\|_\infty}{\|[\tilde{g}_{i,1}(s) \dots \tilde{g}_{i,j-1}(s) \tilde{g}_{i,j+1}(s) \dots \tilde{g}_{i,n}(s)]\|_\infty} \quad (5.71)$$

$h_{i,j} = \infty$, if $[\tilde{g}_{i,1}(s) \dots \tilde{g}_{i,j-1}(s) \tilde{g}_{i,j+1}(s) \dots \tilde{g}_{i,n}(s)]$ is a zero transfer function. $h_{i,j}$ shows the relative dependency of the i^{th} output upon the j^{th} actuator input. The constant matrix $h(\tilde{G}) \triangleq [h_{i,j}]$, for $i, j = 1, \dots, n$ is called the *RDIA* of $\tilde{G}(s)$ in (5.70).

Similar to the case of open-loop stable systems considering the case of actuator degradation, it is not desired that the system to be decoupled, otherwise one of the outputs will be totally or majorly lost. Rather, we want to spread out the dependency of the outputs over all the input channels. Hence, when one actuator fails, the outputs would be affected, but hopefully the effect would be reduced to minimum. In the scenario that one actuator is particularly vulnerable to faults/failures, the problem is which input channel should be selected for this actuator. For this purpose the *i.i.i.* introduced previously is extended to the case of closed-loop systems which reflects how each actuator's input influences the closed-loop system outputs and is naturally based on *RDI*. Input impact index can be defined for closed-loop systems as follows:

Input Impact Index for closed-loop systems: For a closed-loop system the *i.i.i.* of the j^{th} input channel is defined as, for $j=1, \dots, n$.

$$\rho_j \triangleq \max_{i=1, \dots, n} \{h_{i,j}\} \quad (5.72)$$

With such defined input impact index and following a min-max approach, the input channel ϵ which would produce least impact on the system outputs in the case of actuator degradation could be selected as

$$\epsilon \triangleq \arg \min_{\{j=1, \dots, n\}} \{\rho_j\} \quad (5.73)$$

The following procedure can be followed in studying the closed-loop interactions of the system from actuator to the system output.

***RDI-i.i.i.* based procedure for studying closed-loop interactions in case**

of actuator degradation

1. Calculate the *RDIA*, $h(\tilde{G})$, for the MIMO system $\tilde{G}(s)$ from (5.71).
2. Select the *i.i.i.* for each input channel as defined in (5.72)
3. The degraded channel should be selected with the input channel whose *i.i.i.* is minimum defined in (5.73)
4. In the case that more than one ρ 's reaching the minimum value, the second largest *RDI* in each corresponding columns should be compared and the least one among those is to be selected. And this procedure can be repeated accordingly.
5. If two columns of $h(\tilde{G})$ are same, then those two corresponding inputs will have same impact on the system output.

Example 5.2.6 Consider the linearized spacecraft attitude model in terms of Euler's equation of rotational dynamics and the MRP's stated in (2.28-2.31). It was shown that this model can be stabilized using the output feedback control law presented in (3.19) of section 3.6 given as follows:

$$\tau \triangleq T^T [K_2(q_d - q) - K_3 q] \quad (5.74)$$

In (5.74), $T(q)$ is the Jacobian matrix stated in (2.20) and K_2 and K_3 are given as follows: .

$$\begin{aligned} K_2 &= \text{diag}(20, 20, 20) \\ K_3 &= \text{diag} \left[100 \left(\frac{50s}{s+50} \right), 100 \left(\frac{50s}{s+50} \right), 100 \left(\frac{50s}{s+50} \right) \right] \end{aligned} \quad (5.75)$$

In Fig. 5.11, $G_{mrp} \triangleq \left(\begin{array}{c|c} A_{mrp} & B_{mrp} \\ \hline C_{mrp} & D_{mrp} \end{array} \right)$ is the linearized spacecraft attitude model described in (2.28-2.31), Δ is the actuator uncertainty defined in (5.68), $\tau =$

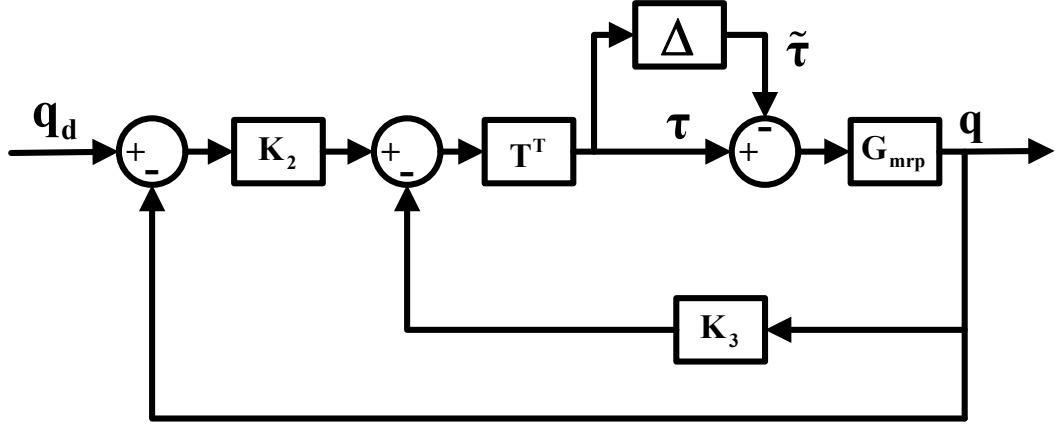


Figure 5.11: Spacecraft attitude stabilization using output feedback

$[\tau_1 \ \tau_2 \ \tau_3]^T$ is the control input described in (5.74) where K_2 and K_3 are the controller gains and q_d is the desired reference. The closed-loop transfer function from the uncertain actuator input to the output from Fig. 5.11 can be written as follows:

$$q = -([I_{3 \times 3} + G_{mrp} T^T (K_2 + K_3)]^{-1} G_{mrp}) \tilde{\tau} = [\tilde{G}_{mrp}] \tilde{\tau} \quad (5.76)$$

The *RDIA* for \tilde{G}_{mrp} in (5.76) from (5.71) can be written as follows:

$$\text{RDIA : } h(\tilde{G}_{mrp}) = \begin{pmatrix} 9.1086 & 0.0617 & 0.0928 \\ 0.0516 & 10.4344 & 0.0808 \\ 0.0849 & 0.0594 & 9.7795 \end{pmatrix} \quad (5.77)$$

The *RDIA*, $h(\tilde{G}_{mrp})$ in (5.77) and the procedure for closed-loop interactions in case of actuator degradations identifies the *i.i.i.* for each input channel of \tilde{G}_{mrp} as follows:

$$\rho_1 = 9.1086, \ \rho_2 = 10.4344, \ \rho_3 = 9.7795 \quad (5.78)$$

Then from (5.73), the first input channel would produce the least impact on the system outputs in the case of actuator degradation. It is worthwhile to mention that the objective of *i.i.i.* and its procedure is not to configure the system structure (actuator-plant pairing) like the open and closed-loop cases discussed previously, but to familiarize a control engineer of the channels least and most prone to the actuator degradation

(channel vulnerability). For example, we have three d.c. motors which are operating on a coupled MIMO system and one of the d.c. motor is more likely to breakdown because of its operational history and durability, then it should be connected to the channel with least input impact i.e. channel corresponding to ϵ in (5.73). From the procedure of *RDIA* and *i.i.i.*, it can be inferred that in example 5.2.6, an actuator degradation in the first channel would least affect the overall performance of the closed-loop system and an actuator degradation in the second channel would produce the maximum effect on the overall performance of the closed-loop system. Similar to the case of predicting channel vulnerability in open-loop stable systems, we verify the effectiveness of *RDIA* and *i.i.i.* based procedure with a performance measure based on the simulation of the closed-loop system and its model.

RMSE based performance measure in case of actuator degradation for closed-loop systems

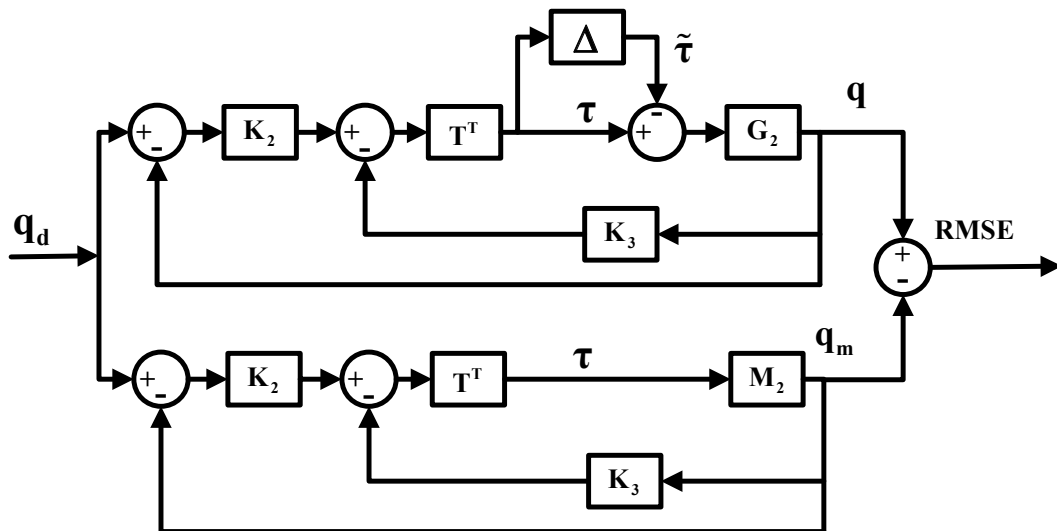


Figure 5.12: RMSE based performance measure in case of actuator degradation for closed-loop systems

Fig. 5.12 shows the plant (G_2) and its model (M_2), discussed in (2.28-2.31) with the output feedback control structure τ described in (5.74). Δ is the actuator uncertainty defined in (5.68). q is the plant output and $q_m = [q_{m1} \ q_{m2} \ q_{m3}]^T$ is the model output. RMSE between the plant affected from actuator degradation and its model (free from

degradation) is given by the following relation:

$$z_1 \stackrel{\Delta}{=} \sqrt{((q_1(i) - q_{m1}(i))^2 + (q_2(i) - q_{m2}(i))^2 + (q_3(i) - q_{m3}(i))^2)} \quad (5.79)$$

when $\Delta = \text{Diag}[0.9, 0, 0]$

$$z_2 \stackrel{\Delta}{=} \sqrt{((q_1(i) - q_{m1}(i))^2 + (q_2(i) - q_{m2}(i))^2 + (q_3(i) - q_{m3}(i))^2)} \quad (5.80)$$

when $\Delta = \text{Diag}[0, 0.9, 0]$

$$z_3 \stackrel{\Delta}{=} \sqrt{((q_1(i) - q_{m1}(i))^2 + (q_2(i) - q_{m2}(i))^2 + (q_3(i) - q_{m3}(i))^2)} \quad (5.81)$$

when $\Delta = \text{Diag}[0, 0, 0.9]$

where N is the number of sampling points.

In (5.79), z_1 is the RMSE between the plant and its model in closed-loop when the first actuator degrades by 90%. In a similar manner (5.80) and (5.81) is the RMSE between the plant and its model in closed-loop when the second and the third actuator degrades by 90%. The simulation is run for 120 seconds with a sampling time of 0.01 seconds and the actuators are degraded at 30 seconds. Figs. 5.13, 5.14 and 5.15 show the attitude stabilization (plant output) when the first, second and third channel actuators degrade by 90% respectively.

Fig. 5.16 shows the RMSE plot when the actuators in channels 1, 2 and 3 degrade. It can be inferred from Fig. 5.16 that the error is minimum when there is a degradation in channel-1 and the error is maximum for a degradation in channel-2. The average values of z_1 , z_2 and z_3 in (5.79, 5.80 & 5.81) can be calculated as follows:

$$\begin{aligned}
z^{(1)} &\triangleq \text{mean}(z_1) \\
z^{(2)} &\triangleq \text{mean}(z_2) \\
z^{(3)} &\triangleq \text{mean}(z_3)
\end{aligned} \tag{5.82}$$

The average values are found to be

$$\begin{aligned}
z^{(1)} &= 0.0164 \\
z^{(2)} &= 0.0599 \\
z^{(3)} &= 0.0590
\end{aligned} \tag{5.83}$$

In order of magnitude $z^{(1)} < z^{(3)} < z^{(2)}$. The performance measure suggests that an actuator fault in channel-1 least affects the overall performance and an actuator fault in channel-2 causes the maximum performance degradation.

The following remarks can be stated as a result of the *RDI*, *i.i.i.* and their performance measure in terms of RMSE.

Remark I: The input channel corresponding to ϵ , defined in (5.73) has the least impact on the system output. Thus, the system would be least affected from the actuator degradation occurrence on that channel and its RMSE defined in (5.79-5.81) is minimum.

Remark II: The input channel corresponding to $\nu \triangleq \arg \max_{\{j=1,\dots,n\}} \{\rho_j\}$, has the largest impact on the system output. Thus, the system would be most affected from the actuator degradation occurrence on that channel and its RMSE is maximum.

Remark III: The input impact index is defined for each input channel. Hence it is also useful for non-square systems.

5.5 Conclusions

In this chapter, a new approach for structure configuration of MIMO systems in open and closed-loop is presented. A simple interaction measure defined in terms of the H_∞ norm of the individual subsystems known as *RDI* was introduced. The *RDI* was shown to help understand the effect of one input on an output of a MIMO system for open-

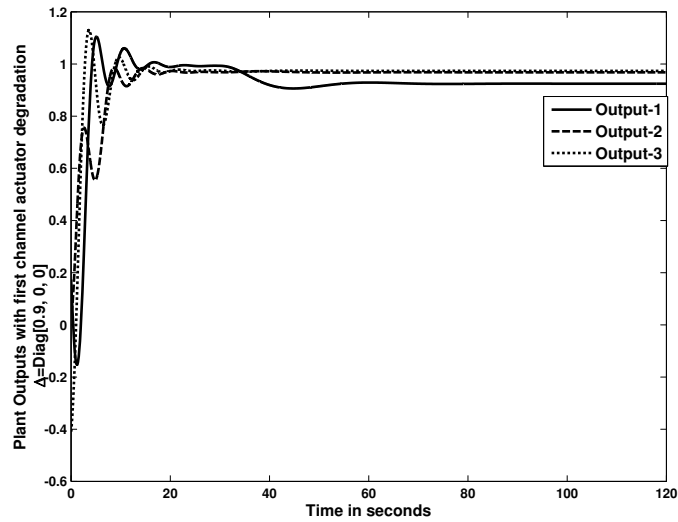


Figure 5.13: Attitude stabilization with channel-1 actuator degradation

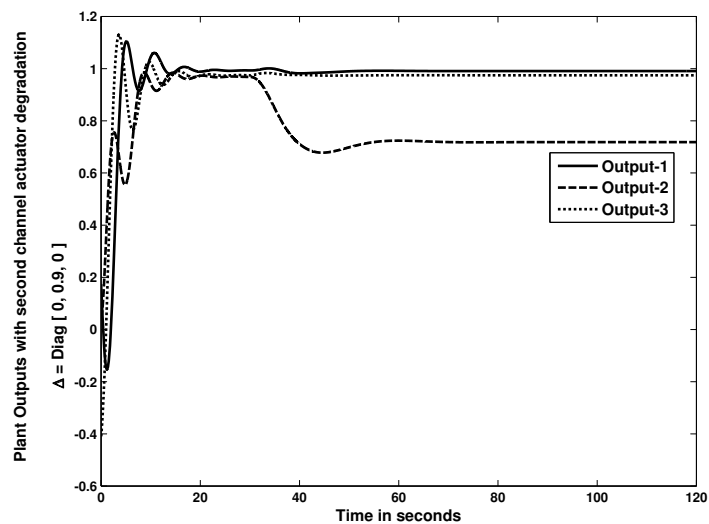


Figure 5.14: Attitude stabilization with channel-2 actuator degradation

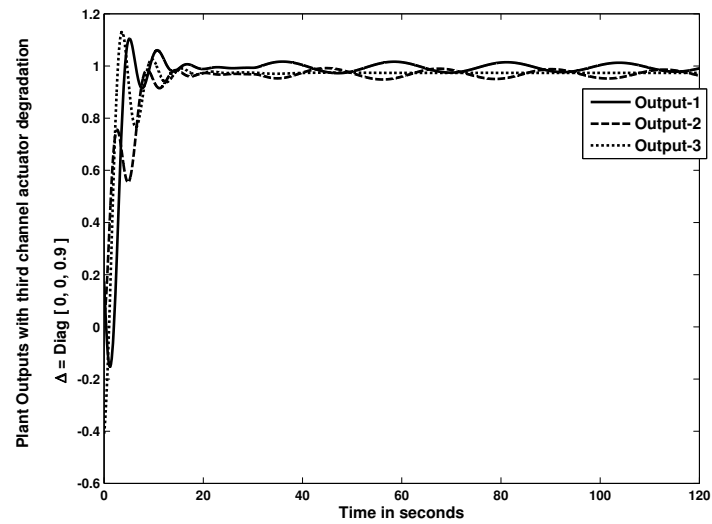


Figure 5.15: Attitude stabilization with channel-3 actuator degradation

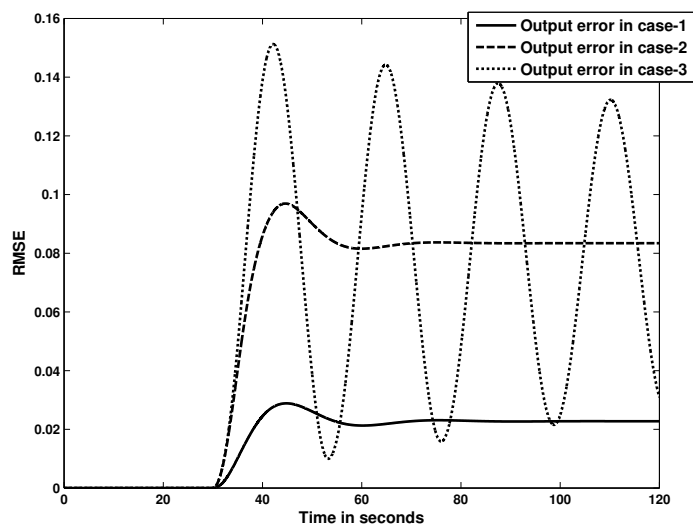


Figure 5.16: RMSE plot for actuator degradation in channels-1, 2 & 3

loop stable and closed-loop systems. Simple guidelines were presented in configuring a system towards decoupling and *RDI* was shown to overcome the drawbacks of the existing interaction measures such as RGA, RIA, ERGA and EREA and the ambiguity associated with them was demonstrated with some examples. The *RDI* was extended to *i.i.i.* in predicting the channel vulnerability in case of actuator degradation for open-loop stable and closed-loop systems. *RDI-i.i.i.* based guidelines were shown to aid a control engineer in identifying the least and most vulnerable channel to an actuator degradation in open-loop stable and closed-loop systems. The effectiveness of *RDI* and *i.i.i.* was illustrated by simulation results and verified using a performance measure defined in terms of RMSE between the plant and its model. The linearized spacecraft model stated in chapter 2 and the output feedback control law proposed in chapter 3 were used as an example in testing the *RDI-i.i.i.* based approach in predicting the channel vulnerability to actuator degradations and this case study was verified using the RMSE based performance measure.

Chapter 6

Conclusions

6.1 Accomplishments

This chapter concludes the thesis by summarizing important contributions and accentuates some future avenues of research which may be pursued as a result of this work. This thesis can be broadly classified into two parts, namely:

1. **Attitude stabilization and control of nonlinear rigid space structures.**
 2. **Study of MIMO subsystems interactions for better performance and fault tolerance.**
1. **Attitude stabilization and control of nonlinear rigid space structures.**

The concept of attitude stabilization and control has been extensively addressed in the literature wherein the attitude control laws are synthesized based on more than one measurement i.e. in addition to the attitude, angular velocity or its rate is assumed measurable. In the event where the angular velocity or its rate was not measurable the control law was designed to have a velocity generating filter formulation which made the control structure very complex. The spacecraft inertia was assumed to be known and if unknown periodic commands were used for its identification. The literature presented in chapter one briefly discussed such

techniques. In this thesis, attitude stabilization is achieved by synthesizing control laws involving just one measurement which is the attitude.

The design problem dealt here is a challenging one, owing to the nonlinear behavior of the plant involving both the kinematics and dynamics, attitude as the only measurement available. This would lead one to think that the performance of the designed controller would be questionable and would be inferior to the previously mentioned control structures in literature. However, the approach developed and presented in this thesis achieves its goal of attitude stabilization and control of nonlinear rigid space structures with simple control design and robust performance. The main conclusions and contributions are now discussed.

- (a) A novel and simple output feedback stabilization approach is proposed for the nonlinear spacecraft attitude model defined by Euler's equation of rotational dynamics and the kinematics in terms of Modified Rodrigues parameters. The control law is shown to globally asymptotically stabilize the nonlinear plant and the overall closed-loop stability is proved in the sense of Lyapunov by proposing a new candidate Lyapunov function. The control structure involves two loops namely, inner and outer, requires only the plant output to be measured, does not directly depend on the spacecraft inertia matrix and is shown to be robust with respect to system parametric uncertainty which is illustrated by simulation results.
- (b) Particle swarm optimization algorithm is used as a tool to infer the optimal controller parameters based on an objective function minimizing the absolute value of the attitude error.
- (c) The novelty and simplicity of the proposed output feedback control structure is further demonstrated by comparing it with two robust control approaches namely, loop-shaping and mixed sensitivity. The robust control approaches stabilize the linearized plant with a higher control effort when compared to the proposed output feedback approach. The output feedback controller

demonstrates good stabilization results for both the linear and nonlinear plant with limited control input, whereas the loop-shaping and mixed sensitivity based approaches show poor stabilization results for the nonlinear plant with a comparatively higher order of controller.

- (d) The output feedback control law is modified by reducing the degree of freedom in the control structure requiring the tuning of six gains instead of the original nine gains. The overall closed-loop stability is proved with a Lyapunov function proving the global asymptotic stability of the modified approach. Simulation results are illustrated in order to demonstrate the attitude stabilization and time varying attitude tracking of the nonlinear plant.
- (e) The output feedback approach is demonstrated in a Quaternion formulation where the nonlinear spacecraft attitude model is defined by Euler's equation of rotational dynamics and Quaternion based kinematics. The output feedback control law is shown to globally stabilize the nonlinear model in the sense of Lyapunov by proposing a new candidate Lyapunov function. Simulation results are illustrated to demonstrate the attitude stabilization and time varying attitude acquisition of the nonlinear model.
- (f) A case study is presented on a LST model developed by NASA, [44] & [48]. Nonlinear fully coupled dynamic equations of motion of the LST model fitted with reaction wheels are derived by taking into account the nonlinear coupling terms, inertia tensors and the angular velocity terms neglected in the original reference [44]. The derived nonlinear coupled dynamic system is combined with a Quaternion based kinematic model to form a nonlinear attitude model of the LST system with three reaction wheels as actuators. The LST attitude model was stabilized with a state feedback control law and time varying attitude tracking was achieved. Simulation results are illustrated to demonstrate the stabilization and control of the coupled and decoupled LST models. Single channel attitude stabilization is shown in order to visualize

the inter-axis coupling.

2. Study of MIMO subsystems interactions for better performance and fault tolerance.

Structure configuration is a principal task in the design of decentralized control systems. The objective is to pair the manipulated and controlled variables such that there is minimum interaction among the input-output channels of a MIMO system. This has been addressed in the literature by means of various interaction measures and their associated guidelines such as RGA, NI, RIA, ERGA and EREA. These measures show inconsistency among each other in the loop configuration of a system as they either depend on the dcgain of a system such as RGA, NI, RIA or a limited bandwidth as in the case of ERGA and EREA. They cannot be used in configuring an unstable system with a controller having a stable closed-loop system. In order to overcome these drawbacks a simple yet effective interaction measure and some guidelines were presented which are effective in structure configuration for open and closed-loop systems and clarify the ambiguity associated with the existing measures. The major conclusions and contributions are now discussed.

- (a) A new measure of interaction known as (*RDI*) and some guidelines were presented for the stable open-loop MIMO systems. *RDI* is defined in terms of H_∞ norm of the individual subsystems and helps in understanding the effect of one input on an output. *RDI* based guidelines were shown to configure a MIMO system structure towards decoupling and the veracity of this approach was verified using a performance measure defined in terms of root mean square error. The effectiveness of the approach was illustrated by simulation results and the approach was compared with the existing measures.

- (b) *RDI* was extended to the case of closed-loop MIMO systems. A similar performance measure was used to verify the *RDI* based approach and its associated guidelines in studying the subsystem interactions. Suitable examples were demonstrated.
- (c) *RDI* was extended to understand the vulnerability of fault and failure and the influence of actuator input on the system output by presenting an index known as *i.i.i.* based on *RDI*. The *i.i.i.* and its associated guidelines were shown to identify the actuator fault/failure that would least and most affect the overall performance of the open-loop stable and closed-loop systems. The effectiveness of the approach was illustrated by examples.

The contributions of this thesis have been accepted as conference publications, namely, [9], [7], [5], [8], [28], [6] and [29]. A few journal papers are currently under preparation.

6.2 Suggestions for Future Work

The work presented in this thesis requires further research, in terms of both design and implementation. These are discussed below.

- The output feedback attitude stabilization and control approach and its modified form presented in chapter 3 can be further improved and investigated by including actuator dynamics, environmental disturbances in the simulations model.
- Practical implementation of the output feedback control structure on a small scale satellite.
- The use of optimal algorithms to infer the best controller parameters in the state feedback control law stabilizing the LST attitude model in chapter 4.
- A Lyapunov stability analysis can be performed ensuring the global asymptotic stability of the LST model using the state feedback approach.

- In chapter 5, the interaction measures namely, *RDI* and *i.i.i.* can be further studied and the possibility of redesigning a control structure based on the subsystem interactions due to the actuator faults and failures can be investigated.

Appendix A

Linearization of Spacecraft Attitude Model based on Euler's Equation of Rotational Dynamics and MRP

A.1 Introduction

The aim of this appendix is to present the detailed Jacobian linearization of the nonlinear spacecraft attitude model defined in terms of MRP's and Euler's equation of rotational dynamics presented in Section 2.9 of Chapter 2.

A.1.1 Linearization

The kinematic differential equation in terms of MRP is stated in (2.20) and the Euler's equation of rotational dynamics is stated in (2.21). Let the inertia matrix and its inverse in (2.21) given by the following:

$$J \triangleq \begin{pmatrix} J_{11} & J_{12} & J_{13} \\ J_{21} & J_{22} & J_{23} \\ J_{31} & J_{32} & J_{33} \end{pmatrix} \quad J^{-1} \triangleq \begin{pmatrix} a & b & c \\ d & e & f \\ g & h & i \end{pmatrix} \quad (\text{A.1})$$

Expanding (2.20) and (2.21), we get the following

$$f_1 \triangleq \dot{q}_1 = \frac{1}{4} [\omega_1(1 + q_1^2 - q_2^2 - q_3^2)] + \frac{1}{2} [\omega_2(q_1q_2 - q_3)] + \frac{1}{2} [\omega_3(q_1q_3 + q_2)] \quad (\text{A.2})$$

$$f_2 \triangleq \dot{q}_2 = \frac{1}{2} [\omega_1(q_1q_2 + q_3)] + \frac{1}{4} [\omega_2(1 - q_1^2 + q_2^2 - q_3^2)] + \frac{1}{2} [\omega_3(q_2q_3 - q_1)] \quad (\text{A.3})$$

$$f_3 \triangleq \dot{q}_3 = \frac{1}{2} [\omega_1(q_1q_3 - q_2)] + \frac{1}{2} [\omega_2(q_2q_3 + q_1)] + \frac{1}{4} [\omega_3(1 - q_1^2 - q_2^2 + q_3^2)] \quad (\text{A.4})$$

$$\begin{aligned} f_4 \triangleq \dot{\omega}_1 = & a[\omega_3(J_{21}\omega_1 + J_{22}\omega_2 + J_{23}\omega_3) - \omega_2(J_{31}\omega_1 + J_{32}\omega_2 + J_{33}\omega_3)] \\ & - b[\omega_3(J_{11}\omega_1 + J_{12}\omega_2 + J_{13}\omega_3) + \omega_1(J_{31}\omega_1 + J_{32}\omega_2 + J_{33}\omega_3)] \\ & + c[\omega_2(J_{11}\omega_1 + J_{12}\omega_2 + J_{13}\omega_3) - \omega_1(J_{21}\omega_1 + J_{22}\omega_2 + J_{23}\omega_3)] \\ & a\tau_1 + b\tau_2 + c\tau_3 \end{aligned} \quad (\text{A.5})$$

$$\begin{aligned} f_5 \triangleq \dot{\omega}_2 = & d[\omega_3(J_{21}\omega_1 + J_{22}\omega_2 + J_{23}\omega_3) - \omega_2(J_{31}\omega_1 + J_{32}\omega_2 + J_{33}\omega_3)] \\ & - e[\omega_3(J_{11}\omega_1 + J_{12}\omega_2 + J_{13}\omega_3) + \omega_1(J_{31}\omega_1 + J_{32}\omega_2 + J_{33}\omega_3)] \\ & + f[\omega_2(J_{11}\omega_1 + J_{12}\omega_2 + J_{13}\omega_3) - \omega_1(J_{21}\omega_1 + J_{22}\omega_2 + J_{23}\omega_3)] \\ & d\tau_1 + e\tau_2 + f\tau_3 \end{aligned} \quad (\text{A.6})$$

$$\begin{aligned}
f_6 \triangleq \dot{\omega}_3 = & g[\omega_3(J_{21}\omega_1 + J_{22}\omega_2 + J_{23}\omega_3) - \omega_2(J_{31}\omega_1 + J_{32}\omega_2 + J_{33}\omega_3)] \\
& -h[\omega_3(J_{11}\omega_1 + J_{12}\omega_2 + J_{13}\omega_3) + \omega_1(J_{31}\omega_1 + J_{32}\omega_2 + J_{33}\omega_3)] \\
& +i[\omega_2(J_{11}\omega_1 + J_{12}\omega_2 + J_{13}\omega_3) - \omega_1(J_{21}\omega_1 + J_{22}\omega_2 + J_{23}\omega_3)] \\
& g\tau_1 + h\tau_2 + i\tau_3
\end{aligned} \tag{A.7}$$

The linearized spacecraft attitude model can be stated as follows:

$$\begin{bmatrix} \dot{q} \\ \dot{\omega} \end{bmatrix} = A_{mrp} \begin{bmatrix} q \\ \omega \end{bmatrix} + B_{mrp} \tau \tag{A.8}$$

$$q = C_{mrp} \begin{bmatrix} q \\ \omega \end{bmatrix}$$

where A_{mrp} , B_{mrp} and C_{mrp} are given as follows:

$$A_{mrp} = \begin{pmatrix} \frac{\partial f_1}{\partial q_1} & \frac{\partial f_1}{\partial q_2} & \frac{\partial f_1}{\partial q_3} & \frac{\partial f_1}{\partial \omega_1} & \frac{\partial f_1}{\partial \omega_2} & \frac{\partial f_1}{\partial \omega_3} \\ \frac{\partial f_2}{\partial q_1} & \frac{\partial f_2}{\partial q_2} & \frac{\partial f_2}{\partial q_3} & \frac{\partial f_2}{\partial \omega_1} & \frac{\partial f_2}{\partial \omega_2} & \frac{\partial f_2}{\partial \omega_3} \\ \frac{\partial f_3}{\partial q_1} & \frac{\partial f_3}{\partial q_2} & \frac{\partial f_3}{\partial q_3} & \frac{\partial f_3}{\partial \omega_1} & \frac{\partial f_3}{\partial \omega_2} & \frac{\partial f_3}{\partial \omega_3} \\ \frac{\partial f_4}{\partial q_1} & \frac{\partial f_4}{\partial q_2} & \frac{\partial f_4}{\partial q_3} & \frac{\partial f_4}{\partial \omega_1} & \frac{\partial f_4}{\partial \omega_2} & \frac{\partial f_4}{\partial \omega_3} \\ \frac{\partial f_5}{\partial q_1} & \frac{\partial f_5}{\partial q_2} & \frac{\partial f_5}{\partial q_3} & \frac{\partial f_5}{\partial \omega_1} & \frac{\partial f_5}{\partial \omega_2} & \frac{\partial f_5}{\partial \omega_3} \\ \frac{\partial f_6}{\partial q_1} & \frac{\partial f_6}{\partial q_2} & \frac{\partial f_6}{\partial q_3} & \frac{\partial f_6}{\partial \omega_1} & \frac{\partial f_6}{\partial \omega_2} & \frac{\partial f_6}{\partial \omega_3} \end{pmatrix} \tag{A.9}$$

$$B_{mrp} = \begin{pmatrix} \frac{\partial f_1}{\partial \tau_1} & \frac{\partial f_1}{\partial \tau_2} & \frac{\partial f_1}{\partial \tau_3} \\ \frac{\partial f_2}{\partial \tau_1} & \frac{\partial f_2}{\partial \tau_2} & \frac{\partial f_2}{\partial \tau_3} \\ \frac{\partial f_3}{\partial \tau_1} & \frac{\partial f_3}{\partial \tau_2} & \frac{\partial f_3}{\partial \tau_3} \\ \frac{\partial f_4}{\partial \tau_1} & \frac{\partial f_4}{\partial \tau_2} & \frac{\partial f_4}{\partial \tau_3} \\ \frac{\partial f_5}{\partial \tau_1} & \frac{\partial f_5}{\partial \tau_2} & \frac{\partial f_5}{\partial \tau_3} \\ \frac{\partial f_6}{\partial \tau_1} & \frac{\partial f_6}{\partial \tau_2} & \frac{\partial f_6}{\partial \tau_3} \end{pmatrix} \quad (\text{A.10})$$

$$C_{mrp} = \begin{pmatrix} 1 & 0 & 0 & 0 & 0 & 0 \\ 0 & 1 & 0 & 0 & 0 & 0 \\ 0 & 0 & 1 & 0 & 0 & 0 \end{pmatrix} \quad (\text{A.11})$$

The elements of A_{mrp} and B_{mrp} in (A.9 & A.10) from (A.2) to (A.7) are found to be

$$\frac{\partial f_1}{\partial q_1} = 0.5(\omega_1 q_1 + \omega_2 q_2 + \omega_3 q_3) \quad (\text{A.12})$$

$$\frac{\partial f_1}{\partial q_2} = 0.5(-\omega_1 q_2 + \omega_2 q_1 + \omega_3) \quad (\text{A.13})$$

$$\frac{\partial f_1}{\partial q_3} = 0.5(-\omega_1 q_3 - \omega_2 + \omega_3 q_1) \quad (\text{A.14})$$

$$\frac{\partial f_1}{\partial \omega_1} = 0.25(1 + q_1^2 - q_2^2 - q_3^2) \quad (\text{A.15})$$

$$\frac{\partial f_1}{\partial \omega_2} = 0.5(q_1 q_2 - q_3) \quad (\text{A.16})$$

$$\frac{\partial f_1}{\partial \omega_3} = 0.5(q_1 q_3 + q_2) \quad (\text{A.17})$$

$$\frac{\partial f_2}{\partial q_1} = 0.5(\omega_1 q_2 - \omega_2 q_1 - \omega_3) \quad (\text{A.18})$$

$$\frac{\partial f_2}{\partial q_2} = 0.5(\omega_1 q_1 + \omega_2 q_2 + \omega_3 q_3) \quad (\text{A.19})$$

$$\frac{\partial f_2}{\partial q_3} = 0.5(\omega_1 - \omega_2 q_3 + \omega_3 q_2) \quad (\text{A.20})$$

$$\frac{\partial f_2}{\partial \omega_1} = 0.5(q_1 q_2 + q_3) \quad (\text{A.21})$$

$$\frac{\partial f_2}{\partial \omega_2} = 0.25(1 - q_1^2 + q_2^2 - q_3^2) \quad (\text{A.22})$$

$$\frac{\partial f_2}{\partial \omega_3} = 0.5(q_2 q_3 - q_1) \quad (\text{A.23})$$

$$\frac{\partial f_3}{\partial q_1} = 0.5(\omega_1 q_3 + \omega_2 - \omega_3 q_1) \quad (\text{A.24})$$

$$\frac{\partial f_3}{\partial q_2} = 0.5(-\omega_1 + \omega_2 q_3 - \omega_3 q_2) \quad (\text{A.25})$$

$$\frac{\partial f_3}{\partial q_3} = 0.5(\omega_1 q_1 + \omega_2 q_2 + \omega_3 q_3) \quad (\text{A.26})$$

$$\frac{\partial f_3}{\partial \omega_1} = 0.5(q_3 q_1 - q_2) \quad (\text{A.27})$$

$$\frac{\partial f_3}{\partial \omega_2} = 0.5(q_3 q_2 + q_1) \quad (\text{A.28})$$

$$\frac{\partial f_3}{\partial \omega_3} = 0.25(1 - q_1^2 - q_2^2 + q_3^2) \quad (\text{A.29})$$

$$\frac{\partial f_4}{\partial q_1} = \frac{\partial f_4}{\partial q_2} = \frac{\partial f_4}{\partial q_3} = 0 \quad (\text{A.30})$$

$$\frac{\partial f_4}{\partial \omega_1} = a(\omega_3 J_{21} - \omega_2 J_{31}) + b(-\omega_3 J_{11} + 2\omega_1 J_{31} + \omega_2 J_{32} + \omega_3 J_{33}) + c(\omega_2 J_{11} - 2\omega_1 J_{21} - \omega_2 J_{22} - \omega_3 J_{23}) \quad (\text{A.31})$$

$$\frac{\partial f_4}{\partial \omega_2} = a(\omega_3 J_{22} - \omega_1 J_{31} - 2\omega_2 J_{32} - \omega_3 J_{33}) + b(-\omega_3 J_{12} + \omega_1 J_{32}) + c(\omega_1 J_{11} + 2\omega_2 J_{12} + \omega_3 J_{13} - \omega_1 J_{22}) \quad (\text{A.32})$$

$$\frac{\partial f_4}{\partial \omega_3} = a(\omega_1 J_{21} + \omega_2 J_{22} + 2\omega_3 J_{23} - \omega_2 J_{33}) + b(-\omega_1 J_{11} - \omega_2 J_{12} - 2\omega_3 J_{13} + \omega_1 J_{33}) + c(\omega_2 J_{13} - \omega_1 J_{23}) \quad (\text{A.33})$$

$$\frac{\partial f_5}{\partial q_1} = \frac{\partial f_5}{\partial q_2} = \frac{\partial f_5}{\partial q_3} = 0 \quad (\text{A.34})$$

$$\frac{\partial f_5}{\partial \omega_1} = d(\omega_3 J_{21} - \omega_2 J_{31}) + e(-\omega_3 J_{11} + 2\omega_1 J_{31} + \omega_2 J_{32} + \omega_3 J_{33}) + f(\omega_2 J_{11} - 2\omega_1 J_{21} - \omega_2 J_{22} - \omega_3 J_{23}) \quad (\text{A.35})$$

$$\frac{\partial f_5}{\partial \omega_2} = d(\omega_3 J_{22} - \omega_1 J_{31} - 2\omega_2 J_{32} - \omega_3 J_{33}) + e(-\omega_3 J_{12} + \omega_1 J_{32}) + f(\omega_1 J_{11} + 2\omega_2 J_{12} + \omega_3 J_{13} - \omega_1 J_{22}) \quad (\text{A.36})$$

$$\frac{\partial f_5}{\partial \omega_3} = d(\omega_1 J_{21} + \omega_2 J_{22} + 2\omega_3 J_{23} - \omega_2 J_{33}) + e(-\omega_1 J_{11} - \omega_2 J_{12} - 2\omega_3 J_{13} + \omega_1 J_{33}) + f(\omega_2 J_{13} - \omega_1 J_{23}) \quad (\text{A.37})$$

$$\frac{\partial f_6}{\partial q_1} = \frac{\partial f_6}{\partial q_2} = \frac{\partial f_6}{\partial q_3} = 0 \quad (\text{A.38})$$

$$\frac{\partial f_6}{\partial \omega_1} = g(\omega_3 J_{21} - \omega_2 J_{31}) + h(-\omega_3 J_{11} + 2\omega_1 J_{31} + \omega_2 J_{32} + \omega_3 J_{33}) + i(\omega_2 J_{11} - 2\omega_1 J_{21} - \omega_2 J_{22} - \omega_3 J_{23}) \quad (\text{A.39})$$

$$\frac{\partial f_6}{\partial \omega_2} = g(\omega_3 J_{22} - \omega_1 J_{31} - 2\omega_2 J_{32} - \omega_3 J_{33}) + h(-\omega_3 J_{12} + \omega_1 J_{32}) + i(\omega_1 J_{11} + 2\omega_2 J_{12} + \omega_3 J_{13} - \omega_1 J_{22}) \quad (\text{A.40})$$

$$\frac{\partial f_6}{\partial \omega_3} = g(\omega_1 J_{21} + \omega_2 J_{22} + 2\omega_3 J_{23} - \omega_2 J_{33}) + h(-\omega_1 J_{11} - \omega_2 J_{12} - 2\omega_3 J_{13} + \omega_1 J_{33}) + i(\omega_2 J_{13} - \omega_1 J_{23}) \quad (\text{A.41})$$

Non-zero equilibrium points are found by solving the six nonlinear equations describing the spacecraft's attitude stated in equations (A.2-A.7). The spacecraft's inertia matrix is given in (2.32) and is taken from [66]. The non-zero equilibrium points are found to be as follows:

$$\begin{aligned}q_1 &= 0.3042 \\q_2 &= -0.3354 \\q_3 &= -0.3475 \\ \omega_1 &= -0.2652 \\ \omega_2 &= 0.2652 \\ \omega_3 &= -0.1107 \\ \tau_1 &= 0.0415 \\ \tau_2 &= 0.1578 \\ \tau_3 &= 0.2785\end{aligned}\tag{A.42}$$

The state space matrices A_{mrp} and B_{mrp} in (A.9 & A.10) are then calculated using the non-zero equilibrium points in (A.42) and are stated in (2.29 & 2.30)

Appendix B

Dynamic Formulation of Euler's Equation of Rotational Dynamics and MRP

B.1 Introduction

The aim of this appendix is to combine the Euler's equation of rotational dynamics and the MRP based kinematic formulation presented in Section 2.9.1 of Chapter 2 and form a second order nonlinear dynamic equation of the Hamiltonian form [52].

B.1.1 Dynamic Formulation

The Euler's equation of rotational dynamics and the kinematic differential equation in terms of MRP is given as follows:

$$J\dot{\omega} = -\omega \times J\omega + \tau \tag{B.1}$$

$$\dot{q} = [T(q)] \omega \tag{B.2}$$

Differentiating the kinematic equations of motion in (B.2) with respect to time we get

$$\begin{aligned}\ddot{q} &= \dot{T}(q)\omega + T(q)\dot{\omega} \\ \ddot{q} &= \dot{T}(q)\omega + T(q)J^{-1}J\dot{\omega}\end{aligned}\tag{B.3}$$

Substituting (B.2 & B.1) in (B.3) we get

$$\begin{aligned}\ddot{q} &= \dot{T}(q)T^{-1}(q)\dot{q} + T(q)J^{-1}(J\omega \times \omega + \tau) \\ \ddot{q} &= \dot{T}(q)T^{-1}(q)\dot{q} + T(q)J^{-1}J\omega \times \omega + T(q)J^{-1}\tau \\ \ddot{q} &= \dot{T}(q)T^{-1}(q)\dot{q} + T(q)J^{-1}JT^{-1}(q)\dot{q} \times T^{-1}(q)\dot{q} + T(q)J^{-1}\tau\end{aligned}\tag{B.4}$$

Multiplying throughout by $T^{-T}(q)JT^{-1}(q)$ we get

$$\begin{aligned}T^{-T}(q)JT^{-1}(q)\ddot{q} &= T^{-T}(q)JT^{-1}(q)\dot{T}(q)T^{-1}(q)\dot{q} + \\ &T^{-T}(q)JT^{-1}(q)T(q)J^{-1}JT^{-1}(q)\dot{q} \times T^{-1}(q)\dot{q} + \\ &T^{-T}(q)JT^{-1}(q)T(q)J^{-1}\tau\end{aligned}\tag{B.5}$$

Defining

$$P(q) \triangleq T^{-1}(q), P^T(q) \triangleq T^{-T}(q),\tag{B.6}$$

we get

$$\begin{aligned}P^T(q)JP(q)\ddot{q} &= P^T(q)JP(q)\dot{T}(q)P(q)\dot{q} + \\ &P^T(q)JP(q)P^{-1}(q)J^{-1}JP(q)\dot{q} \times P(q)\dot{q} + \\ &P^T(q)JP(q)P^{-1}(q)J^{-1}\tau\end{aligned}\tag{B.7}$$

$$\begin{aligned}
P^T(q)JP(q)\ddot{q} &= P^T(q)JP(q)\dot{T}(q)P(q)\dot{q} + \\
&P^T(q)JP(q)\dot{q} \times \\
&P(q)\dot{q} + P^T(q)\tau
\end{aligned} \tag{B.8}$$

$$J^*(q)\ddot{q} - J^*(q)\dot{T}(q)P(q)\dot{q} - P^T(q)JP(q)\dot{q} \times P(q)\dot{q} = P^T(q)\tau \tag{B.9}$$

$$J^*(q)\ddot{q} - J^*(q)\dot{T}(q)P(q)\dot{q} - P^T S(JP(q)\dot{q})P = P^T(q)\tau \tag{B.10}$$

Hence the nonlinear dynamic model of spacecraft is given by the following equation

$$J^*(q)\ddot{q} + C^*(\dot{q}, \ddot{q})\dot{q} = P^T \tau \tag{B.11}$$

where

$$\begin{aligned}
J^*(q) &\triangleq P^T(q)JP(q) \\
C^*(q, \dot{q}) &\triangleq -J^*(q)\dot{T}(q)P(q) - P^T(q)S(JP(q)\dot{q})P(q)
\end{aligned} \tag{B.12}$$

For ease of notation we simplify $J^*(q) = J^*$, $P(q) = P$ and $C^*(q, \dot{q}) = C^*$

Appendix C

Dynamic Formulation of Euler's Equation of Rotational Dynamics and Quaternions

C.1 Introduction

The aim of this appendix is to combine the Euler's equation of rotational dynamics and the Quaternion's based kinematic formulation presented in Section 2.9.2 of Chapter 2 and form a second order nonlinear dynamic equation of the Hamiltonian form [52].

C.1.1 Dynamic Formulation

The Euler's equation of rotational dynamics and the kinematic differential equation in terms of Quaternion's is given as follows:

$$J\dot{\omega} = -\omega \times J\omega + \tau \tag{C.1}$$

$$\dot{\beta}_q = [B(\beta_q)] \omega \equiv B \omega \tag{C.2}$$

Differentiating the kinematic equations of motion in (C.2) with respect to time we get

$$\begin{aligned}\ddot{\beta}_q &= \dot{B}\omega + B\dot{\omega} \\ \ddot{\beta}_q &= \dot{B}\omega + BJ^{-1}J\dot{\omega}\end{aligned}\tag{C.3}$$

Substituting (C.2 & C.1) in (C.3) we get

$$\begin{aligned}\ddot{\beta}_q &= \dot{B}B^{-1}\dot{\beta}_q + BJ^{-1}(J\omega \times \omega + \tau) \\ \ddot{\beta}_q &= \dot{B}B^{-1}\dot{\beta}_q + BJ^{-1}J\omega \times \omega + BJ^{-1}\tau \\ \ddot{\beta}_q &= \dot{B}B^{-1}\dot{\beta}_q + BJ^{-1}JB^{-1}\dot{\beta}_q \times B^{-1}\dot{\beta}_q + BJ^{-1}\tau\end{aligned}\tag{C.4}$$

Multiplying throughout by $B^{-T}JB^{-1}$ we get

$$\begin{aligned}B^{-T}JB^{-1}\ddot{\beta}_q &= B^{-T}JB^{-1}\dot{B}B^{-1}\dot{\beta}_q + \\ &B^{-T}JB^{-1}BJ^{-1}JB^{-1}\dot{\beta}_q \times B^{-1}\dot{\beta}_q + \\ &B^{-T}JB^{-1}BJ^{-1}\tau\end{aligned}\tag{C.5}$$

Defining

$$\xi \triangleq B^{-1}, \xi^T \triangleq B^{-T},\tag{C.6}$$

we get

$$\begin{aligned}\xi^T J \xi \ddot{\beta}_q &= \xi^T J \xi \dot{B} B^{-1} \dot{\beta}_q + \\ &\xi^T J \xi B J^{-1} J B^{-1} \dot{\beta}_q \times B^{-1} \dot{\beta}_q + \xi^T J \xi B J^{-1} \tau\end{aligned}\tag{C.7}$$

$$\xi^T J \xi \ddot{\beta}_q = \xi^T J \xi \dot{B} B^{-1} \dot{\beta}_q + \xi^T J \xi \dot{\beta}_q \times B^{-1} \dot{\beta}_q + \xi^T \tau \quad (\text{C.8})$$

$$M^* \ddot{\beta}_q - M^* \dot{B} B^{-1} \dot{\beta}_q - \xi^T J \xi \dot{\beta}_q \times B^{-1} \dot{\beta}_q = \xi^T \tau \quad (\text{C.9})$$

$$M^* \ddot{\beta}_q - M^* \dot{B} \xi \dot{\beta}_q - \xi^T S(J \xi \dot{\beta}_q) \xi = \xi^T \tau \quad (\text{C.10})$$

Hence the nonlinear dynamic model of spacecraft is given by the following equation

$$M^*(\beta_q) \ddot{\beta}_q + N^*(\dot{\beta}_q, \beta_q) \dot{\beta}_q = \xi^T \tau \quad (\text{C.11})$$

where

$$\begin{aligned} M^*(\beta_q) &\triangleq \xi^T(\beta_q) J \xi(\beta_q) \\ N^*(\beta_q, \dot{\beta}_q) &\triangleq -M^*(\beta_q) \dot{B}(\beta_q) \xi(\beta_q) - \xi^T(\beta_q) S(J \xi(\beta_q) \dot{\beta}_q) \xi(\beta_q) \end{aligned} \quad (\text{C.12})$$

For ease of notation we simplify $M^*(\beta_q) = M^*$, $\xi(\beta_q) = \xi$ and $N^*(\beta_q, \dot{\beta}_q) = N^*$

Appendix D

Reaction Wheel Specifications

D.1 Introduction

The aim of this appendix is to give the technical details of the reaction wheel manufactured by SSBV Space and Ground Systems, UK [1]. The details mentioned in this appendix are taken from the company's web site. The physical characteristics mentioned here are used in calculating the reaction wheel inertia of the LST model discussed in chapter four.

D.1.1 Functional Characteristics

Max wheel torque: 20 mNm

Max wheel momentum: 0.65 Nms

Speed range: -9000 to +9000 rpm

Rotor moment of inertia: $1.0 \times 10^{-3} \text{ kgm}^2$

Speed control tracking error: <1 rpm

Current consumption: 40 mA / mNm

D.1.2 Physical Characteristics

Mass: 1550g

Dimensions: 102 x 102 x 105 mm

Static unbalance: < 5 g mm

Operating temperature -30 to +60C

D.1.3 Current Consumption

0 rpm: 45 mA

100 rpm: 65 mA

4000 rpm: 165 mA

D.1.4 Interfaces

Power supply: 28V unregulated unregulated

Data: RS422

Bibliography

- [1] www.satserv.co.uk.
- [2] Large space telescope phase a final report. *Program Development Directorate, George C. Marshall Space Flight Center, Huntsville, Alabama, 1972.*
- [3] M. A. Abido. Optimal design of power system stabilizers using particle swarm optimization. *IEEE Transactions on Energy Conversion*, 17:406–413, 2002.
- [4] J. Ahmed, V. T. Coppola, and D. S. Bernstein. Adaptive asymptotic tracking of spacecraft attitude motion with inertia matrix identification. *Journal of Guidance, Control and Dynamics*, 21:684–691, 1998.
- [5] R. Ahmed, H. Chaal, and D. W. Gu. Spacecraft controller tuning using particle swarm optimization. *ICCAS-SICE 2009, International Joint Conference, Fukuoka, Japan, 2009.*
- [6] R. Ahmed, D. W. Gu, , and I. Postlethwaite. System structure configuration and actuator degradation. *23rd Chinese Control and Decision Conference, CCDC-2011, Mianyang, China, 2011.*
- [7] R. Ahmed, D. W. Gu, and I. Postlethwaite. Attitude tracking of a rotating rigid body system. *11th IASTED International Conference on Control and Applications, CA 2009, Cambridge, United Kingdom, 2009.*

-
- [8] R. Ahmed, D. W. Gu, and I. Postlethwaite. A case study on spacecraft attitude control. *48th IEEE Conference on Decision and Control and 28th Chinese Control Conference, Shanghai, China, 2009.*
- [9] R. Ahmed, D. W. Gu, and I. Postlethwaite. A simple stabilization approach for a nonlinear spacecraft attitude model using a Lyapunov function. *Proceedings of ICEAE, International Conference and Exhibition on Aerospace Engineering, Bangalore, India, 2009.*
- [10] J. L. Boiffier. *The Dynamics of Flight: The Equations.* John Wiley & Sons, 1998.
- [11] E. H. Bristol. On a new measure of interactions for multivariable process control. *IEEE Transactions on Automatic Control*, 11:133–134, 1966.
- [12] E. H. Bristol. Recent results on interactions in multivariable process control. *Proceeding of the 71st Annual AIChE meeting, Houston, TX, USA*, pages –, 1979.
- [13] D. Chen and D. E. Seborg. Relative gain array analysis for uncertain process models. *AIChE J*, 48:302–310, 2002.
- [14] S. M. Chen and Y. F. Dong. Satellite attitude tracking controller optimization based on particle swarm optimization. *Procedia Engineering*, 15:526–530, 2011.
- [15] S. M. Chen, Y. F. Dong, and J. Su. Sliding mode control using RBF neural network for spacecraft attitude tracking. *Intelligent Computing and Intelligent Systems*, 2:211–214, 2010.
- [16] R. O. Doruk. Linearization in satellite attitude control with modified rodriguez parameters. *Aircraft Engineering and Aerospace Technology*, 81:199–203, 2009.
- [17] W. Feng and I. Postlethwaite. A simple robust control scheme for robot manipulators with only joint position measurements. *International Journal for Robotics Research*, 12:490–496, 1993.

-
- [18] J. P. Gagnepain and D. E. Seborg. Analysis of process interactions with applications to multiloop control system design. *Industrial and Engineering Chemistry Research*, 21:5–11, 1982.
- [19] N. Gollu and L. Rodrigues. Control of large angle attitude maneuvers for rigid bodies using sum of squares. *Proceedings of American Control Conference*, 2007.
- [20] D. W. Gu, P. Hr. Petkov, and M. M. Konstantinov. *Robust control design with matlab*. Springer, 2005.
- [21] K. E. Haggblom. Control structure analysis by partial relative gains. *Proceedings of the 36th Conference on Decision and Control, San Diego, California, USA*, 1997.
- [22] W. K. Ho, T. H. Lee, and O. P. Gan. Tuning of multiloop proportional-integral-derivative controllers based on gain and phase margin specifications. *Industrial and Engineering Chemistry Research*, 36:2231–2238, 1997.
- [23] D. Hu, A. Sarosh, and Y. F. Dong. An improved particle swarm optimiser for parametric optimization of flexible satellite controller. *Appl Math Comput*, 217(21):8512–8521, 2011.
- [24] H. P. Huang, M. Ohshima, and I. Hashimoto. Dynamic interaction and multiloop control system design. *Journal of Process Control*, 4:15–27, 1994.
- [25] P. C. Hughes. *Spacecraft Attitude Dynamics*. Wiley, 1986.
- [26] J. Kennedy. The particle swarm: social adaptation of knowledge. *Proceedings of IEEE International Conference on Computation*, pages 303–308, 1997.
- [27] A. Khaki-Sedigh and B. Moaveni. *Control Configuration Selection for Multivariable Plants*. Springer, 2009.
- [28] N. Khan, R. Ahmed, and D. W. Gu. A fault tolerant scheme for attitude estimation. *7th International Bhurban Conference on Applied Sciences and Technology, IBCAST 2010, Islamabad, Pakistan*, 2010.

-
- [29] N. Khan, S. Fekri, R. Ahmed, and D. W. Gu. Robust state estimation in spacecraft attitude control. *50th IEEE Conference on Decision and Control and European Control Conference, CDC-ECC-2011, Orlando, Florida, USA*, 2011.
- [30] M. Krstić and P. Tsiotras. Inverse optimal stabilization of a rigid spacecraft. *IEEE Transactions on Automatic Control*, 44:1042–1049, 1999.
- [31] B. G. Lipták. *Instrument Engineer's Handbook: Process Control and Optimization Volume II*. CRC Press, 2006.
- [32] F. Lizarralde and J. T. Wen. Attitude control without angular velocity measurements: A passivity approach. *IEEE Transactions on Automatic Control*, 41:468–472, 1996.
- [33] D. McFarlane and K. Glover. A loop shaping design procedure using H_∞ synthesis. *IEEE Transactions on Automatic Control*, 37:749–769, 1992.
- [34] G. Meyer. Design and global analysis of spacecraft attitude control. *Nasa Technical report*, R-361, 1971.
- [35] M. Monshizadeh-Naini, A. Fatehi, and A. Khaki-Sedigh. Input-output pairing using effective relative energy array. *Industrial and Engineering Chemistry Research*, 48:7137–7144, 2009.
- [36] A. Niederlinski. A heuristic approach to the design of linear multivariable interacting control systems. *Automatica*, 7:691–701, 1971.
- [37] B. A. Ogunnaike, J. Lemaire, M. Morari, and W. H. Ray. Advanced multivariable control of a pilot plant distillation column. *AIChE J*, 29:632–640, 1983.
- [38] A. E. Olsson. *Particle Swarm Optimization: Theory, Techniques and Applications*. Nova Science Publishers, 2011.

- [39] P. Grosdidier P. and M. Morari. A computer aided methodology for the design of decentralized controllers. *Journal of Computers and Chemical Engineering*, 11:423–433, 1987.
- [40] S. Salcudean. A globally convergent angular velocity observer for rigid body motion. *IEEE Transactions on Automatic Control*, 36:1493–1497, 1991.
- [41] M. E. Salgado and A. Conley. MIMO interaction measure and controller structure selection. *International Journal of Control*, 77:367–383, 2004.
- [42] H. Schaub and J. L. Junkins. *Analytical Mechanics of Space Systems*. AIAA, 2003.
- [43] H. Schaub, S. R. Vadali, and J. L. Junkins. Feedback control law for variable speed control moment gyros. *Journal of the Astronautical Sciences*, 46:307–328, 1998.
- [44] W. O. Schiehlen. A fine pointing system for the large space telescope. *NASA Report, No. NASA TN D-7500, National Aeronautics and Space Administration, Washington, D.C.*, 1973.
- [45] R. Sharma and A. Tewari. Optimal nonlinear tracking of spacecraft attitude maneuvers. *IEEE Transactions on Automatic Control*, 12:677–682, 2004.
- [46] M. D. Shuster. A survey of attitude representations. *Journal of Astronautical Sciences*, 41:439–517, 1993.
- [47] M. J. Sidi. *Spacecraft Dynamics and Control: A Practical Engineering Approach*. Cambridge University Press, 1997.
- [48] D. D. Siljak. *Large-Scale Dynamic Systems*. Dover Publications, 1978.
- [49] S. Skogestad and M. Morari. Implications of large rga elements on control performance. *Industrial and Engineering Chemistry Research*, 26:2323–2330, 1987.
- [50] S. Skogestad and I. Postlethwaite. *Multivariable Feedback Control*. John Wiley & Sons, 1996.

- [51] J. J. E. Slotine and M.D. Di Benedetto. Hamiltonian adaptive control of spacecraft. *IEEE Transactions on Automatic Control*, 35:848–852, 1990.
- [52] J. J. E. Slotine and W. Li. *Applied Nonlinear Control*. Prentice Hall, 1990.
- [53] K. J. Åström and B. Wittenmark. *Adaptive Control*. Addison-Wesley Publishing Company, 1995.
- [54] S. Tavakoli and A. Banookh. Robust PI control design using particle swarm optimization. *Journal of Computer Science and Engineering*, 1:36–41, 2010.
- [55] A. Tewari. *Atmospheric and Space Flight Dynamics*. Birkhäuser, 2007.
- [56] P. Tsiotras. New control laws for the attitude stabilization of rigid bodies. *Proceedings, IFAC Symposium on Automatic Control in Aerospace*, pages 316–321, 1994.
- [57] P. Tsiotras. Further passivity results for the attitude control problem. *IEEE Transactions on Automatic Control*, 43:1597–1600, 1998.
- [58] L. S. Tung and T. F. Edgar. Analysis of control-output interactions in dynamic systems. *AIChE J*, 27:690–693, 1981.
- [59] K. Valarmathi, D. Devraj, and T. K. Radhakrishnan. Particle swarm optimization based PI controller tuning for fermentation process. *Computational Intelligence for Modelling, Control and Automation*, pages 1043–1048, 2005.
- [60] J. T. Y. Wen and K. Kreutz-Delgado. The attitude control problem. *IEEE Transactions on Automatic Control*, 36:1148–1162, 1991.
- [61] J. R. Wertz. *Spacecraft Attitude Determination and Control*. D. Reidel, 1978.
- [62] B. Wie. *Space Vehicle Dynamics and Control*. AIAA, 1998.
- [63] B. Wie and P. M. Barbara. Quaternion feedback for spacecraft large angle maneuvers. *Journal of Guidance, Control and Dynamics*, 8:360–365, 1985.

-
- [64] B. Wie, H. Weiss, and A. Arapostathis. Quaternion feedback regulator for spacecraft eigenaxis rotations. *Journal of Guidance, Control and Dynamics*, 12:375–380, 1989.
- [65] M. F. Witcher and T. J. McAvoy. Interacting control systems: steady-state and dynamic measurement of interaction. *ISA Transactions*, 16:35–41, 1977.
- [66] H. Wong, M.S. De Queiroz, and V. Kapila. Adaptive tracking control using synthesized velocity from attitude measurements. *Automatica*, 37:947–953, 2001.
- [67] R. K. Wood and M. W. Berry. Terminal composition control of a binary distillation column. *Chemical Engineering Science*, 28:1707–1717, 1973.
- [68] Q. Xiong, W. J. Cai, and M. J. He. A practical loop pairing criterion for multivariable processes. *Journal of Process Control*, 15:741–747, 2005.
- [69] Z. X. Zhu. Variable pairing selection based on individual and overall interaction measures. *Industrial and Engineering Chemistry Research*, 35:4091–4099, 1996.
- [70] Z. X. Zhu and A. Jutan. A new variable pairing criterion based on Niederlinski index. *Industrial and Engineering Chemistry Research*, 121:235–250, 1993.